THE MESSENGER

EL MENSAJERO

Munich

La Silla
La Serena
Santiago

No. 44 – June 1986

ESO Observations of Bright Supernova in Centaurus A

An extensive observing campaign is underway at the European Southern Observatory in an attempt to unravel some of the mysteries of massive stellar explosions, known as supernovae. It has been triggered by the sudden appearance of a comparatively bright supernova in the peculiar galaxy NGC 5128, located in the southern constellation Centaurus. This galaxy is one of the strongest radio emitters in the southern sky and is as such designated Centaurus A (Cen A).

The supernova, which has received the official designation 1986G by the International Astronomical Union, was discovered on May 3.5 UT by Reverend R. Evans, an amateur astronomer in Australia who has more than a dozen earlier discoveries to his credit. It appeared as a "new star", southeast of the centre of Cen A and almost in the middle of the broad dust band that girdles this unusual galaxy (see Figure 1). The magnitude was estimated as 12. No supernovae have been detected in this galaxy before. This event is of particular interest, because comparatively bright supernovae are rather rare and also because of the peculiar nature of the parent galaxy. The most recent supernova of a similar magnitude was in 1980, in the northern, spiral galaxy NGC 6946.

Supernovae are believed to represent a late evolutionary stage of massive stars in which the star runs out of atomic fuel. It can no longer support its own weight and collapses. Immediately thereafter follows a dramatic thermonuclear explosion during which the outer layers are blown into the surrounding space. A small and very compact object may remain at the centre. The best known historical supernova was seen in the year 1054, giving birth to the Crab Nebula and an associated neutron star, which was detected as a radio pulsar in 1967. Most, if not all, heavy elements in the Universe have been generated in the exceedingly hot interiors of stars in the supernova phase. Supernovae are very rarely discovered before they reach their maximal brightness and little is known about the early phases. Currently, about 20–25 supernovae are detected per year in ex-

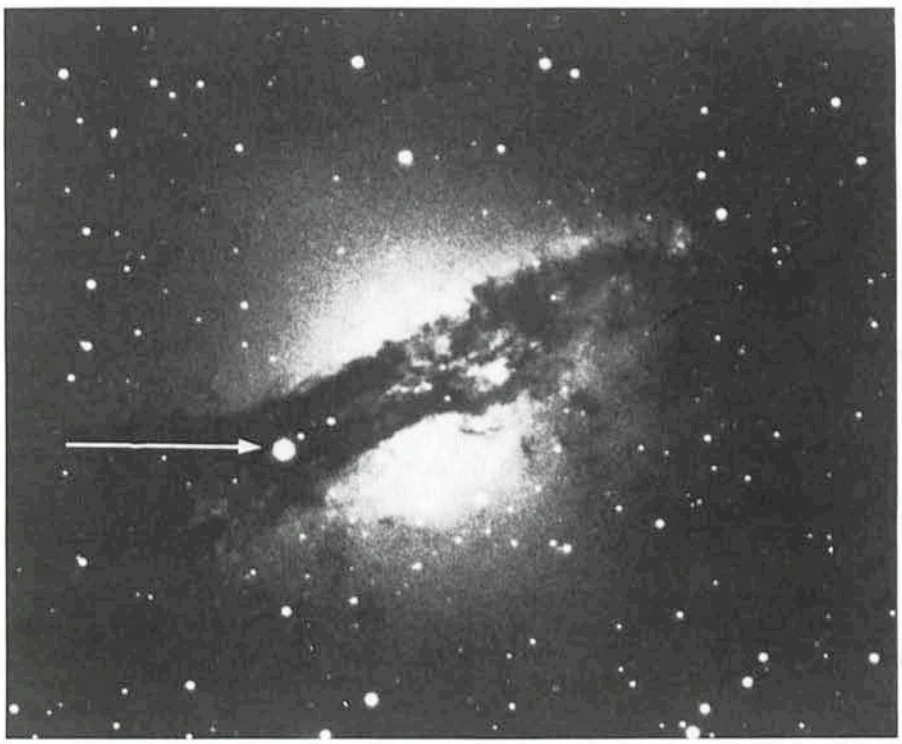

Figure 1: *This picture of the newly discovered supernova 1986 G in the peculiar, southern galaxy Centaurus A (= NGC 5128) was obtained on 1986 May 8.0 UT with the ESO 40-cm double astrograph (GPO) on La Silla. Exposure: 90 minutes on blue-sensitive IIa–O emulsion. Observer: H. Duerbeck, visiting astronomer from Astronomisches Institut, Münster, FRG. The 11.5-mag supernova (indicated with an arrow) is situated in the extensive dust band that surrounds the galaxy.*

terior galaxies; the last one in our own galaxy, the Milky Way, appears to be the one found by Kepler in the constellation Ophiocus in 1604.

Observations at ESO with the 1-m and 50-cm photometric telescopes have shown that supernova 1986G was still brightening at a rate of about 0.05 mag/day on May 11.2 UT. On this date, the V-magnitude was 11.4 and colour index (B-V) was 1.1 magnitude. CCD images in different colours were exposed at the Danish 1.5-m telescope (cf. the note by Galletta in this *Messenger*). Low-dispersion IDS and CCD spectra have been obtained with the ESO 1.5-m spectroscopic telescope and with the 2.2-m telescope (cf. the note by di Serego Alighieri). They show a typical Type I supernova spectrum before maximum, significantly reddened by absorption in Cen A. Of special interest are very high dispersion spectral observations, obtained with the CASPEC spectrograph at the ESO 3.6-m telescope. The CaII H and K lines and the NaI D lines show a complicated structure with no less than six very deep absorption components. From a preliminary analysis, it would appear that four of these are caused by absorption of the light from the supernova in four separate interstellar clouds in Cen A. One is due to matter in the Milky Way and one may belong to an intergalactic cloud between Cen A and the Milky Way, the existence of which was surmised in an earlier ESO study of this galaxy (D'Odorico et al., 1985, *Ap. J.* **299,** p. 852).

These observations, and the position near the middle of the dust band, indicate that the supernova is situated well inside the galaxy and that its light is dimmed by about 4 magnitudes due to obscuring dust. Had it been situated in an unobscured region, its magnitude would have been about 7.5, making it the brightest supernova in this century. Due to Cen A's peculiar structure (some astronomers consider it to be the result of a collision among two galaxies), it has not yet been possible to measure an accurate distance to this galaxy. However, if the intrinsic brightness of 1986G is that of a normal Type I supernova, then the distance to Cen A would be around 2–3 Megaparsec (7–10 million light-years), or only 3–4 times farther away than the Andromeda Nebula. Cen A may therefore even be an outlying member of the Local Group of Galaxies. At a distance of 3 Megaparsec, the total radio energy would be around 10^{58} ergs, corresponding to 10^4 solar masses. Clearly, a most energetic event has taken place in Cen A rather recently; the velocity dispersion of the interstellar clouds may be a relict of it.

The ESO observations are continuing. The following ESO staff and visiting astronomers have participated so far: I. Bues, P.R. Christensen, S. di Serego Alighieri, H. Duerbeck, G. Galletta, L. Kohoutek, P. Magain, P.E. Nissen, D. Reimers, R. Schulte Ladbeck and J. Sommer-Larsen. *The editor*

CCD Observations of Supernova 1986G in Cen A

G. GALLETTA, Astronomical Institute, University of Padova, Italy

A CCD image of the newly discovered supernova in NGC 5128 was obtained with the Danish 1.52-m telescope on May 8, 1986. By comparison with previous images of the same area it appears that the supernova is located in a luminous portion of the dust band, similar to a hole in the disk of gas surrounding the galaxy (Fig. 1).

This disk and the related dust lane is probably the result of a recent collision with a gas cloud or a gas-rich system, whose age has been estimated to about 3×10^8 years (Tubbs, A.D., 1980, *Ap. J.* **241,** 969). A convincing proof of this is that the rotation axis of the gas coincides with the major axis of the underlying galaxy (Graham, J.A., 1979, *Ap. J.* **232,** 60; Marcelin, M. et al., 1982, *Nature,* **297,** 38) while the stars within the galaxy share a cylindrical rotation around the minor axis (Bertola et al., 1985, *Ap. J.,* **292,** L 51), i.e. perpendicular to the gas rotation axis.

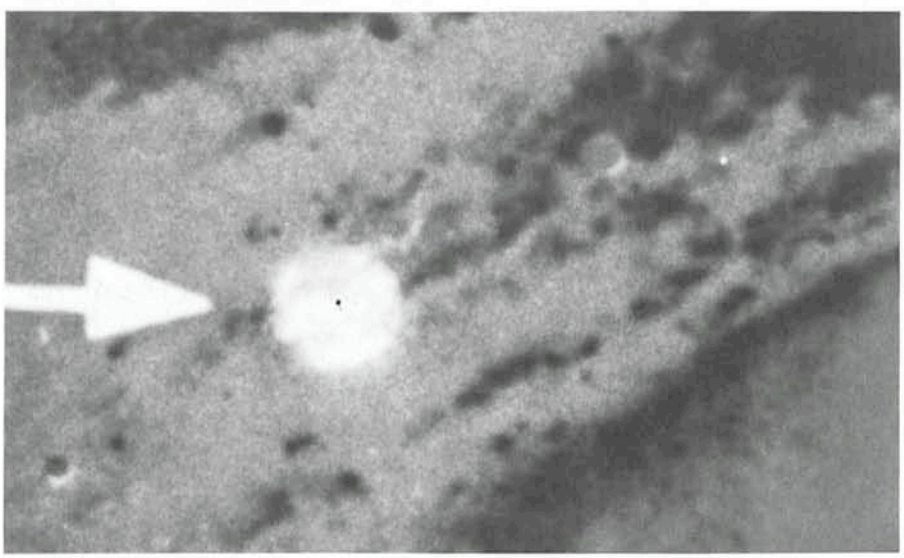

Figure 1: *A sandwich of two photographs of Cen A, one taken before the explosion of the supernova and one after. The small point at the centre of the white circle is the position of 1986G, as measured on a CCD frame, obtained with the Danish 1.54-m telescope. The diameter of the white circle is about 18 arcseconds.*

On the basis of these investigations, it appears that, in the region where the supernova is located, the mean gas motions relative to the sun are around 340–380 kms^{-1}, but that the stellar motions, extrapolated to the same point, would be around 500 kms^{-1} or more. Accordingly, the supernova in this peculiar galaxy (which is not oblate but triaxial) must belong to the old population of the underlying stellar system, if its velocity is higher than 450 kms^{-1}. However, the velocity of the central object of the supernova can only be measured at a later stage, when it is well past maximum. The interstellar absorption lines which were observed at ESO at high resolution then represent different layers (clouds) in the dust band. On the contrary, if the supernova belongs to the stars connected to the gas disk, its velocity must be lower, but in that case we shall be obliged to revise the age of the collision phenomenon (cf. the article by Tubbs). This hypothesis is also in contradiction with the Type I appearance of 1986G.

Clearly, it is of great importance to continue the observations of this interesting object.

Low Resolution Spectroscopy of the Supernova 1986G Near Maximum Brightness

S. DI SEREGO ALIGHIERI, ST-ECF, ESO*

Being at La Silla shortly after the supernova 1986G was discovered, I had the opportunity to take two spectra before it reached maximum brightness and quasi simultaneously with ultraviolet spectra taken with IUE. My first spectrum (Fig. 1) was taken on May 7 at 03 : 56 UT with the Boller & Chivens spectrograph and CCD # 5 at the 2.2-m telescope, with a resolution of 10 Å. It shows the features typical of type I supernovae – e.g. the broad one at 6120 Å. The sodium D doublet at 5890/96 Å, which was so nicely resolved in the CASPEC spectra, is visible here in blend.

* Affiliated to the Astrophysics Division, Space Science Department, European Space Agency.

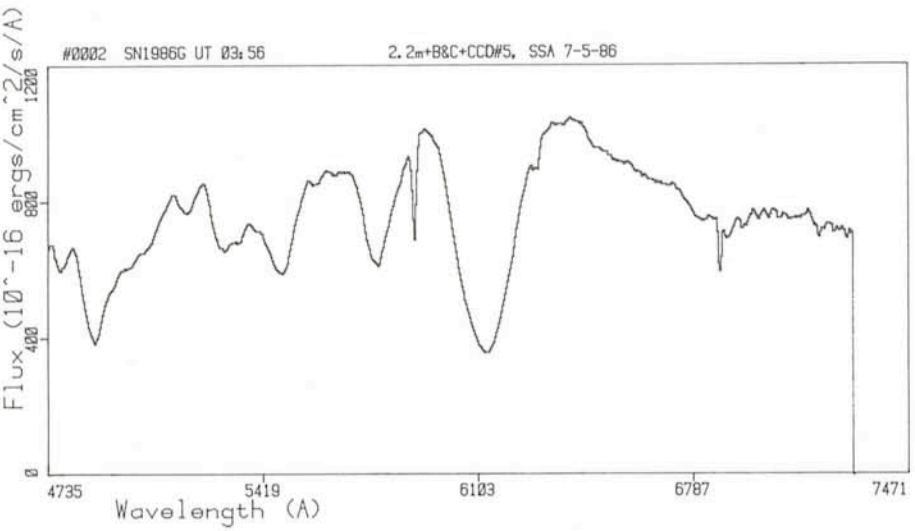

Figure 1: *The spectrum of the supernova 1986G taken on May 7 at 03 : 56 UT.*

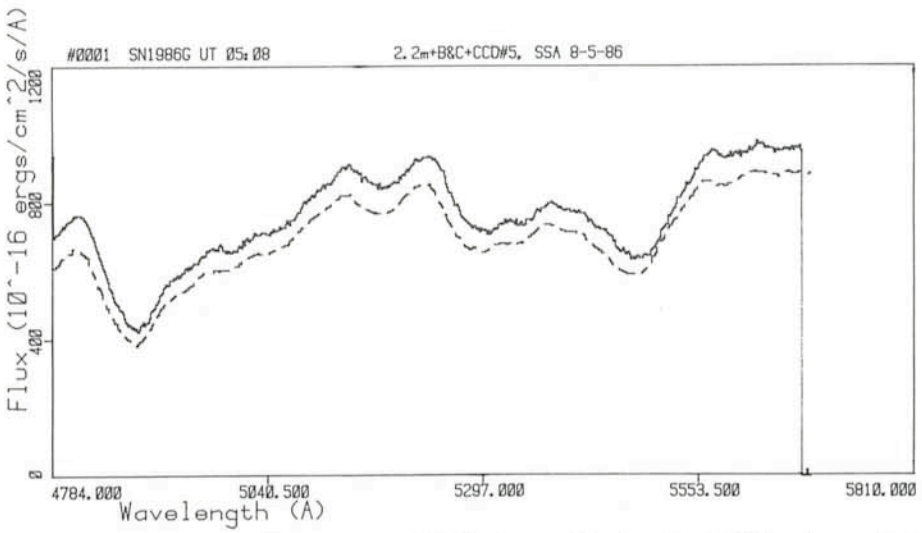

Figure 2: *The spectrum of the supernova 1986G taken on May 8 at 05 : 08 UT (continuous line) together with the one of the previous night (dashed line).*

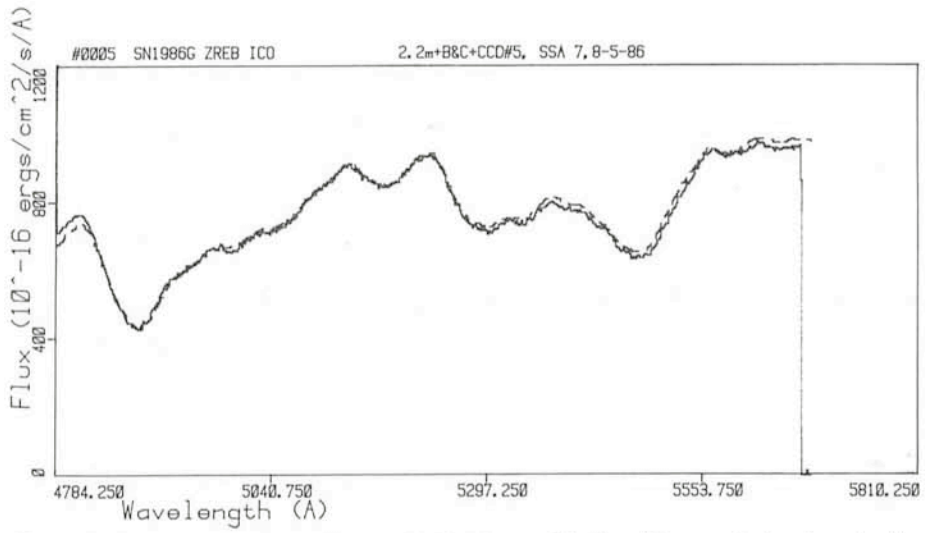

Figure 3: *The spectra of the supernova 1986G taken on May 7 and 8, corrected as described in the text.*

The second spectrum (Fig. 2) was taken on May 8 at 05 : 08 UT with the same instrumentation but a resolution of 3 Å. The comparison of the two spectra shows that the second is brighter – in agreement with the fact that the supernova was still rising – and is shifted slightly to the red. By applying to it an intensity correction of 0.11 magnitude and a velocity shift of 230 km/s, it overlaps very well to the spectrum of the previous night, as shown in Figure 3. The velocity shift can be interpreted as due to the fact that, as the emitting shell due to the explosion expands and gets thinner, we see deeper into it and therefore observe material moving towards us with smaller velocity. It would be interesting to follow this behaviour as the supernova reaches maximum brightness and beyond. I would therefore very much welcome collaboration with later observers to this end.

Tentative Time-table of Council Sessions and Committee Meetings in 1986

August 26	Finance Committee
October 3	Scientific Technical Committee, Venice
November 17–18	Finance Committee
November 18	Scientific Technical Committee
December 8–9	Observing Programmes Committee
December 11–12	Committee of Council

All meetings will take place at ESO in Garching unless stated otherwise.

Oxigen Abundances in Horizontal Branch Stars

R. NESCI, Istituto Astronomico, Università di Roma

The history of galactic nucleosynthesis may be followed by looking at the element abundances in stars of different age. It is generally believed that, besides hydrogen, helium und traces of a few light elements, all the other elements have been essentially produced in the stellar interiors and then injected into the interstellar medium by supernova explosions and stellar winds, giving eventually origin to more and more metal rich new stellar generations. As the amount of a given element produced by a star is a function of its mass, a study of the chemical enrichment of our galaxy makes it possible to test the predictions of stellar nucleosynthesis and to cast some light on the behaviour of the star formation rate and the mass function in the past.

The oxigen abundance in stars of different iron content has already been measured in some main-sequence stars, subdwarfs, field and globular cluster red giants, but few observations of horizontal branch stars have been done for this purpose up to now, namely three field HB stars by Kodaira and Tanaka (1972) and one star belonging to the globular cluster M4 by Peterson (1985). The main result of all these studies is that [O/Fe] increases slowly with decreasing [Fe/H] reaching eventually a plateau about [O/Fe]~+0.6 (see Pilachowsky, Sneden and Wallerstein 1983 for a review). There are, however, some globular clusters of intermediate metallicity which do not show an oxigen enhancement, a feature that can be considered as a signature of non-homogeneity in the process of chemical enrichment of our galaxy. Quite recently, however, this result has been questioned by Butler et al. (1986) who found, from a sample of 20 field RR Lyrae stars that [O/Fe] increases with increasing [Fe/H].

The aim of this work was to look at the oxigen abundance in globular cluster HB stars, in order to check the results from their red giants, using the capability of the CASPEC spectrograph at the ESO 3.6-m telescope to reach 14-magnitude stars with a good resolving power (~0.2 Å) and adequate signal to noise ratio. Two globular clusters were selected, one oxigen-rich (NGC 6397) and the other oxigen-poor (NGC 6752), essentially on the basis of their HB stars' apparent magnitude. A number of field HB stars were also included in the programme in order to see whether they showed a similar bimodal distribution. The spectral feature looked for was the infrared triplet at 7772–7775 Å, which is practically the only measurable oxigen feature in metal poor A-type stars, with an expected total equivalent width of about 500 mÅ. This triplet, however, is formed in strong non-LTE conditions, so that its interpretation in terms of abundance is not straightforward.

Since the beginning of the observing run (June 11–14, 1985) it was clear that, due to the bad seeing and atmospheric transparency, the cluster HB stars could be observed with a reasonable S/N ratio only by reducing the resolving power. The CCD was therefore binned in both directions (along and across the dispersion) and the slit set up at 500 microns (3.5 arcseconds) giving, at 7775 Å, a net peak continuum level of about 300 counts/pixel with a two-hour exposure. In such a time, the number of cosmic rays collected by the CCD was, however, very high (about 1,000), the majority of them involving two or three pixels. Removing the resulting spikes from the images poses no problems if they occur between the spectral orders, but is quite questionable if they are on an absorption line of the stellar spectrum. This is a warning for first-time observers to limit the exposure time to less than one hour,

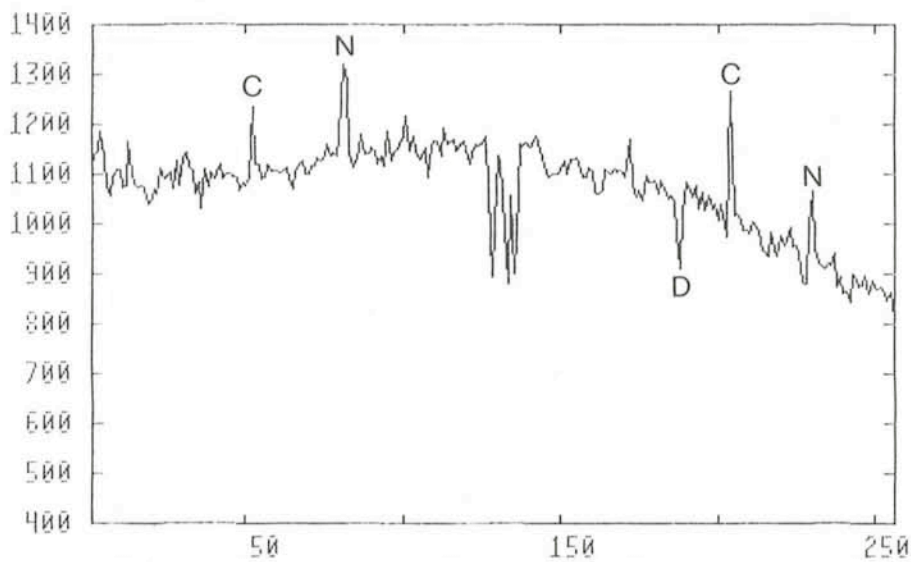

Figure 1: *Flat-fielded spectrum of HD 74721 showing the OI triplet: C are cosmic-rays spikes, N are night-sky lines, D is a CCD defect. Abscissa is in pixels, ordinate is in total net counts. A width of five pixels was used to extract the spectral order.*

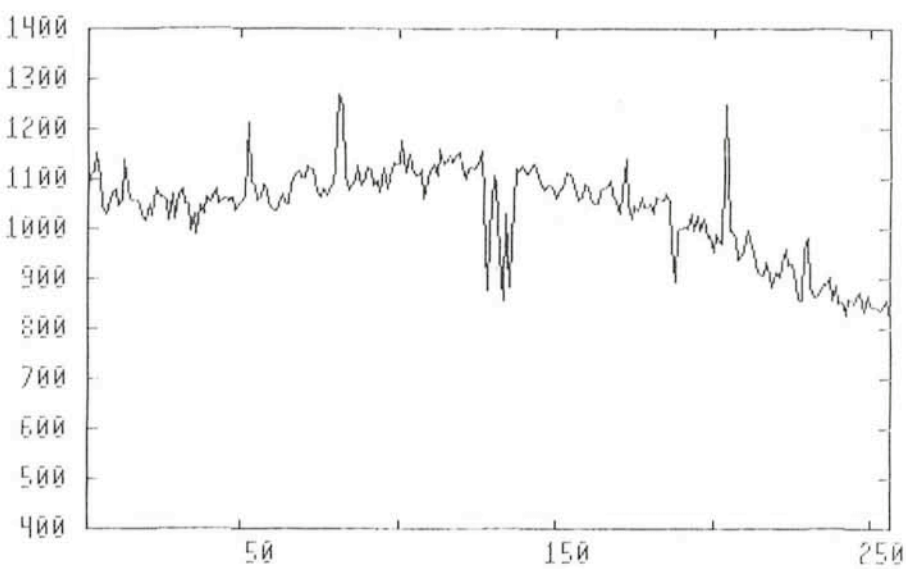

Figure 2: *Same as Figure 1 but with the flat-field correction applied after the spectral order extraction as explained in the text. A width of 11 pixels was used to extract the flat-field spectral order and of 5 pixels for the star.*

taking, if necessary, several spectra of the same star. In addition, one should not forget that cosmic rays are detected by the CCD also when the shutter is closed, so that it is not possible to interrupt an exposure for, say, one hour (due to the clouds, for instance) and then continue: the CCD will be filled by cosmic rays spikes!

For sake of homogeneity with the spectra of the cluster stars, the field HB stars, which were intended as comparison stars, were taken with the same instrumental configuration, so they are actually not the best that can be obtained with the CASPEC. Eventually, they came out to be the only useful observations of this unlucky run. Indeed, bad weather conditions and a number of technical troubles prevented us from securing blue spectra for any programme star and allowed only two stars of NGC 6397 to be observed in the infrared. Unfortunately, these last spectra showed an atmospheric emission line at 7774 Å which largely overfilled the stellar OI absorption triplet, located at the same wavelength due to the low radial velocity of the cluster. One would expect night-sky subtraction to be possible for CASPEC spectra, as the slit used was higher than the stellar image diameter. As a matter of fact, due to the CCD binning and the bad seeing, only one pixel at each side of the stellar spectrum was left to estimate the night sky luminosity, not enough to safely evaluate the emission line strength and recover the stellar absorption line.

Two main problems were found during the data reduction, which was performed at the Rome Astronomical Institute with home-made software. The first was that the stellar spectrum does not always fall completely on the same pixels as the flat-field spectrum. This is due to the fact that, during the observations, it is difficult to know if the star is on the slit centre as the slit is not actually visible on the guide monitor. One way to overcome this point would be to take the stellar spectrum through one of the small apertures of the spectrograph decker (beside the slit, obviously) reserving the full slit width to the flat-field spectrum. Unfortunately, this procedure was developed only towards the end of the observing run. A posteriori, two ways are left to retrieve the data: one is to use another flat-field exposure which better matches the stellar spectrum position; the other is to extract both the stellar and the flat-field spectrum of a given order from the raw data and then divide the stellar spectrum by the flat-field one. Although this procedure is in principle not correct, I found that it gave nearly the same result as the normal flat-fielding procedure: differences may be judged from a comparison of Figure 1 and Figure 2.

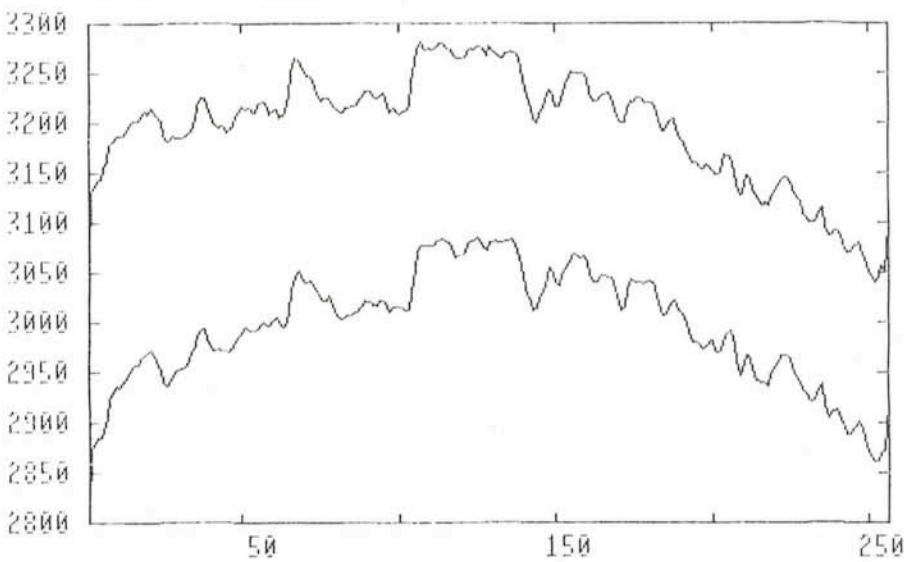

Figure 3: *Flat-field spectra of the order containing the OI triplet taken in different nights. Abscissa is in pixels, ordinate is in net counts/pixel. The spectra have been vertically shifted for a better comparison.*

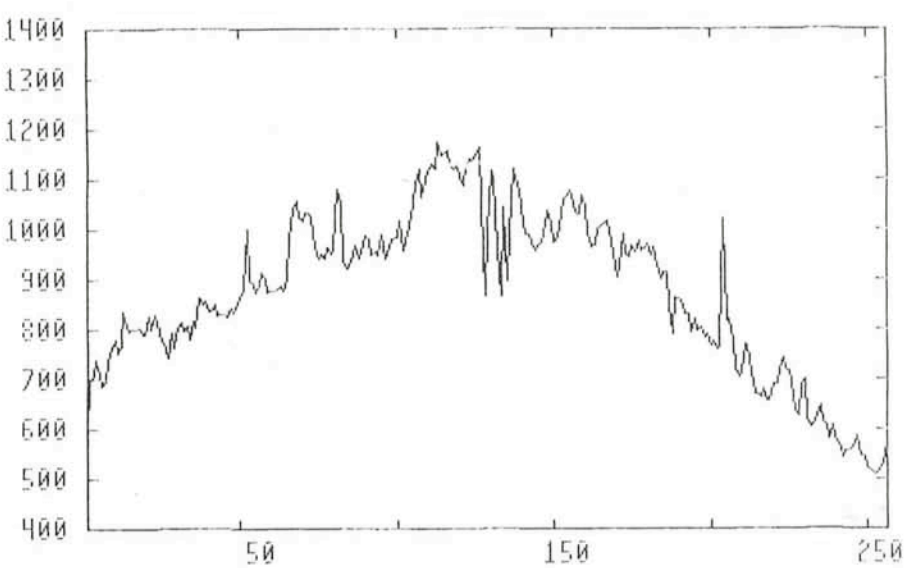

Figure 4: *Spectrum of HD 74721 without flat-field correction: the effect of the interference fringes is quite evident. Scales as in Figure 1. The spectrum of Figure 2 is obtained dividing this spectrum by the (normalized) flat-field spectrum of Figure 3.*

The second problem was a small non-linearity in the response of the CCD, which can hardly be corrected *a posteriori*. During the observing run, 3 consecutive flat-field spectra were taken with exposure times of 1, 2 and 3 seconds, to roughly test the CCD linearity. Then a given order was extracted from each exposure and the resulting spectra compared with each other: no differences were found in the interference patterns and the count levels were proportional to the exposure times within the limit of the clock accuracy. However, when flat-field exposures taken in different nights were compared, small variations in the fringes amplitude and in the overall shape of the flat-field spectrum were found (see Fig. 3). A further signature of a small non-linearity are the long-term wavy pattern of the flat-fielded stellar continuum and the incomplete correction, at a 4% level, of the interference fringes: the importance of this effect may be estimated by comparing the raw spectrum of Figure 4 with the corrected spectrum of Figure 1.

The wavelength range of the spectra obtained was from about 6870 to 7900 Å. Few absorption lines, besides the atmospheric HO and O bands, are present in metal-poor A-type stars in this spectral region. Besides the strong OI triplet, some CI, NI, FeII and MgII lines were expected but none of them was unambiguously detected. Preliminary equivalent widths, obtained simply summing up the depth of each pixel

TABLE 1

Star	W(A)	[O/H]	[Fe/H]			[Ca/H]
HD 2857	0.41	−0.4	−1.3	−1.9		
HD 74721	0.61	+0.1			−1.2	0.0
HD 86986	0.57	0.0		−1.1	−1.6	−2.0
HD 117880	0.58	0.0				−1.0
HD 130095	0.32	−0.7	−0.6			−0.6
HD 139961	0.53	−0.1				−1.6
HD 213468	0.43	−0.3				<−1.1

Values of [Fe/H] are (from left to right) from Kodaira and Davis Philip (1981), Danfort and Lea (1981), Klochkova and Panchuk (1985). [Ca/H] values are from Rodgers (1972).

normalized to the continuum level, are shown in the second column of Table 1 for all the programme field HB stars. Their accuracy should be of the order of 15%, the main source of error being the continuum position. A comparison with previous observations may be done only for HD 86986, whose OI triplet equivalent width was found 0.65+0.13 Å by Kodaira and Tanaka from an image-tube spectrum. Given the observational errors, the agreement may be considered good.

As it was told above, the formation of this OI absorption triplet happens in strong non-LTE conditions, which have been extensively studied by Baschek, Scholz and Sedlmayr (1977). From their computations it is clear that temperature and gravity differences have only a small effect on the total equivalent width of the triplet for HB A-type stars, while major effects are expected from microturbulence and metal content variations. Several determinations of Te and log(g) are available for the present stars (see Huenemoerder, de Boer and Code 1984 for the most recent results) all in fair agreement among them. On the contrary, microturbulence has been measured for only 4 stars, and there is no agreement between different authors. However, the spread of this parameter is not large when stars observed with the same instrument are compared, and the resulting maximum spread in the triplet equivalent widths should be less than 20%. If one assumes, as a first approximation, that microturbulence is nearly the same for all the programme stars, then the ranking in oxigen equivalent width may be considered as a ranking in abundance too.

From the paper of Baschek et al. one may roughly derive that $\Delta \log [O/H]^- 2.8\ \Delta \log (W_\lambda)$ for $[O/H]^- -1$ and a microturbulence of 5 km/s. This allows a preliminary conversion from equivalent widths to relative abundances to be made, which is shown in column 3 of Table 1, where HD 86986 is taken as reference star. The definition of the trend of [O/H] vs [Fe/H] is not possible by now, because a homogeneous set of [Fe/H] determinations is not available and the published values, also collected in Table 1, are clearly inadequate. A first result that can be remarked, however, is that the oxigen abundances found span a range of about a factor 6 within this star sample, with the most oxigen-poor star being relatively iron rich. It may also be noted that the [Ca/H] ranking found by Rodgers (1972) from the H and K line intensities in low dispersion spectra does not agree with the present (preliminary) [O/H] ranking. A homogeneous set of spectroscopic (blue) observations of these stars is clearly needed to derive their microturbulence and [Fe/H] values and then the trend of [O/Fe].

References

Baschek, B., Scholz, M., Sedlmayr, E., 1977, *Astron. Astrophys.* **55,** 375.

Butler, D., Laird, J.B., Eriksson, K., Manduca, A., 1986, *Astron. J.* **91,** 570.

Danfort, S.C., Lea, S.M., 1981, *Astron. J.* **86,** 1909.

Huenemoerder, D.P., de Boer, K.S., Code, A.D., 1984, *Astron. J.* **89,** 851.

Klochkova, V.G., Panchuk, V.E., 1985, *Sov. Astron.* **29,** 320.

Kodaira, K., Tanaka, K., 1972, *Publ. Astron. Soc. Japan* **24,** 355.

Kodaira, K., Davis Philip, A.G., 1981, IAU Coll. No. 68, 153.

Peterson, R.C., 1985, *Astrophys. J.* **289,** 320.

Pilachowsky, C.A., Sneden, C., Wallerstein, G., 1983, *Astrophys. J. Suppl.* **52,** 241.

Rodgers, A.W., 1972, *Mon. Not. R. Astron. Soc.* **146,** 71.

The Optical Counterpart of OH/IR 17.7−2.0

T. LE BERTRE, ESO

Type-II OH sources are characterized by maser emission at 1,612 MHz (18 cm), with a double-peaked velocity pattern. The emission is supposed to arise in an expanding circumstellar shell, the blue-shifted peak being produced in its front side, and the red-shifted peak in its back side. In such a model, the velocity separation is equal to twice the expansion velocity of the circumstellar envelope. Very often, these sources are associated with long-period variables of spectral type later than M5, such as Miras or supergiants whose spectral energy distributions peak at ~ 2 μm. Systematic radio surveys have led to the discovery of numerous type-II OH masers not associated to previously known stellar objects. Research of counterparts at infrared wavelengths have led to the discovery of objects extremely red to the point that they could not be identified optically. For that reason, these new objects have been designated "unidentified OH/IR sources". As they show similarities, in the OH and IR properties, with Miras or supergiants, they have been considered to be cool stars in the late stages of evolution on the Ascending Giant Branch (AGB), or core-helium burning supergiants (de Jong, 1983). These stars are in a phase of enhanced mass loss and, consequently, produce an envelope so dense that they are completely hidden to observers at short wavelengths; this phase is assumed to precede the planetary nebula stage. Usually, the energy distribution is dominated by reradiation from circumstellar dust grains and, except for a feature at 10 μm, it is similar to that of a blackbody at a temperature lower than $\sim$ 1,000 K. The 10 μm feature is generally attributed to silicate grains and characterizes oxygen-rich circumstellar matter. The prototype of this class of objects is OH/IR 26.5+0.6: its spectrum, comparable to the one of a blackbody at $\sim$ 400 K, peaks around 10 μm and it is not detected at $\lambda < 2$ μm. It is variable in the IR and OH emissions, with a very long period ($P \sim 1{,}630$ days). From the OH spectrum, the expansion velocity is $\sim$ 14 km s^{-1}. Using the Very Large Array (VLA), Herman et al. (1985) resolved the OH-shell structure and showed it to be

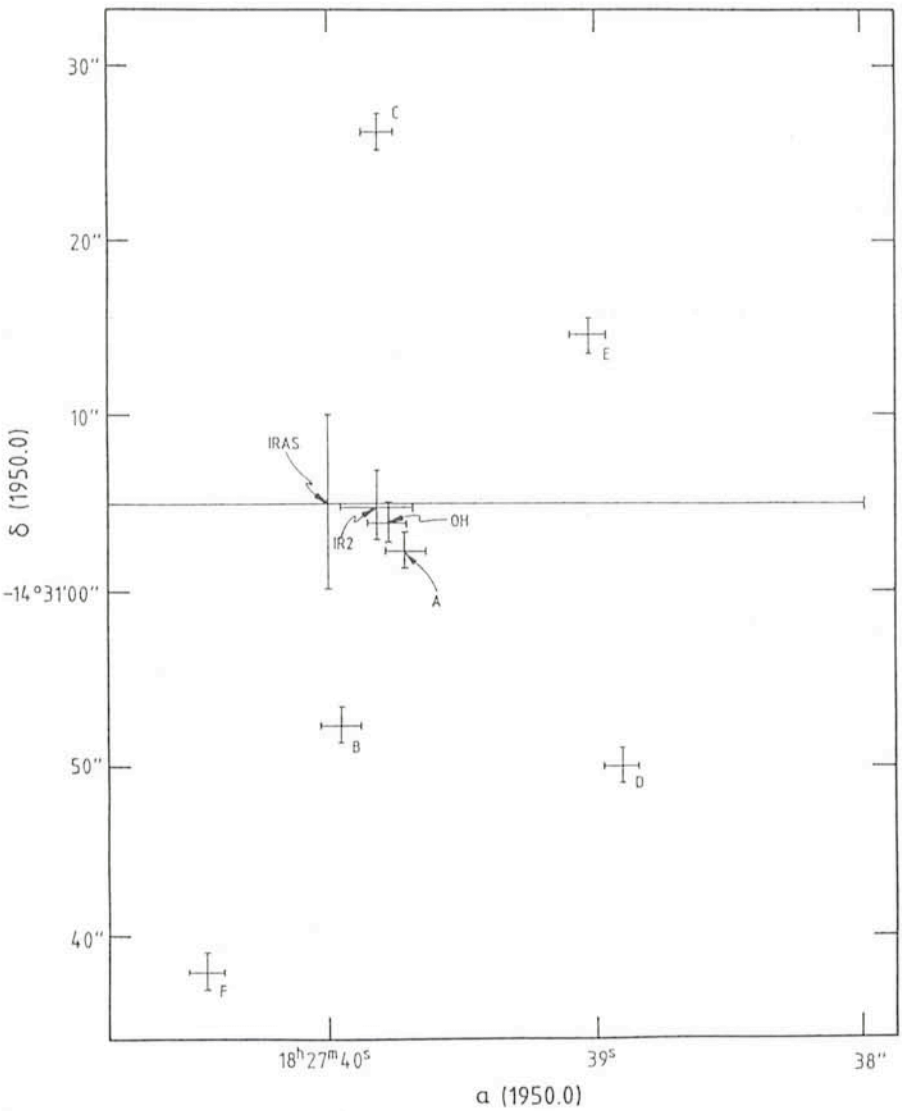

Figure 1: *Positions of OH/IR 17.7–2.0, measured in different wavelength ranges (IRAS [10–100 μm]; IR2 [2 μm]; OH [18 cm]; A [0.5 μm]). Positions of some field objects (B, C, D, E, F) are also indicated.*

spherical with a radius of 2.2″; measuring the phase delay between the blue and the red peaks of OH emission, they deduce a distance of 1 kpc. At this distance, the luminosity is $\sim 18 \times 10^3\ L_\odot$, and the mass-loss rate, $5 \times 10^{-5}\ M_\odot\ yr^{-1}$.

Another famous unidentified OH/IR source is OH/IR 17.7–2.0. It has a typical type-II OH spectrum, indicative of an average expansion velocity (Ve ~ 14 km s^{-1}). As its energy distribution is peaking at 30 μm, there should be no hope to find any optical counterpart. Nevertheless, in some aspects this object appears to be peculiar. Bowers et al. (1981), using also the VLA, showed that the structure is not spherical, but elongated (3.1 × 1.4″). Norris et al. (1984) discovered in the OH spectrum a high-velocity feature (600 km s^{-1}) which might indicate that a violent phenomenon is occurring in this source. Finally, Sèvre (1984) discovered what could be an optical counterpart of OH/IR 17.7–2.0.

As stated above, such an identification was absolutely unexpected and, consequently, deserved careful attention. As this source is in a region near the galactic plane, which is very crowded, there was a high probability of confusion. Also, it could be possible that a background star was exactly coincident with the real OH/IR source. Clearly, the first step was to select or obtain the best possible coordinates in different wavelength ranges.

Bowers et al. (1981), with the VLA, measured a radio position (labelled OH on Figure 1) which is accurate to ± 1″. In the visible, by using the Optronics machine of ESO-Garching, it is possible to measure positions on Schmidt plates with an accuracy of ± 1″; this has been done for the objects in the field of the OH position (labels: A, B, C, D, E, F). At this level of investigation, it appears that the Sèvres' object (A) is the only possible counterpart of the OH source, visible on the Sky Atlas plates. The near infrared position of the OH/IR source could be measured, using the 1-m telescope on La Silla. With this telescope, in the pointing mode, by referring to Perth 70 astrometric stars, it is possible to measure absolute positions to within ~ 7″. Using it in the offset mode, it is possible to obtain relative positions accurate to ~ 2″. By doing so, and using a nearby star whose coordinates were measured with the Optronics machine, the position of the IR source was obtained, at 2 μm, with an accuracy of ~ 3″ (label IR2). Once again, the only possible optical counterpart is object A. The IRAS satellite measured a position in the (10–100 μm) range which is labelled IRAS on Figure 1. Due to the field of view of the detectors and to the scanning mode of observation, the error box is wide and elongated; nevertheless, it is interesting to note that all the three posi-

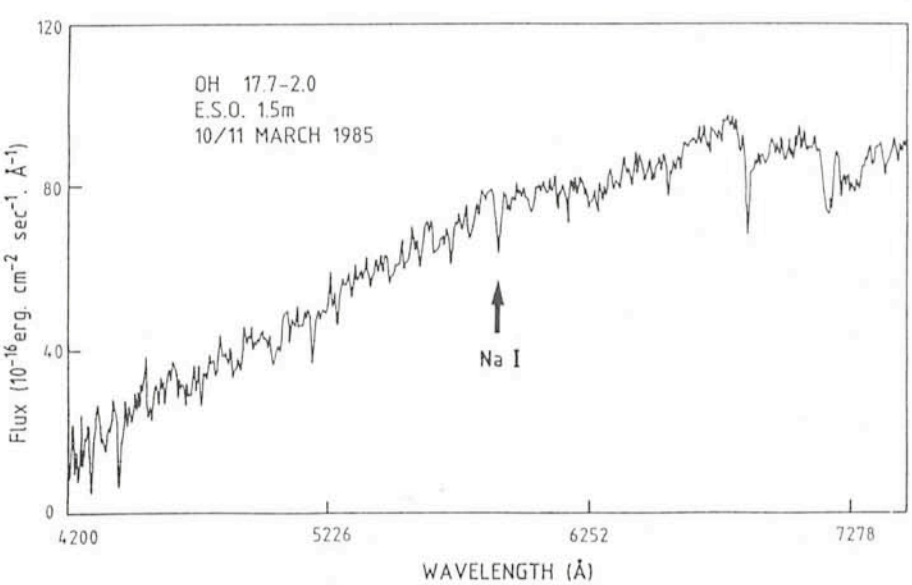

Figure 2: *(4200–7500 Å) IDS spectrum of the optical counterpart of OH/IR 17.7–2.0. The spectral resolution is ~ 15 Å; the calibration in fluxes is accurate to ~ 30 %.*

tions, obtained in very different wavelength ranges and with different instruments, are consistent with A.

This positional agreement does not imply a physical association between A and OH/IR 17.7–2.0. On March 10/11 1985, a spectrum of A was obtained with the Bollers & Chivens spectrograph attached to the 1.5-m telescope and equipped with an IDS detector. This spectrum is presented in Figure 2; the resolution (FWHM) is ~ 15 Å. Whereas one would have expected a spectrum dominated by molecular bands, such as those due to TiO and, eventually, VO, like in Mira or M supergiants, at first glance, it looks desperately flat. A few absorption features, like the NaI doublet at 5893 Å, are visible and point towards an early K-type object. Could it be that the object A is a star, merely coincident with the OH/IR source?

To elucidate this problem, the 1-m telescope was again used, but, this time, for obtaining the broad band energy distribution between .4 and 20 μm. This telescope may be equipped with two photometers, one for the visual range, and one for the infrared. In June 1985, (U, B, V, R, I) data were obtained with the visible photometer and a Quantacon photomultiplier; as the field is very crowded, the sky was measured at positions predetermined with the Optronics on Schmidt plates. The IR photometer equipped with an InSb detector was used to measure the source in the (J, H, K, L, M) bands; similarly, care was taken for avoiding pollution from the chopped beams. Fluxes at 10 and 20 μm were measured with a bolometer detector. All these data are plotted in Figure 3, together with those obtained by the IRAS satellite during 1983. The whole spectrum is characterized by a continuity in the variations of the fluxes, indicating that no misidentification has been made. From the (N1, N2, N3) measurements one suspects the presence of the 10 μm silicate feature in absorption. It is difficult to explain quantitatively this kind of spectrum by the addition of spectra produced by two different objects, such as the one of a typical OH/IR source peaking at 30 μm, and the one of a K star; from (U, B, V, R, I) data, a K background star could not be very much reddened, and, with such a modelling, a deficit of energy appears in the 1–5 μm range. In fact, this kind of spectrum seems to be typical of stars embedded in an axi-symmetrical dust shell; for instance, the bipolar nebula CRL 2688 has a very similar broad band energy distribution (Ney et al., 1975).

The observations with the 1-m telescope point towards a physical association between the IR source and object A. This interpretation could be strengthened by a confirmation of the central star spectral type independent of optical observations of A. Low resolution spectra can be recorded in the infrared by using the standard ESO photometers; Circular Variable Filters (CVF) are included in those and give a spectral resolution of ~ 60. M stars are characterized in the 1–5 μm region by the presence of molecular absorption features, mainly due to CO and H_2O. As the object is relatively faint, it was necessary to observe it with the 3.6-m telescope. The recorded spectrum is presented in Figure 4. Once again, the surprising character is the absence of absorption features, in particular, the usually strong absorption band due to CO at 2.3 μm is obviously not present. This absence indicates that the underlying star is of spectral type earlier than K5 and, consequently, is a confirmation of the physical association between OH/IR 17.7–2.0 and A.

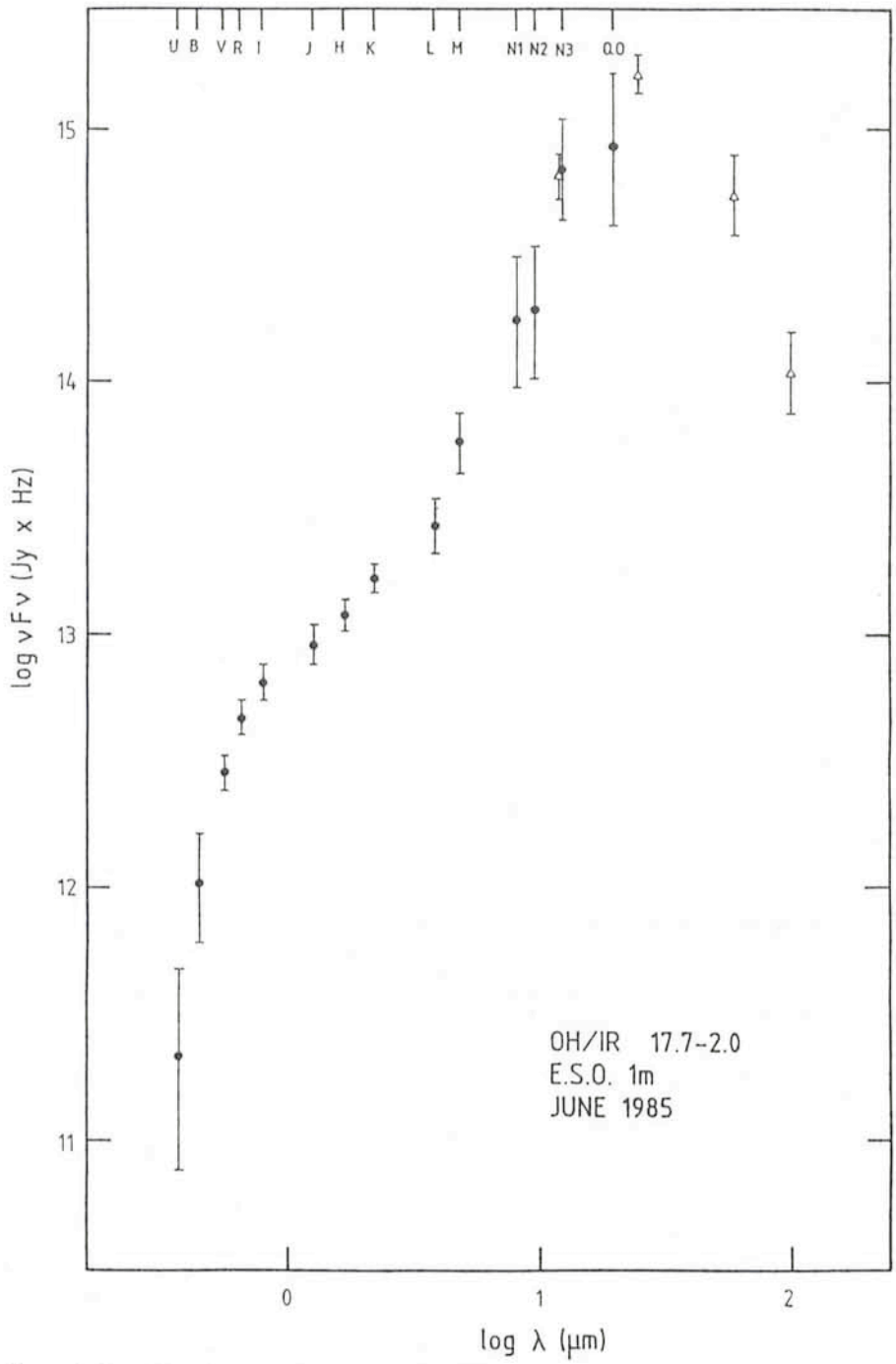

Figure 3: *Broad band energy distribution of OH/IR 17.7–2.0. The filled circles (●) correspond to data obtained with the 1-m telescope; the triangles (△), to IRAS data.*

OH/IR 17.7–2.0 appears now to be not so "unidentified" as previously thought. The CVF and IDS spectra indicate that it is in a more evolved stage than the one of AGB or M supergiant stars. Objects like OH/IR 17.7–2.0, while they are still type-II OH emitters, could be already evolving towards the

planetary stage, through an axi-symmetrical structure reminiscent of bipolar nebulae. Further observations exploiting this still unique opportunity of studying the central star of a type-II OH/IR source are in progress; and, of course, other optical counterparts are actively searched for.

References

Bowers, P.F., Johnston, K.J., and Spencer, J.H.: 1981, *Nature* **291,** 382.

Herman, J., Baud, B., Habing, H.J., and Winnberg, A.: 1985, *Astron. Astrophys.* **143,** 122.

de Jong, T.: 1983, *Astrophys. J.* **274,** 252.

Ney, E.P., Merrill, K.M., Becklin, E.E., Neugebauer, G., and Wynn-Williams, C.G.: 1975, *Astrophys. J. Letters* **198,** L129.

Norris, R.P., Booth, R.S., Diamond, P.J., Graham, D.A., and Nyman, L.-A.: 1984, IAU Symposium 110, 323.

Sèvre, F.: 1984, Personal communication.

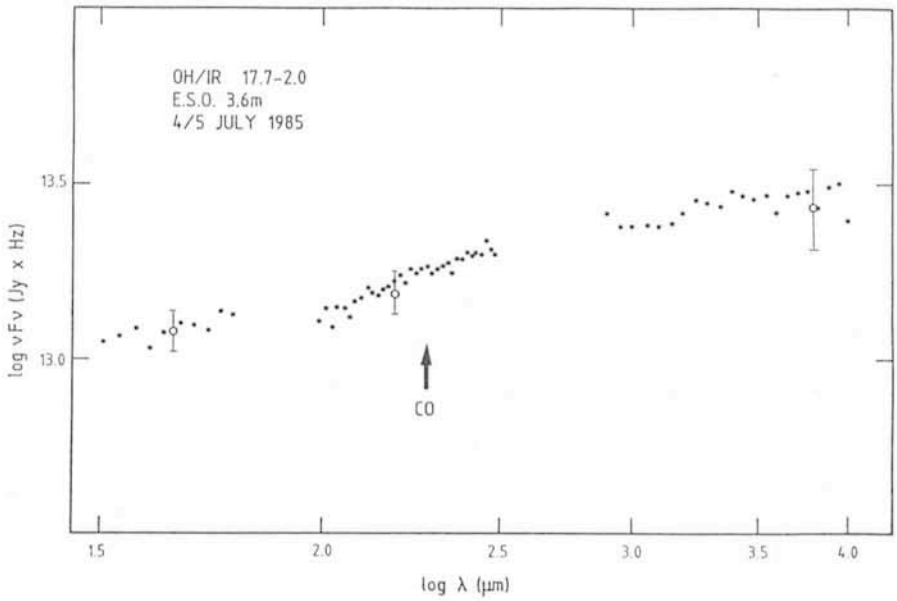

Figure 4: *(1.5–4 μm) CVF spectrum of OH/IR 17.7–2.0. The empty circles (o) correspond to the broad band (H, K, L) data obtained at the 1-m telescope (same as in Figure 3). The arrow indicates the position of the 2.3 μm absorption band produced by CO, and, normally, found in M stars.*

Infrared Observations of Comet Halley Near Perihelion

T. LE BERTRE, P. BOUCHET and A. CHALABAEV, ESO
A.C. DANKS, Michigan State University
T. ENCRENAZ and N. EPCHTEIN, Observatoire de Paris-Meudon

Ground-based observations of periodic Comet Halley near its perihelion passage were important due to the increased activity of its nucleus as it approached the sun and, in this specific case, due to the planned spacecraft flybys several weeks later. As with all comets, it naturally reached its maximum brightness at perihelion, but, of course, it was then so close to the sun that it was difficult to see or measure. It is the cometary astronomers misfortune that the best moments to catch a comet at its brightest are just before sunrise, or just after sunset. Few ESO telescopes can be used to observe the comet so close to the sun. Among them, the GPO which can almost be pointed to the horizon, and the 1-m telescope which, when equipped for IR observations, can be used for daytime observing. Our principal interest was to monitor the comet progress and evolution in the IR using both the ESO 3.6-m and 1-m telescopes. As a single group, we had sufficient time spaced around perihelion to monitor the comet fairly well. In addition, we were able to fill some of the remaining holes with the kind cooperation of 1-m observers B. Reipurth, H. Cuypers and G. Hahn, who allowed us to observe 1 or 2 hours each day during their observing runs.

During this time, between December 24, 1985, and March 3, 1986, the 1-m telescope was used for approximately three periods of two weeks each. The orbit of the comet brought it from the northern hemisphere to the southern hemisphere, steadily brightening, and, from February 17 to March 3, the comet was undoubtedly well located ($\delta \sim -14°$) for observations from La Silla. The comet was west of the sun in this period and, consequently, observable in the morning; due to the configuration of the Andes the sunrise was delayed by approximately 15 minutes. These 15 minutes or so were crucial in the period from February 17 to 18 when the comet was at less than 20° from the sun. The 1-m telescope was equipped with an InSb detector for the 1 to 5 μm range or a bolometer for the 8 to 20 μm range. Both instruments employ a focal plane chopper, and chopping was carried out in the east-west direction with a 30 arcseconds amplitude. This naturally means, due to the large angular size of the comet, that with one beam centred on the nucleus, the other beam was somewhere in the coma.

In Figure 1, the broad band flux distribution is shown plotted against wavelength. Although the dust grains expelled from the nucleus constitute, in mass, only a minor fraction of the material, they are the dominant element responsible for the observed broad-band IR spectrum. The flux distribution can be seen to consist of two different regimes: from 1 to ~ 3 μm, the spectrum is dominated by dust-scattered sunlight, whereas at wavelengths longer than 3 μm, thermal emission from the dust is dominating, and described well by a 400°K blackbody (no wavelength dependence of emissivity has been taken into account). The spectrum is qualitatively similar to that found in comets Bennett, Kohoutek and Bradfield (see e.g., Ney, E.P.: 1974, *Icarus* **23,** 551).

In Figure 2, the evolution of individual bands and colours is shown with time, over the period between February 17 and March 3, 1986. One measurement a day was made at approximately 10 hours UT, and the observations were, therefore, carried out during day time, centring the comet by maximizing the detector signal. This procedure worked well as there was found to be no wavelength dependence with this

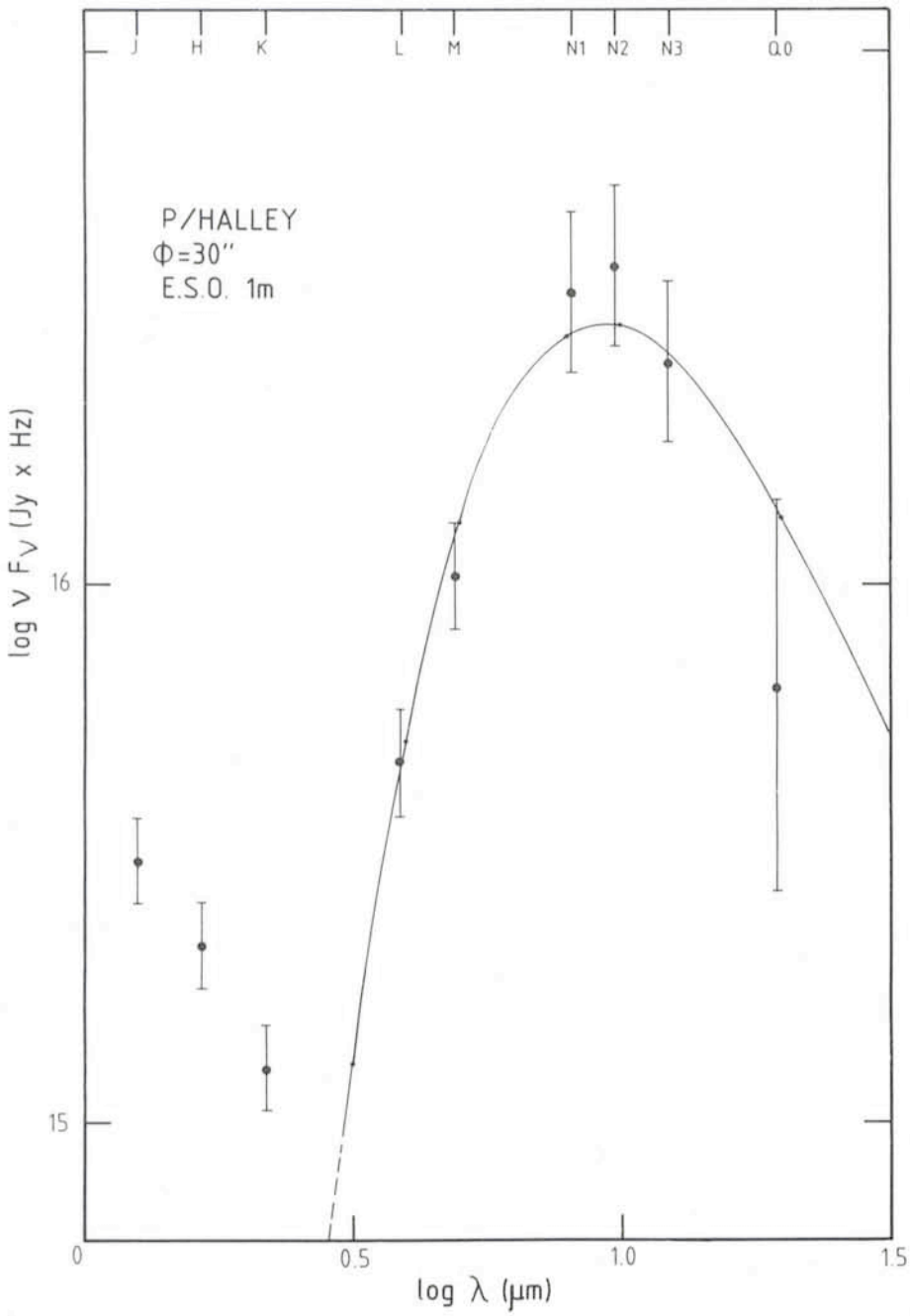

Figure 1: *Broad band spectral energy distribution of the central part of comet P/Halley (∅ = 30") obtained in January 1986 with the 1-m telescope. The labels in the upper part of the frame indicate the positions of the broad band filters that have been used.*

technique; also we had checked, before, that the IR centre corresponded to visual centring to within 2 to 3 arcseconds. Throughout, we used the IHW ephemeris to locate the comet, and we also took the cometary motions from there to set the telescope tracking rate; both proved extremely accurate. Figure 2 shows that strong fluctuations in individual bands were seen from day to day superimposed on a monotonic variation. In some cases, fluctuations of up to 1.5 magnitudes are seen within 24 hours (i.e. a factor of 4 in flux). These fluctuations were present in all filters and appear to be well correlated (to help visualize this correlation, linear regression lines are also shown). This means that these fluctuations are almost identical in the emitted and in the scattered fluxes, and, consequently, that they are mainly due to variations in the mass-loss rate ("outbursts"). Of course, it is well known that comets exhibit both a gas tail and a dust tail, and it is therefore not surprising that we have noted a correlation between these outbursts and the apparition of tail features. The origin of these rapid variations in the mass-loss rate may be multiple. It could be in part due to the elongated shape of the nucleus; depending on the orientation of the nucleus with respect to the sun, the surface area exposed to the sun's radiation, and hence solar heating, would be different, consequently varying the amount of heat absorbed, and therefore the amount of matter released. Such a geometrical effect could alone account for a factor 4 in the variation of mass loss, only if the nucleus is highly prolate (4:1). In fact, recent pictures obtained by Giotto suggest that the nucleus is of the order of 12 by 5 kms (i.e. ~ 2:1). Another source of the outbursts could be inhomogeneities in the composition of the nucleus. Present models suggest that the cometary nuclei are made of snows or ices, with a clathrate or porous like structure in which the dust particles are held. Solar heating results in sublimation of these snows with the consequent release of gases and dust. Furthermore, varying composition or crystallization of the ices would result in varying specific heats and hence varying production rates. In both cases, the rotation of the nucleus should be reflected in the light-curve by some sort of periodicity. If this periodicity were due solely to geometrical effects, the observed period would be twice as high as that produced from a rotating active region. More likely, both effects are present, with several active regions, to produce a more complex variation.

The monotonic variations are most probably due to changes in the distances between the comet, sun and earth. Part of them are almost certainly observational effects. As the chopping throw used was fixed at 30 arcseconds, it follows then that, as the earth-comet distance changes, we effectively compare the nuclear region to physically different parts of the coma. The coma itself, being fed by mass loss from the nucleus will also be varying in brightness.

Variations of colour with time are also seen; although the effect is small in comparison with the individual magnitude, it is real and was especially apparent around March 1. The rapid colour fluctuations could be indicative of an evolution in the scattering and emitting properties of the dust as ist moves outwards from the nucleus. The monotonic variations in K-J most probably are due to changes in the scattering angle, whereas the L-M index would more probably reflect the decrease in dust temperature as the comet recedes from the sun. Finally, time variations study of the observed fluxes from different diaphragms is also possible due to the high quality of the detector beam profiles,

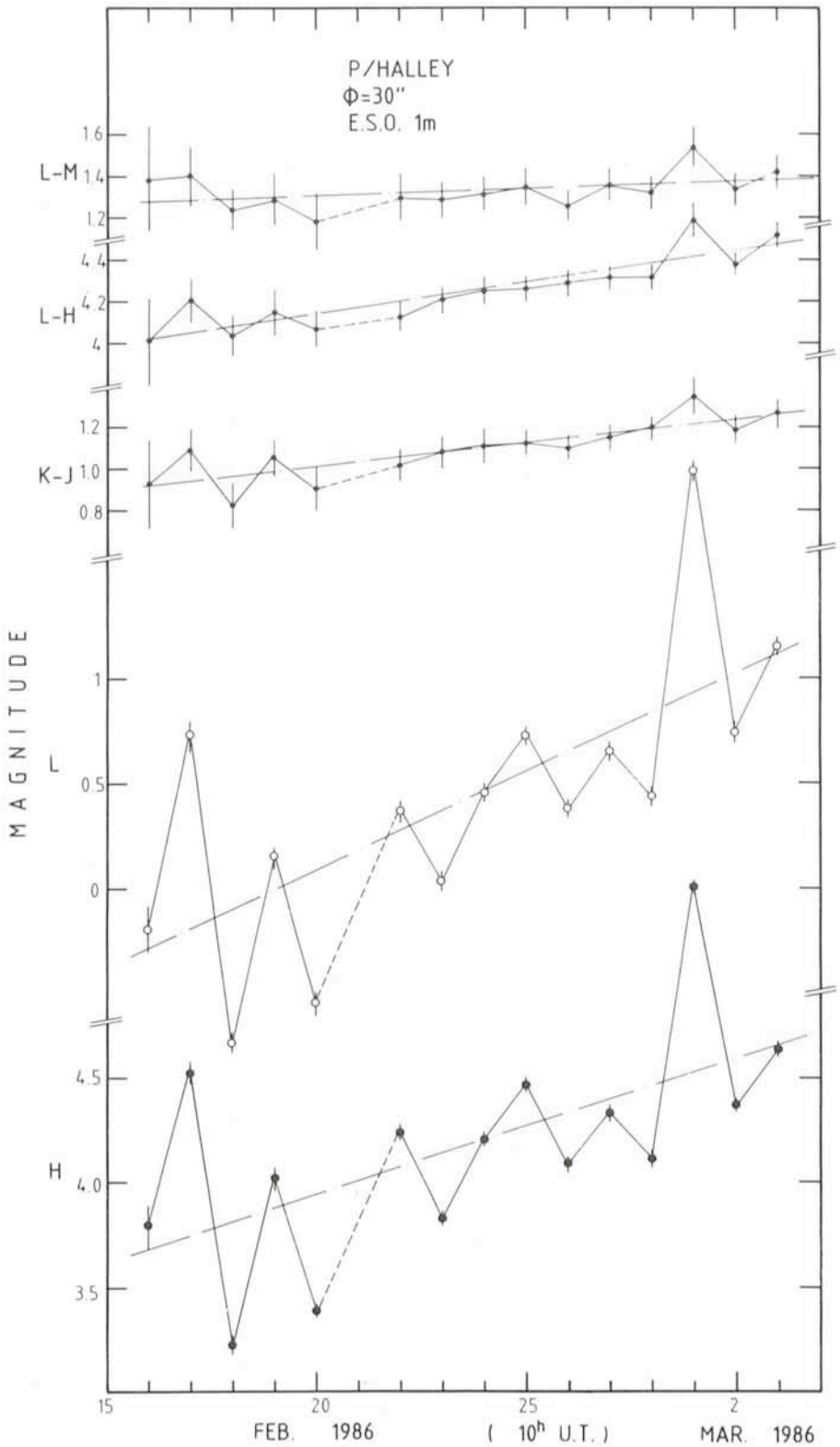

Figure 2: *Infrared light-curves of comet Halley between February 17 and March 3 are shown. Observations were made with a diaphragm of 30". Filled circles (●): H-curve (scattered flux); empty circles (○): L-curve (emitted flux); small dots (•): colours (K-J, L-M and L-H) -curves. There was no observation on February 21.*

and initial results indicate the outward dust propagation from the nucleus.

An impressive amount of IR data has already been collected at ESO and is being analysed. The first data on Halley were obtained with the 1-m telescope in September 1985, and we plan to pursue, with it, our monitoring further on, at least till July 1986.

We are thankful to R. Vega who always, even after a long observing night, helped us with enthusiasm and skillfulness.

ESO Exhibition at the Amateur Astronomy Fair at Laupheim

Soon after the ESO exhibition at the Reuschel Bank in Munich closed on 30 April, it was transported to the city of Laupheim, about 150 km west of Munich. Here it was one of the highlights during the 3-day Amateur Astronomy Fair on May 17–19, 1986. The fair which was organized by Volkssternwarte Laupheim for the fifth time attracted more than 5,000 amateur astronomers from all over Germany and was a great success.

The photo on page 24 of this issue shows a model of the ESO New Technology Telescope (scale 1 : 20) which joined models of La Silla, the ESO 3.6-m and the future ESO VLT 16-m telescope in Laupheim. The ESO exhibition which also includes large colour pictures of the most beautiful objects in the southern sky, is available for similar occasions. Societies, institutions, etc. who are interested in borrowing (part of) the exhibition should contact the ESO Information and Photographic Service.

ESO Press Releases

The following material has been published since the last issue of the *Messenger*. It has been sent to about 350 addresses in the ESO member countries and beyond. The distribution is limited for practical reasons, but members of the press are welcome to apply for inclusion to the ESO Information and Photographic Service (address on last page).

PR s/n: The ESO 16-m Optical Telescope (VLT) – a Colour Brochure (20 March).

PR 07/86: Big Radio Galaxy Is Nearer Than Previously Thought (13 May; with photo of NGG 5128 = Cen A).

Note also that an ESO Halley Slide Set has now become available, see the announcement on page 17 in this issue of the *Messenger*.

ESO Book to Appear in 1987

It has been decided that the ESO Book "An Outlook to the Southern Sky", cf. the *Messenger* 43, p. 25 (March 1986), shall now be published in 1987, on the occasion of ESO's 25-year anniversary. A publishing contract with a major European publishing house is in the final stages of negociation.

Spatial Distribution of Constituents in the Coma of Comet Halley, an Observing Programme at the ESO 1-m Telescope

K. JOCKERS, Max-Planck-Institut für Aeronomie, Katlenburg-Lindau, FRG
E.H. GEYER and A. HÄNEL, Observatorium Hoher List, Daun, FRG

1. Scientific Objective

When a comet visits the inner solar system the sun's radiation sublimates part of the nucleus' matter. The liberated gases drag some dust particles with them and form the coma of the comet. It has an approximately spherical shape and an extent of several hundred thousand kilometres. The sublimated gas particles are dissociated and ionized by solar UV radiation, charge exchange and, in the inner coma, by collisions. In the inner coma chemical reactions between the different coma species will form new types of radicals and ions. Ultimately, all gas molecules and their daughter products will be ionized and swept away by the solar wind into the cometary ion tail. The dust particles are removed from the coma by solar radiation pressure and form the dust tail.

The observing programme to be described in the following was devoted to a study of the different constituents in the cometary coma. Such a study should give information on the chemical composition of the cometary nucleus. The neutral radicals, which are observable from the ground like CN, C_2, C_3, CH, NH and NH_2, are chemically processed and therefore relate only indirectly to the so-called mother substances of the nucleus. Many ions, however, e.g. CO^+, CO_2^+ and H_2O^+, are ions of presumable nucleus constituents. Consequently, the interest concentrated on the cometary ions. Their behaviour, however, is influenced by their interaction with the solar wind, which leads to the formation of ion rays and streamers. Therefore, a study of cometary ions must include their kinematical behaviour. As Comet Halley was investigated by an armada of space probes, we have the unique opportunity to compare the ground-based observations with *in situ* measurements.

2. The Instrument

For the observations the focal reducer of the Observatory Hoher List was used at the ESO 1-m telescope. For the comet observations the Max-Planck-Institute for Aeronomy supplemented this instrument with two dioptric cameras (Carl Zeiss, Oberkochen) for the near UV (365–500 nm) and visual (425–660 nm) spectral ranges. A two-stage proximity-focused image intensifier (Proxitronic, Bensheim) with bialkali cathode was attached to the UV camera and the image was recorded on plates (mostly hypersensitized IIIa-F) pressed against the exit window of the intensifier. The optical arrangement is shown in Figure 1. The telescope beam behind the Cassegrain focus (a) is recollimated via a field lens (b) and a collimator triplet (c), and a new image, reduced in size by a factor of 5, is formed by the lens (g) on the photocathode of the image intensifier (h). At the 1-m telescope a field of 25 arcminutes is obtained which corresponds at Comet Halley to about 10^6 km (depending on its geocentric distance).

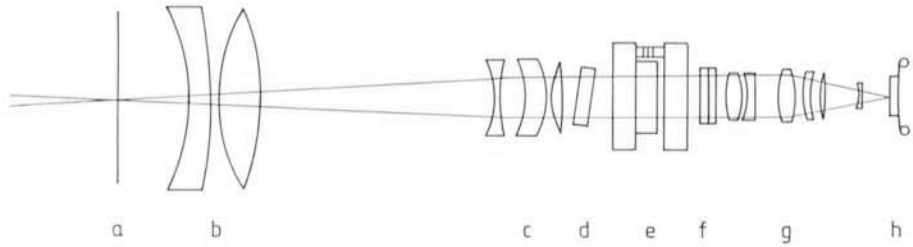

Figure 1: *Optical arrangement of the focal reducer in the imaging mode. a: Cassegrain focus; b: field lens; c: collimator lens; d: coloured glas prefilter; e: tunable Fabry-Perot filter; f: interference filter; g: camera lens f/2.8; h: two-stage image intensifier.*

The instrument was used in three modes. In the imaging mode (Figure 1) pictures of the comet were obtained through interference filters combined with a tunable narrow-gap Fabry-Perot filter (Queensgate Instruments, Sunbury near London, B. Halle, Berlin). The Fabry-Perot works in the wavelength interval of 350–430 nm. It has a bandpass (FWHM) of about 6 Å and a free spectral range of about 100 Å. In the field spectroscopy mode (Geyer et al., 1979) a slit mask with a pattern of 70 0.2 mm wide slits was inserted into the Cassegrain focal plane. Instead of the Fabry-Perot filter a direct vision grating prism was put into the parallel beam to produce 70 simultaneous spectra at different places in the cometary coma. The resulting saving of observing time was essential for the success of the programme, in particular when the comet was still close to the sun. Two gratings with 300 and 600 lines/mm were used and gave an inverse dispersion of 207 and 103 Å/mm, respectively. One plate was obtained with a double grating prism. The resulting pairs of inverted spectra should allow the determination of radial velocities (Geyer and Nelles, 1985). The field spectroscopy mode is in some sense similar to the octopus spectrograph introduced recently at the ESO 3.6-m telescope (Lund and Surdej, 1986). In a third mode, another Fabry-Perot etalon with a fixed plate separation of 0.5 mm was added to the optical arrangement of Figure 1 in an attempt to derive Doppler velocities of the cometary ions. A few very weakly exposed interferograms were obtained in the light of the CO^+ and CH^+ ions. It seems questionable if they will allow derivation of ion speeds. Most plates exposed in the direct imaging and field spectroscopy modes were photometrically calibrated with the ESO spot sensitometer, with exposures of the bipolar nebula NGC 6302 and with a set of mercury standard lamps. Besides the focal reducer, three

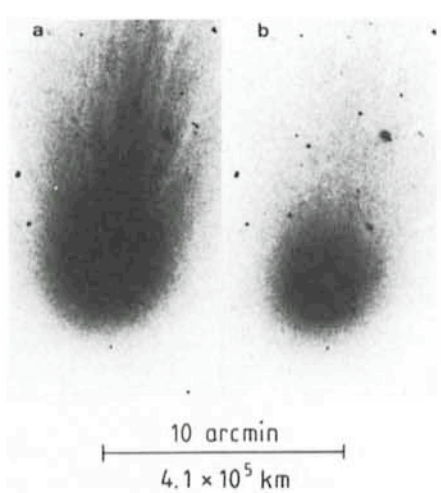

Figure 2: *Images of Comet Halley obtained March 15. a: CO^+ at 367.4 nm; b: "continuum" at 365.0 nm. Exposure times: 10 minutes.*

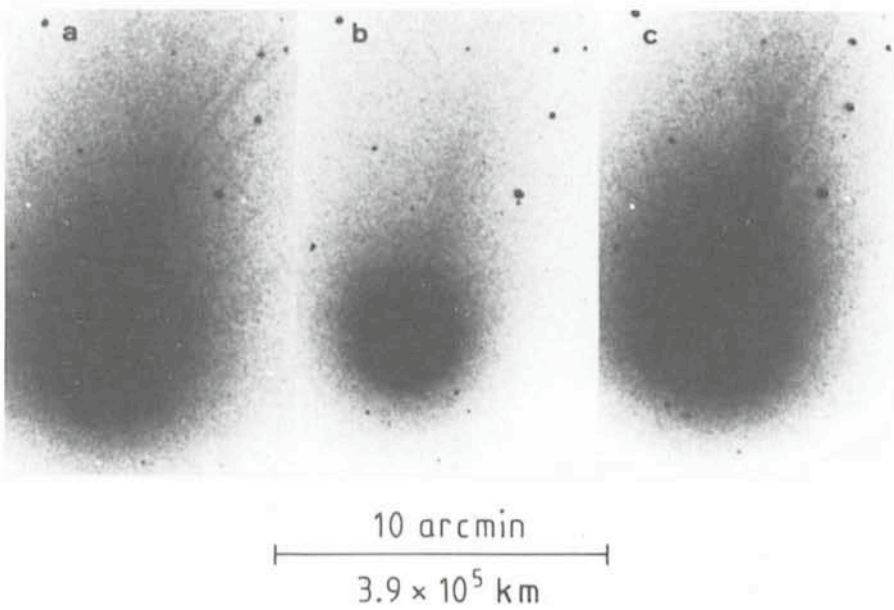

Figure 3: *Images of Comet Halley obtained March 16. a: CO^+ at 401.9 nm; b: "continuum" at 407.4 nm; c: N_2^+ at 391.2 nm. Exposure times: a and b: 1 minute; c: 4 minutes.*

cameras, attached to the top ring of the telescope, were used to obtain wide-field images and slitless wide-field spectra in the visible and UV spectral ranges.

3. The Observations

The observations were performed in the two periods March 10–16 and April 4–11, 1986. As there has not been enough time yet for a detailed quantitative analysis of the data, only some raw data are presented. Figure 2 shows a pair of images taken on March 15 at 367.4 nm (CO_2^+) and 365.0 nm ("continuum"). Both images were taken through the same interference prefilter but correspond to different settings of the Fabry-Perot filter. Comparison of the two images indicates a strong signal at the wavelength of CO_2^+. The weak ion features present in the "continuum" picture may be caused by weak plasma emissions in the "continuum" window or, more likely, by spectral impurity of the Fabry-Perot filter. Note the regular pattern of ion streamers surrounded by a plasma envelope which is missing in the continuum picture. In Figure 3 we see three images, obtained at 401.9, 407.4 and 391.2 nm respectively, corresponding to the 3-0 $A^2\,\pi_{3/2} - X^2\Sigma^+$ transition of CO^+, "continuum" and the O-O $B^2\Sigma_u^+ - X^2\Sigma_g^+$ transition of N_2^+. The N_2^+ emission is present but weaker than CO^+ and N_2^+. There is a neutral gas coma visible in the CO^+ and N_2^+ pictures which is due to C_3 and CH, respectively. In the second observation period the comet was observable almost all night. The development of the inner tail of the comet during 6 hours is illustrated in Figure 4. Dramatic changes are seen in the light of the CO^+ and CO_2^+ ions. The images in the light of the two molecular ions look similar but there seem to be systematic differences. They need not to correspond to differences in column density ratio but may be caused by Greenstein effect (change in fluorescence efficiency caused by Doppler shift of the solar spectrum as seen by the moving cometary ions). An example of a multi slit spectrum is presented in Figure 5. It covers the region between 350 and 430 nm. To show the location of the comet relative to the slits, with most spectra a calibration exposure was obtained by removing the grating and taking a double exposure. Direct images of the slits were exposed, then the slit mask was removed and an image of the comet was taken through an interference filter of 10 nm passband centred at 369 nm. The spectra show all major ions except H_2O^+ which has no emissions between 350 and 430 nm. Note the varying line ratios in the different spectra. The ion emissions are also seen in spectra which do not correspond to a visible ion streamer. CO^+ ions are even seen upstream of the comet, confirming the notion of an extended CO^+ ion source region.

Figure 6 shows an example of a wide-field slitless tail spectrum taken with the Zeiss UV Sonnar with 104 mm focal length. The spectrum was taken through a UG 5 filter and covers the wavelength range from 309 to 395 nm. A direct, unfiltered, blue image of the comet is presented at the same scale for comparison. The wide-field images were taken simultaneously with the two latest

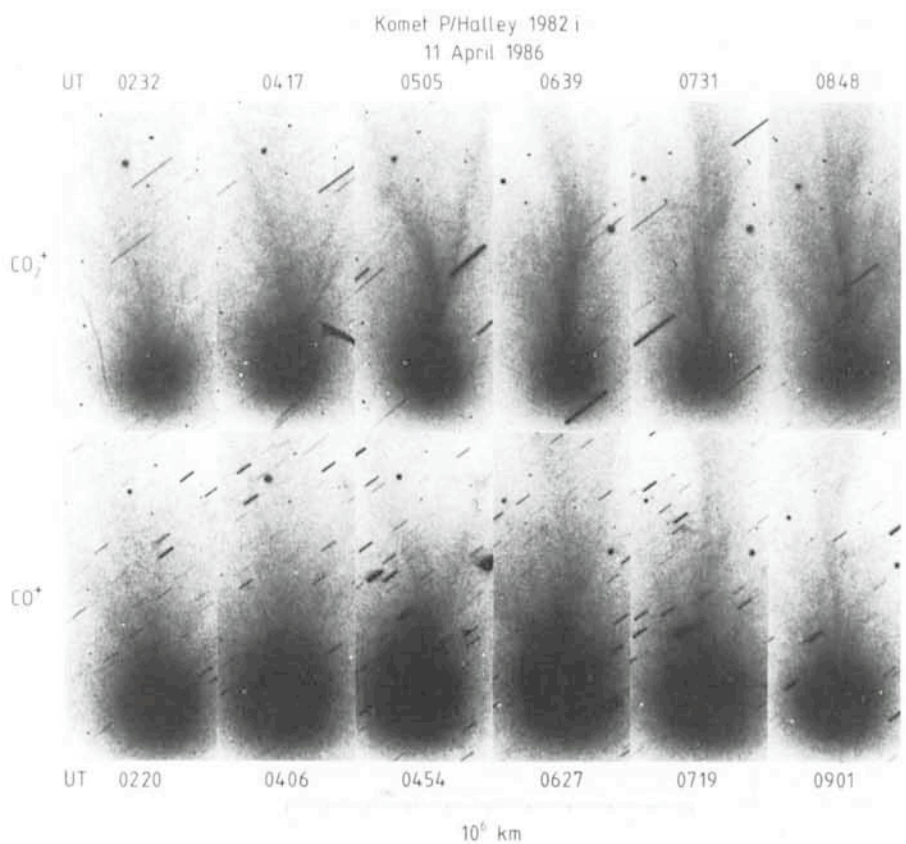

Figure 4: *Motions in the inner plasma tail of comet Halley recorded in the light of the CO_2^+ and CO^+ ions (April 11). Exposure times: CO_2^+: 13 minutes; CO^+: 4 minutes.*

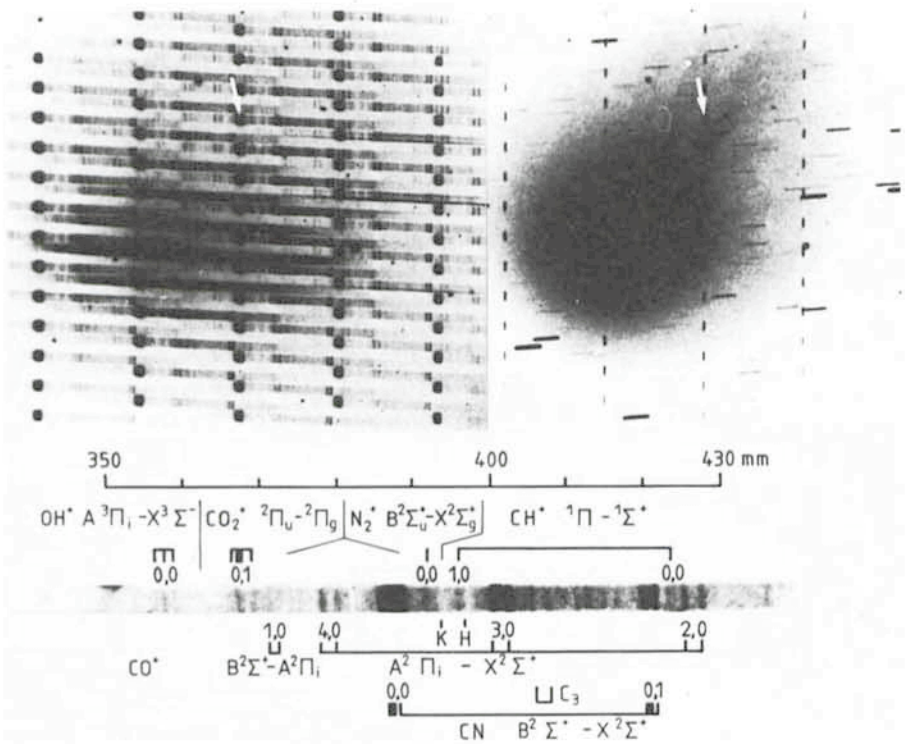

Figure 5: *Multi-slit spectrum of Comet Halley obtained on April 10. Top left: Spectrum plate; top right: slit position plate. The arrows point to the slit and the corresponding spectrum, which is reproduced in enlarged form in the bottom to explain the individual spectrum features. Exposure time of spectrum: 30 minutes.*

pictures of Figure 4 but the spatial scale is almost 10 times larger. The extended CN coma in the wide-field picture would cover almost half of the frames of Figure 4.

Acknowledgement

We are indebted to W.I. Axford, H. Rosenbauer and V.M. Vasyliunas for a generous support of the ground-based comet camera project. The work would not have been possible without the helping hands of engineers and workers in the shops of the Max-Planck Institute of Aeronomy and the Observatory Hoher List. We are very grateful for the possibility to conduct the observations under the cloudless skies of the European Southern Observatory and for the invaluable assistance provided by ESO staff at La Silla and Garching.

References

Geyer, E.H., Hoffmann, M., Nelles, B.: 1979, *Astron. Astrophys.* **80,** 248.

Geyer, E.H., Nelles, B.: 1985, *Astron. Astrophys.* **148,** 312.

Lund, G., Surdej, J.: 1986, *Messenger* **43,** 1.

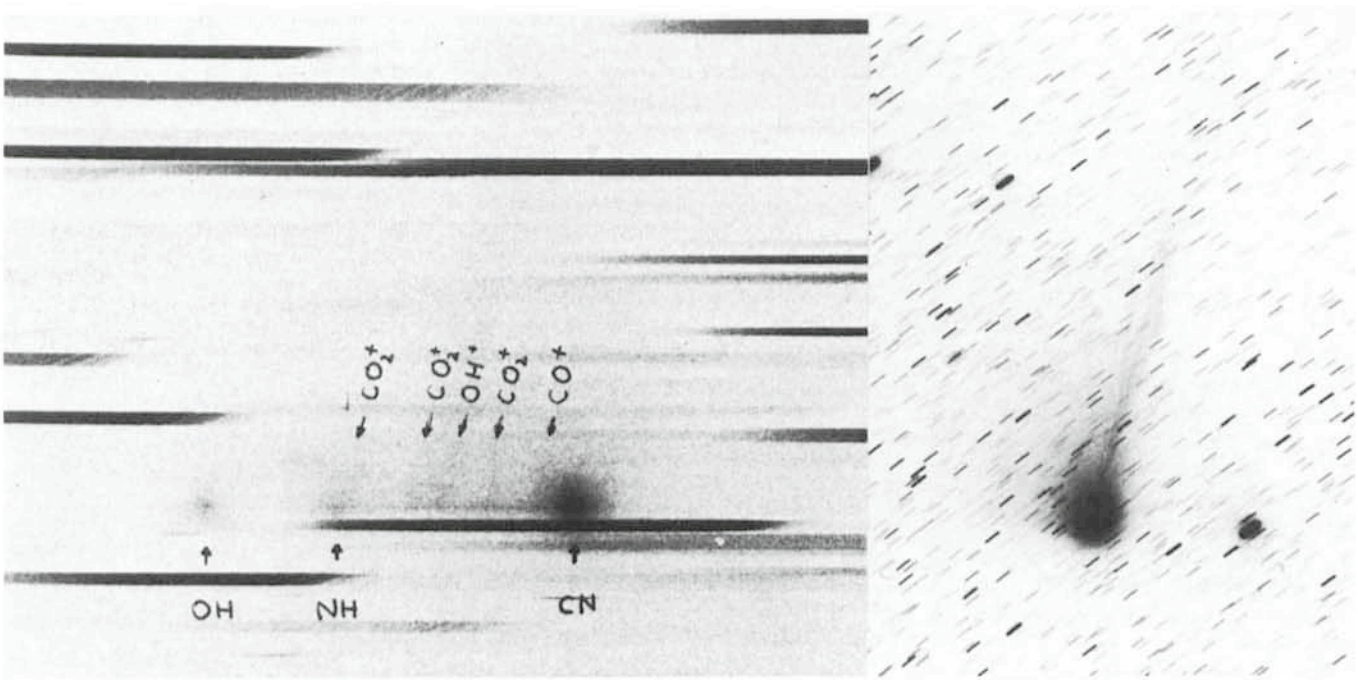

Figure 6: *Slitless wide-field spectrum and direct photograph of Comet Halley. Wavelength range of spectrum 309–395 nm. Dispersion E-W. Wavelength increases to the right. Exposure time of spectrum: 1 hour at f/4.5 on IIa-O plate.*

STAFF MOVEMENTS

Arrivals

Europe:

ELLES, Daniel (F), Procurement Officer
IOVINO, Angela (I), Fellow

Chile:

MURPHY, David (USA), Telescope Software Scientist
OLBERG, Michael (D), Telescope Software Scientist
SCHWARZ, Hugo (NL), Astronomer

Departures

Europe:

ANGEBAULT, Pascal (F), Fellow
FONTANA, Silvana (I), Head of Personnel Service
GARAY, Guido (RCH), Fellow
JÖRSÄTER, Steven (S), Fellow

Chile:

GRANBOM, Sven (S), Head of Operations
URQUIETA, Arturo (USA), Senior Optical Technician
ZUIDERWIJK, Eduardus (NL), Astronomer

Optical Spectroscopy of the Coma of Comet Halley at ESO

R. FALCIANI[1,2], L.A. SMALDONE[2] and G.P. TOZZI[1]

[1] *Arcetri Astrophysical Observatory, Florence, Italy*

[2] *Physics Department, University of Naples, Italy*

The present observing programme performed at La Silla is part of a more comprehensive coordinated project for the study of the coma of comet Halley, a joint collaboration between the Arcetri Astrophysical Observatory, the Astronomy Institute of the University of Florence and the Physics Department of the University of Naples.

The main scientific objectives of the coordinated project can be summarized as follows:

(a) determination of the coma radiance at various heliographic distances and over the widest spectral range, to improve the knowledge of the main mechanisms for the coma formation and evolution, to study the cometary activity and to check the existence (and the possible causes) of highly variable phenomena (bursts, jets, etc.);

(b) the detailed analysis of the dynamic equilibrium conditions of the most abundant gaseous chemical elements within the coma and also their spatial distribution (from the inner coma region, partially influenced by the collision, to the outer coma, collisionless and optically thin);

(c) the study of the physical conditions of the dust and gas components within the coma together with the determination of their ratio along various lines-of-sight within the coma, for a better understanding of the physical mechanisms of their production and evolution.

To reach the above-mentioned objectives it was necessary to perform contemporary measurements over wide spectral ranges, with sufficient spectral resolution, together with the highest possible spatial resolution. Moreover, the whole observing programme had to be repeated during the pre- and post-perihelion phase to study the strong irradiation effects induced by the Sun.

Visible range spectroscopy supplies important information especially on the points (b) and (c), by measuring the diffusion of solar radiation by the coma dust and the molecular and atomic resonant scattering, of some of the main gaseous "daughter" components. Spatial resolution could be obtained by putting a long spectrographic slit on various parts of the coma image.

For the pre-perihelion phase we obtained the optical spectra (3550–6800 Å) of the Halley coma with the 1.5-m telescope of the Astronomy Department of the University of Bologna in Loiano (Italy), equipped with a Boller and Chivens spectrograph and an EMI 9914 image tube.

For the post-perihelion phase we used the 1.52-m ESO telescope equipped with the Boller and Chivens spectrograph. As detectors, we used the EMI 9914 image tube for 4 nights and the Reticon for the remaining 1 night. The best compromise between spectral resolution, luminosity and spectral range, with the EMI tube, has been obtained by using the 1,200 l/mm diffraction grating (ESO # 26) with the entrance spectrograph slit of 150 μm width × 25 mm decker height. With the image linear scale of 19.4 arcsec/mm and reciprocal dispersion of ~59 Å/mm, given by the telescope and spectrograph, we then could have a spectral resolution of ~3 Å and a sky coverage of 8.09 arcminutes with a linear resolution along the slit of ~3 arcseconds (roughly corresponding to an extension of 2.8×10^5 km and the resolution of 1,700 km on the Halley coma for the days of observation). The whole optical range has been covered with only two spectra (3500–5400 Å; 5400–7300 Å).

A total of 25 spectra were obtained during the nights of March 19–22, 1986, with different exposure times, wavelength range, slit positions and orientations (parallel and perpendicular to the sunward direction). The exposure times ranged from 1 minute up to 60 minutes in order to correctly expose the most intense features (e.g., the CN 3883 band) near the photometric nucleus as well as the weakest features in the outer coma regions. Two examples of the obtained spectra are given in Figures 1 and 2. At a first glance the quality of the spectra seems to be very good. This photographic material has been digitized by means of a PDS microdensitometer and is presently being elaborated. We would like to remark here the great extension of the scattered solar radiation (see, e.g. the strength of H_β, H and K lines along the slit direction) that roughly implies a very extended dust component.

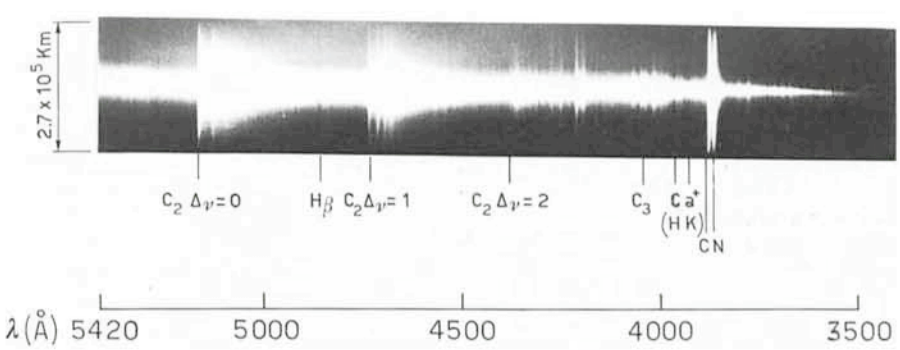

Figure 1: *Example of a spectrum in the 3500–5400 Å range taken on March 21 at 8h 01m UT. The slit was perpendicular to the sunward direction and the exposure time was 10 minutes. Identification of some lines are reported.*

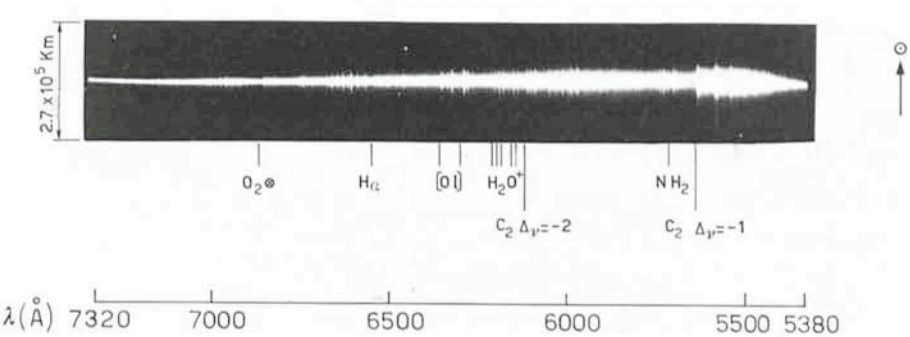

Figure 2: *Spectrum in the 5400–7300 range taken on March 20 at 8h 06m UT. The slit was parallel to the sunward direction. Exposure time was 8 minutes. Identification of some lines are reported.*

The Reticon has been used for 1 night in the spectral range 8500–10000 Å to study the CI atoms in the metastable level $2p^2\ ^1D_2$. The atoms in this level can give emission, by resonant scattering of solar radiation, at 1931 Å, and by spontaneous decay to the $2p^2\ ^3P_{1,2}$ ground state, at 9823 and 9850 Å. Measurements of the 1931 Å line with IUE, for other comets, have shown a very fast decreasing of $^1D_2$ population with heliocentric distance, indicating the possible presence of collisional sources (Feldman, 1983). It would then have been important to measure the two near infrared lines in various parts of the coma to map the CI atoms in this metastable level. Unfortunately, also in the spectrum taken with the longest exposure on the photometric nucleus, there was no presence of these lines. These spectra are still under study in order to evaluate upper limits to be compared with ultraviolet measurements.

References

Feldman, P.D.: 1983, *Science,* **219,** 347.

Halley Through the Polaroids

R. HAEFNER and K. METZ, Universitäts-Sternwarte München

According to ancient tales a comet brings severe misfortune to people. This was again confirmed by the appearance of Comet Halley (see photo on page 18). We had in mind to perform linear and circular narrow band polarimetric measurements of this comet using the new ESO polarimeter. However, mostly due to a damage of the polarization optics which happened last year on transport from Europe to La Silla, this instrument was not available for the scheduled observations in March 1986.

To get the best out of it, we decided to convert the one-channel photometer at the ESO 50-cm telescope into an auxiliary polarimeter. Since during our observing time the comet could be measured only for about 30 minutes to 100 minutes in the very last part of the night, this had to be done without affecting preceding photometric investigations of other objects. Inserting sets of specially prepared Polaroid sheets into the filter wheel of the photometer provided an uncomplicated and economic solution. There were different reasons to restrict ourselves to circular polarimetric measurements: Whereas a large amount of linear polarimetric observations has been performed during the past years, only very few circular measurements exist up to now. To determine linear polarization, at least three sets of Polaroids are necessary whereas two sets are sufficient to derive the circular polarization. Since the different sets can be used only sequentially, the time to complete one measurement is much longer and therefore the required tracking accuracy must be much higher for linear polarimetric observations. Furthermore, measuring linear polarization requires a very precise alignment of the Polaroid sets relatively to each other, whereas the circular polarization can be determined without specially fixed positions of the two sets. Moreover, long-lasting calibration measurements of polarized standard stars are necessary in order to determine the coordinate system of the instrument for the linear polarimetry. Finally, the linear polarization is much more affected by the sky background polarization, especially shortly before and during dawn.

We prepared two sets of Polaroid sheets fabricated by E. Käsemann Ltd., each containing one Polarex polarizer and two quarter wave foils (retarders). The first quarter wave foils were placed in front of the polarizers and aligned with the fast axes at +45° respectively −45° versus the polarization axes of the polarizers. So, within the limits imposed by the effective wavelength (approx. V band, given by the spectral response of the Polaroids and the photomultiplier as well as the spectral distribution of the comet), these sets exhibit maximum transparency for + circular respectively − circular polarization. The remaining retarders were each placed behind the polarizers in such a way that the linear polarized light leaving the polarizers was again transformed into circular polarized light, thus avoiding the instrumental problems arising from the recording of linear polarized light. A consecutive measurement through these two sets (A and B) allows then the determination of the circular polarization.

What is the accuracy of such an arrangement? The one-channel version does not allow for a seeing compensation and causes together with the absorption of the Polaroids a light-loss of about 70%. To shorter and longer wavelengths the retarders deviate gradually from the quarter wave characteristics, thus producing a depolarization. The same holds for the cometary emission lines, especially the C_2 λ 5165 complex. Based on tests in the laboratory and on previous experiences with such Polaroids, we estimate the error of a single polarization determination to be of the order of 0.5%. This means that the circular polarization of Halley to be detected by this device must be of the order of a few per cent.

Indeed, theory predicts circular polarization in comets up to 4% (Dolginov, A.Z., and Mitrofanov, I.G., 1975, *Russ. Astron. J.* **52,** 1268). However, no hint for circular effects was found in either Comet Kohoutek or Bradfield or West (Michalsky, J.J., 1981, *Icarus* **47,** 388) or Tago-Sato-Kosaka (Wolf, G.W., 1972, *Astron. J.* **77,** 576). The reason for this could be that the measurements were made using too large apertures (up to 42″) centred on the core of the comet, thus averaging over too large areas. Indeed, the dusty Comet Bennet showed up to 5% and even once 18% circular polarization when measured through a 14″ aperture placed on different areas within the coma (Metz, K., 1970, Thesis University Munich).

After some test runs in situ, five successful observing runs between March 16 and 20, 1986, could be obtained. Halley showed a pronounced condensation of a few seconds of arc around the nucleus as seen through the view finder. This allowed an accurate positioning of selected areas to be measured using its cross wire and concentric rings. These areas are shown in Figure 1. The tracking speed of the telescope has been adjusted to the actual motion of the comet. However, due to differential refraction (high air mass at start time), there remained a very small uncompensated motion which could influence the subsequent measurements. To overcome this, the sequence ABBA was taken for one polarization measurement. Normally the smallest aperture (10″) was used since obviously the measured degree of polarization decreases with increasing diameter of the diaphragm. This is well known for linear polarization and suspected to hold also for the circular one. An integration time of 20 seconds per Polaroid set proved to be appropriate. Several unpolarized standard stars of solar type were measured every night at the beginning and the end of the Halley run in order to derive the instrumental effects. There was no moon and perfect meteorologi-

cal conditions prevailed all the time except one night when some cirri were present. Altogether about 170 polarimetric observations for different parts in Halley's coma could be obtained.

The reduction revealed that nearly all measured areas around the core (except position 2) exhibited a circular polarization between 0.5% and 0.9%. Though these values are very near to the detection limit of our device, it is important to note that the sign of the polarization did not change, it was always left-handed. Area 7 did not reveal any polarization. However, area 2 was variable in its polarization from night to night with polarization degrees up to about 2% decreasing for the distance of 15″ and 60″ as well. These variations were evidently correlated with the strengthening and faintening of red dust jets emanating from the sun-heated side of the core. The jets showed a length of about 20″ during our observing runs as seen through the Bochum 61-cm telescope (Celnik, W., 1986, private communication). The changing activity did, however, never affect the sign of the polarization at all. This indicates that the measured polarization is not an artifact photometrically produced by these events. Furthermore, subsequent measurements using 21″ and 10″ apertures revealed that the observed polarization was diminished by a factor of 8 for the larger aperture whereas the result for the smaller one remained the same. This also seems to prove that the circular polarization is (at least in area 2) a small-scale effect. The core was measured also using different apertures. A maximum circular polarization of about 0.9% was determined for an aperture of 15″ decreasing appreciably with increasing or decreasing apertures.

How can our measurements be interpreted in terms of the present theories concerning the mechanisms for producing circular polarization in comets? Basically an admixture of non-metallic particles within the coma is needed for scattering processes of the sun light. If these particles are non-spherical, they must be aligned either by magnetic fields or by radiative pressure at least for single scattering. This type of scattering, however, should be excluded by the fact that the sign of the polarization in different areas remained always the same. It is highly improbable that the alignment of the particles is everywhere the same in view of such an active nucleus. Multiple scattering in the dust rich area near the nucleus seems to give a more promising explanation. This process would not necessarily need non-spherical aligned particles for a phase angle (Sun-Comet-Earth) not too far away from 90°. Both, degree and sign of the circular polarization, depend then on the actual phase angle which was around 66° during our observing runs. The results of multicolour observations obtained at roughly the same phase angle are needed to support this interpretation.

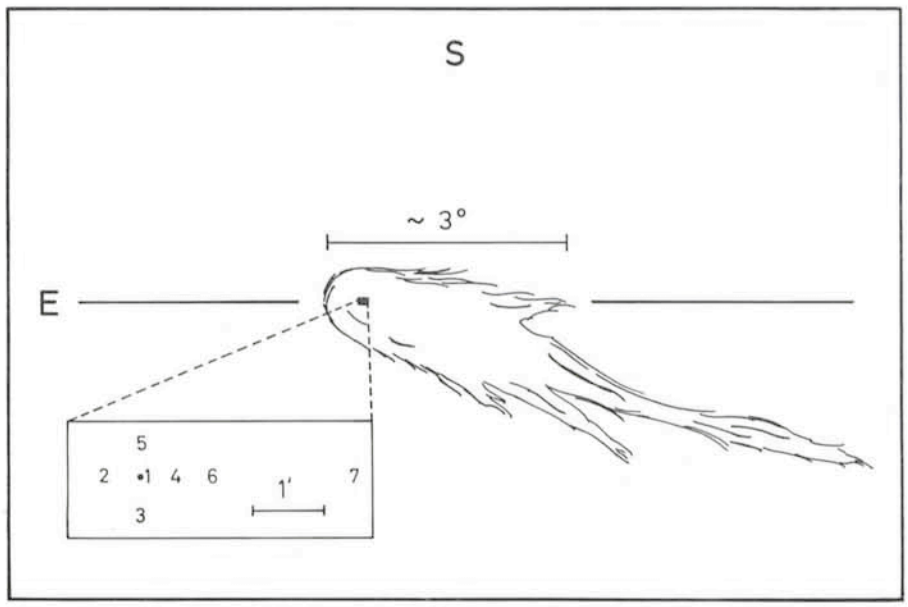

Figure 1: *Sketch of Comet Halley as it appeared during the observing runs. The enlarged portion shows the different positions of the measurements. The core is indicated by 1. Positions 2, 3, 4 and 5 refer to a distance of 30″ from the core and are those areas where most of the measurements were obtained. Additional observations were also performed for distances of 15″ and 60″ in those directions. Position 6 corresponds to a distance of 60″ and position 7 to a distance of 180″. (10″ correspond to a length of roughly 9,000 km on Halley.)*

Acknowledgement

We thank A. Urquieta for his technical support on La Silla and Dr. W. Schlosser for his help in obtaining the Halley photograph (page 18).

Images of Comet Halley – A Slide Set

ESO announces the publication of a limited edition of this slide set. It is composed of some of the best images of Comet Halley, obtained at La Silla during the period December 10, 1982, to April 30, 1986. The slide set only includes direct images, although other types of observations – for instance photometry and spectroscopy – were also carried out at ESO, cf. the articles in this *Messenger* issue. The 20 slides are in colour and B/W and emphasize the different observing techniques. They start with the first CCD images, which were obtained with the Danish 1.5-m telescope, when Halley was still more than 10 A.U. from the sun. The set also includes the recovery image on February 15, 1986, which was made only six days after perihelion. A spectacular disconnection event on March 10, 1986, is documented with three Schmidt pictures and the impressive changes in the tail can be followed on Wide-Field CCD images. Some slides are very beautiful, like a colour picture of Halley in the southern Milky Way.

The slide set is accompanied by a comprehensive text, giving details about the instruments used and the circumstances of each image. This set is therefore particularly useful for educational purposes. Copies may be obtained by sending DM 35,–, which is the equivalent of the cost price including postage, to:

ESO Information and Photographic Service
Karl-Schwarzschild-Strasse 2
D-8046 Garching bei München
Federal Republic of Germany

Do not forget to indicate your name and accurate address. Please note that the delivery time may be 3–4 weeks.

Comet Halley as seen on March 21, 1986, from La Silla (photograph: R. Haefner).

IRSPEC: ESO's New Infrared Spectrometer

A. MOORWOOD, P. BIEREICHEL, G. FINGER, J.-L. LIZON, M. MEYER, W. NEES, J. PAUREAU, ESO

Introduction

IRSPEC is a cryogenically cooled grating spectrometer equipped with an array detector for spectroscopy at R = 1,000–2,500 between 1 μm and 5 μm. It was successfully installed at the 3.6-m telescope in November 1985, underwent further testing in February 1986 and will be available for Visiting Astronomers from October 1986 as announced in the *Messenger* No. 42 and in the Announcement for Applications in Period 38. In this article we describe the instrument, discuss its performance with reference to some of the test spectra obtained and comment on its possible evolution.

Instrument Concept

The main characteristics of IRSPEC are summarized in Table 1. In order to meet our requirements for a large collimated beam diameter, high optical and mechanical quality and flexibility in the future choice of detector arrays, the overall concept departs substantially from the usual approach of designing infrared instruments to fit within the cold space in commercially available storage cryostats. Instead, the spectrometer design is rather classical except that all the optical components are cooled to ~80 K by a continuous flow liquid N_2 system and the detector to ≃50 K by solid N_2 contained in a separate cryostat inside the vacuum vessel. Figure 1 is a photograph of the instrument with the upper parts of the vacuum vessel and radiation shield removed. Various design aspects are described in more detail in the following sections.

Optical Design

The optical arrangement is shown schematically in Figure 2. As IRSPEC was designed for use at the 3.6-m F/8 Cassegrain focus (before implementation of the F/35 chopping secondary) and eventually at one of the F/11 Nasmyth foci of the 3.5-m NTT, it was necessary to incorporate the input opti-

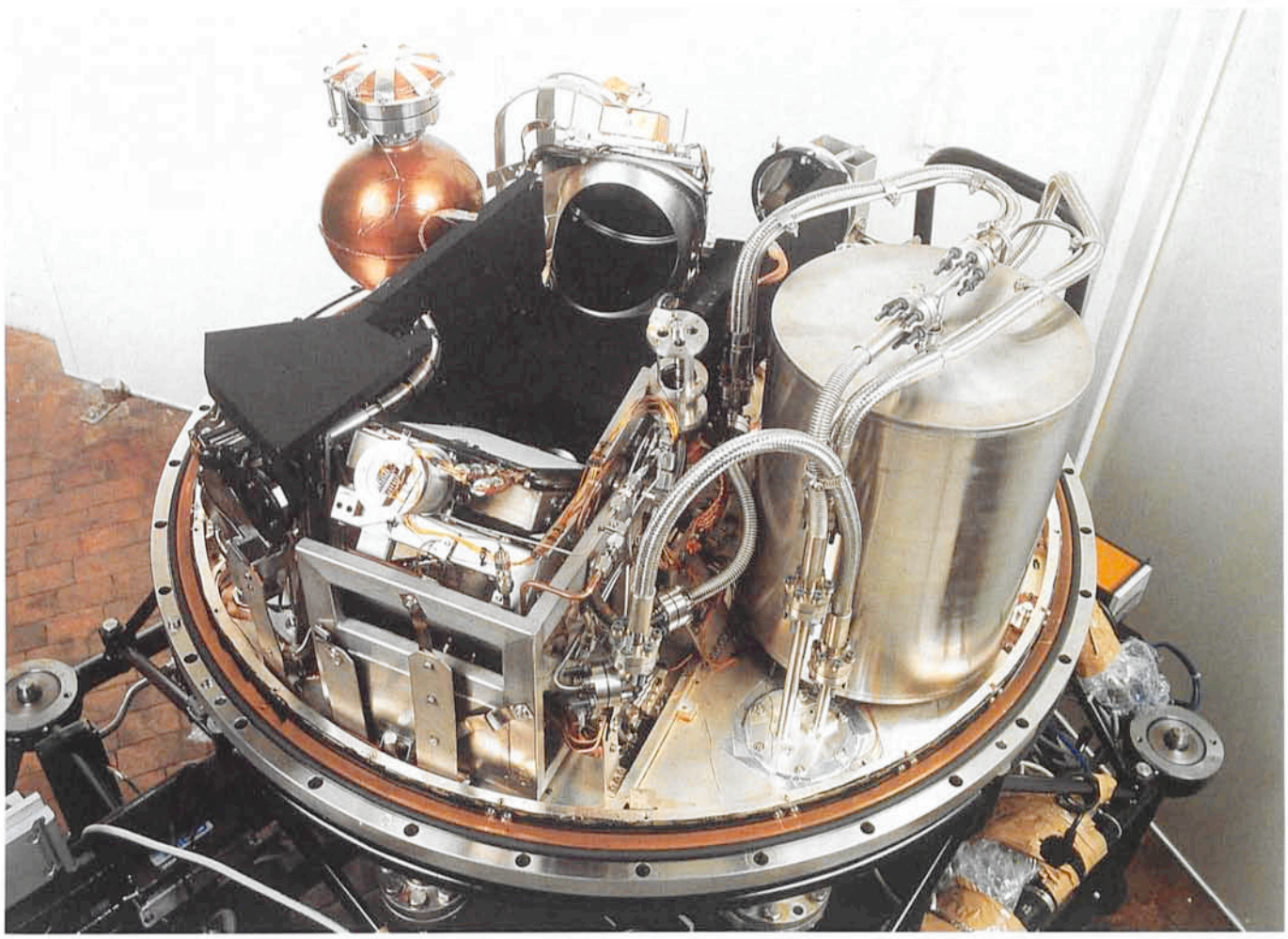

Figure 1: *IRSPEC with the upper parts of its radiation shield and vacuum vessel removed. The spectrometer is cooled by a continuous flow of liquid N_2 supplied either by the internal reservoir on the right or from an external tank while the detector array is cooled by solid N_2 contained in the copper cryostat (upper left).*

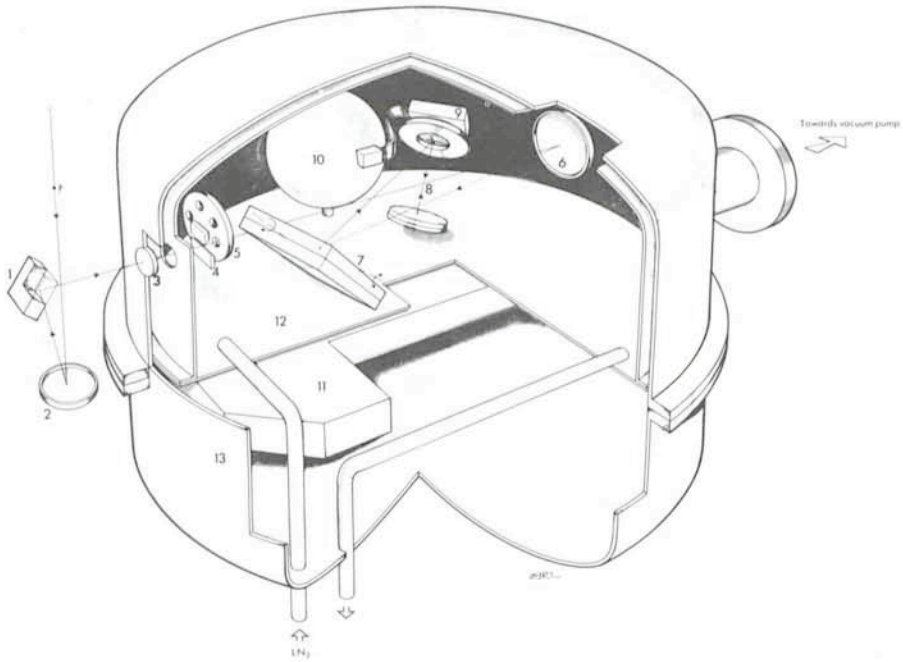

Figure 2: *Schematic of the optical arrangement.*

cal system comprising a spherical relay mirror (2 in Fig. 2) and a cylindrical mirror (1), on which the telescope pupil is imaged by 2 and which can be "wobbled" to provide for sky chopping. The slit unit (4) consists of a classical moving blade system plus a decker which can be scanned along the slit to define the projected detector size and position once the instrument is cold. Both the slit and decker blades are highly polished and slightly tilted to permit viewing of the field by a TV camera which is not shown in Figure 2. Behind the slit is the 8 position order sorting filter wheel (5) and just in front, a field lens which images the telescope pupil on a cold baffle at the off-axis (9°) parabolic collimator mirror (6). This latter has a focal length of 740 mm, accepts an F/7.4 beam from the field lens and directs a 100 mm diameter parallel beam to the two interchangeable gratings (120 × 150 mm ruled) which are mounted back to back (7) and operated in the Littrow Mode to maximize their efficiency and dispersion. Finally, an F/2 Pfund type camera (8) focusses the spectrum on the detector array (9).

As described below, the spectrometer is mounted on an uncooled optical bench to avoid misalignment during cooling. It is aligned interferometrically when warm, and after cooldown it is only necessary to optimize the spectrometer focus (using a three position Hartmann mask in front of the collimator) and the decker position. For calibration purposes, the slit can be illuminated by either of two spectral line lamps (Ne and Kr) or a variable temperature blackbody source which are permanently installed and remotely controllable via the instrumentation computer.

Mechanical and Cryogenic System

In order to minimize mechanical and thermal flexure, the optical elements are supported by a thermally isolated optical bench (11 in Figure 2) supported by a rigid frame attached to the telescope flange. This frame also carries the vacuum vessel which is mechanically decoupled from the spectrometer by means of bellows, however, and plays no structural role. Cooling of the spectrometer is by liquid N_2 flowing through a tube attached to the bottom plate of the radiation shield (12) to which the optical elements are attached via silver straps or copper braids. Additionally, liquid N_2 is also passed through a heat exchanger sandwiched between the two gratings in order to achieve a cooldown time of $\simeq$ 10 hours. The N_2 can be supplied from an external tank (usually during cooldown) or from the internal stainless steel reservoir visible in Figure 1. Temperature sensors are used to automatically control the N_2 flow both to limit temperature gradients during cooldown and to maintain the selected final steady state temperature ($\simeq$ 80 K). A separate copper cryostat (upper left in Figure 1) containing N_2 solidified by an external pump is used to cool the detector (to $\simeq$ 48 K) and also a small volume of active charcoal which acts as a cryogenic pump to maintain the vacuum.

The most complex mechanical unit is the grating support shown in Figure 3 which enables the two back to back mounted gratings to be interchanged by a 180° rotation and also rotated about their ruled surfaces for spectrum scanning. In order to achieve maximum accuracy and reproducibility the gratings are supported in a cradle mount and driven by a high precision "transroll" screw. All functions, except for the collimator drive and Hartmann mask, are remotely controlled via either DC motors and absolute encoders (slit, decker, grating rotation and drive) or stepper magnets (filter wheel, calibration source selector mirror). As the control shafts (plus all cryogenic and electrical connections) only penetrate the lower shell of the vacuum vessel, removal of the upper parts of the vacuum vessel and radiation shield is relatively straightforward and provides easy access for alignment, maintenance, modification, etc. as can be seen in Figure 1.

Detector

At present this is a monolithic array of 32 InSb diodes (each 200 μm × 200 μm) operated in the integrating mode and multiplexed onto a single amplifier. Their wavelength response is from 1 μm to 5 μm with a maximum quantum efficiency of ~ 70% at the long wavelength end. Under normal operating conditions at T $\simeq$ 50 K the charge capacity is $\simeq 10^7$ e, dark currend $< 10^4$ e/s and the read noise is close to the kTC limit of 10^3 e. The readout electronics (Fig. 4) comprises the "Head" electronics mounted on IRSPEC and modules in CAMAC. The Head electronics generates the readout clock signals, the detector bias voltage and the timing signals for the 15 bit A/D converter, while the CAMAC modules generate the readout sequence commands and the timing pattern for the wobbling mirror accord-

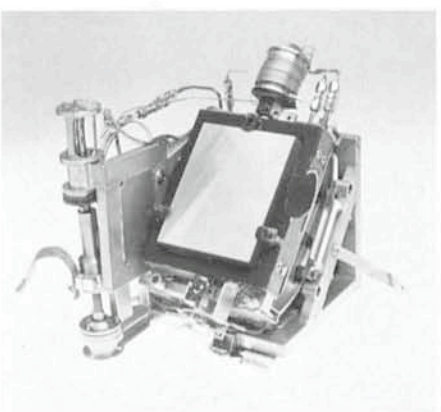

Figure 3: *The grating cradle support which permits interchange of the two back to back gratings and precision scanning about their ruled surfaces.*

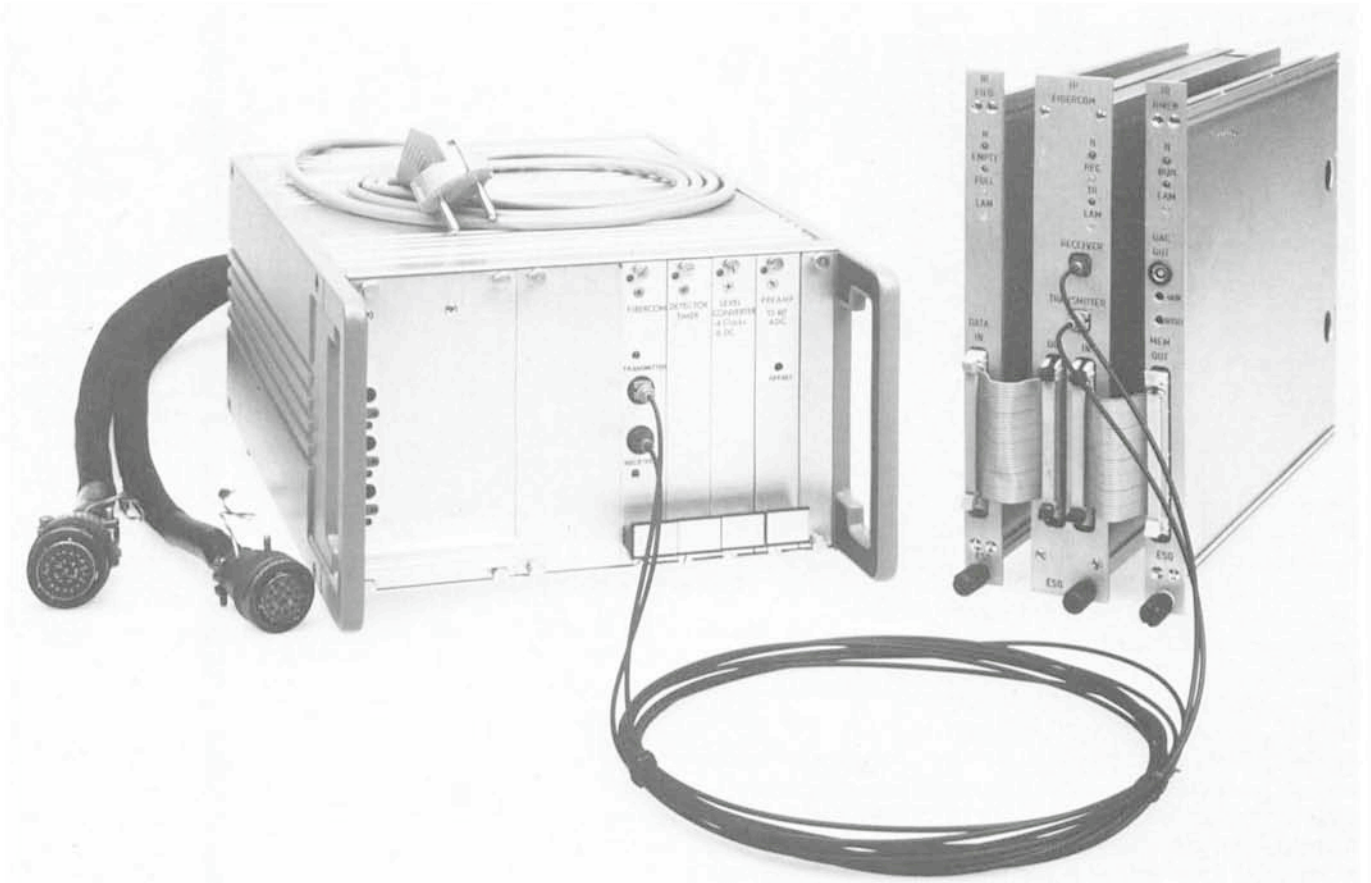

Figure 4: *Detector array electronics comprising the "Head" electronics (left) and modules in CAMAC which communicate via a fibre optic link.*

ing to the observing mode and integration parameters selected by the observer. All power is derived from the mains, thus eliminating the need for battery changes, and ground loops are avoided by employing a fibre optic link for communication between CAMAC and the sensitive (4.5 μV in a 10^5 Hz bandwidth) Head electronics.

Operating Modes and Software

As with the other major ESO instruments, user interaction with IRSPEC is by means of form filling, function keys and typed commands at the HP instrumentation computer console in the control room. One novel feature, however, is the provision of a colour Ramtek display of the complete instrument and measurement status. The complete instrumental set-up can also be saved in a file at any time and restored later by typing a simple command and the appropriate file name. IHAP is used for data acquisition plus spectrum displays and plots and is available to the user for on-line reduction during any spare moments.

Three basic operating modes can be selected via the function keys. Most measurements are made in the Observing Mode which is used to acquire and store (disk and magtape) astronomical spectra at either a fixed grating position (Discrete) or with automatic stepping of the grating to cover a specified wavelength range (Continuous). The desired centre wavelength or wavelength range is entered directly and translated into grating position by the software via a master calibration curve made at higher than the normal resolving power by centring lines from the spectral line lamps in the small gaps (20 μm) between pixels. Discrete spectra can be made at sub-pixel intervals to achieve a better sampling of specific spectral lines and the segments of Continuous spectra can be specified to overlap by any number of pixels from 0 to 16. With no pixel overlap, 10–15 grating steps are required to cover each of the standard J, H, K, L and M photometric windows. A complete measurement comprises a number (1–49) of cycles corresponding to a user specified integration time in the case of DC and chopped observations and a complete ABBA sequence when telescope beam switching is employed. All cycle measurements, plus the standard deviations computed for each pixel from the elementary detector integrations, can be displayed and are stored in the database together with the final average and standard deviations on the mean. Each spectrum file also contains all the instrument settings, coordinates, airmass, time and any comments entered by the user.

The Calibration Mode is similar but used to obtain spectra of the spectral line lamps and the blackbody for wavelength calibration and flat fielding respectively. As the wavelength calibration appears to be stable and flat field-

TABLE 1: IRSPEC Characteristics

Wavelength Range:	1 μm–5 μm
Resolving Power:	1,000–2,500
Sensitivity (1 σ, 60 s):	m ≃ 10.5–11 (1–2.4 μm), 6–7 (3–5 μm)
Slit:	6 × 6 arcseconds (= 200 μm pixel)
Detector:	32 element InSb integrating array
Optics:	Littrow arrangement 2 interchangeable gratings (120×150mm ruled) parabolic collimator, F/2 Pfund camera
Cryogenic System:	continuous flow liquid N_2 for spectrometer (80K) solid N_2 cryostat for detector (~48 K)

ing better achieved on stars, however, this mode will probably not be used much by Visiting Astronomers except on cloudy nights.

A Peak-up Mode is available for use whenever it is required to centre an object by maximizing its infrared signal. Selection of this mode overrides any grating stepping and telescope beam switching, suppresses the storage of data and automatically displays each cycle measurement as intensity versus pixel number on the graphics terminal. An analogue signal corresponding to any selected pixel or to the average is also output to a chart recorder allowing either the continuum or any strong spectral line (whose pixel number can be identified on the graphics screen) to be peaked-up in the usual way.

Field recognition and centring of visible objects is possible using the normal Cassegrain adapter functions and/or the TV slit viewer (down to $m_v \sim 20$ on a dark sky). The standard ESO autoguider can also be used on the Cassegrain adapter guide probe, except if beam-switching when autoguiding is only possible at present on the slit viewer and is severely limited by the small field (no stars) and the fact that the object itself is usually not visible with the nominal 6″ slit width.

Test Results

Both the installation and tests of IRSPEC went remarkably smoothly and with extremely satisfactory results in general. The most potentially serious technical problem arose towards the end of the second test when a rapid increase in friction caused us to restrict our remaining observations to a single order sorting filter rather than risk completely jamming the filter wheel drive. This problem was not entirely unexpected, however, because the bearing responsible had not been surface treated for low temperature and vacuum conditions due to lack of time and was due to be replaced anyway as soon as possible. No particular problems were experienced with the more complex functions. The grating drive proved to be reliable and reproducible to within 20 μm while the cryogenic system yielded hold times of 17 hours and nearly 5 days for the internal reservoir and the detector cryostat respectively and a pressure of $\simeq 2.10^{-6}$ τ for 9 days. Detector read noise was actually slightly lower than the best values achieved during laboratory testing and extremely close to the theoretical limit for this type of readout system. Although initially too high, mechanical flexure was finally reduced to less than 25 μm at the detector within zenith distances of up to ~ 50°.

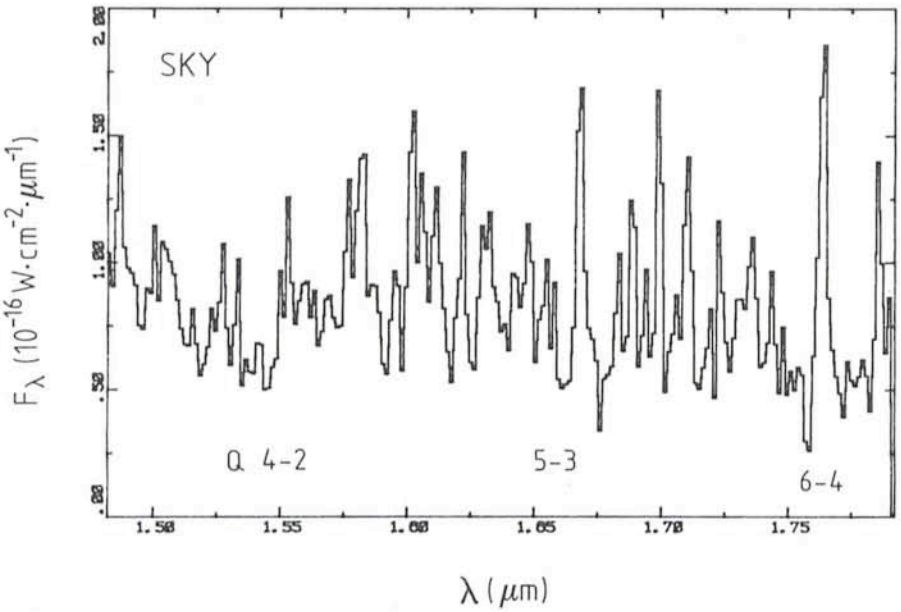

Figure 5: *Sky emission in the H band which is dominated by P, Q and R branch lines in the $\Delta v = 2$ system of OH. The spectrum was obtained in DC mode with 20s integration.*

The present resolving power is thus limited by the pixel size of 200 μm rather than the slit width (6 arcseconds), the optical quality (25 μm) or the mechanical stability of the spectrometer.

Sensitivity figures for the various wavelength range/order combinations were circulated with the Period 38 Announcement and will be documented in more detail in the Operating Manual. Between 1 μm and 2.4 μm the r.m.s. noise for a 1-minute observation corresponds to $m \simeq 10.5-11$ or $\sim 3.10^{-21}$ W.cm^{-2} in the best case. At longer wavelengths the instrument becomes background limited at $m \simeq 6-7$ or 2.10^{-20} W.cm^{-2}.

Spectra

A sample of spectra which illustrate the capabilities of IRSPEC in its different modes are reproduced in Figures 5–10. These were all reduced using IHAP, following the simplest approach of dividing object and standard star spectra to remove the instrumental response and telluric absorption features and then

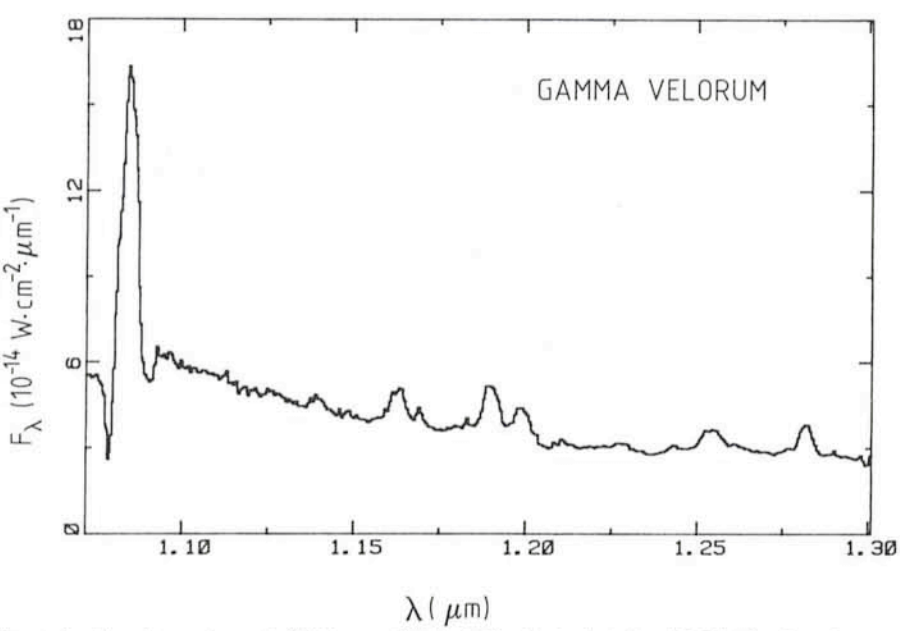

Figure 6: *J band spectrum of γ^2 Velorum (WC8+O8) obtained at R = 1,900 in the Continuous mode with sky chopping and 12s integration. Note the P. Cygni profile of the strong HeI (1.083μm) line. The other lines are from HI, HeI, CIII and CIV. Additional noise between 1.1μm and 1.15μm is due to the presence of strong atmospheric absorption features which are, nevertheless, removed quite well after division by the standard star.*

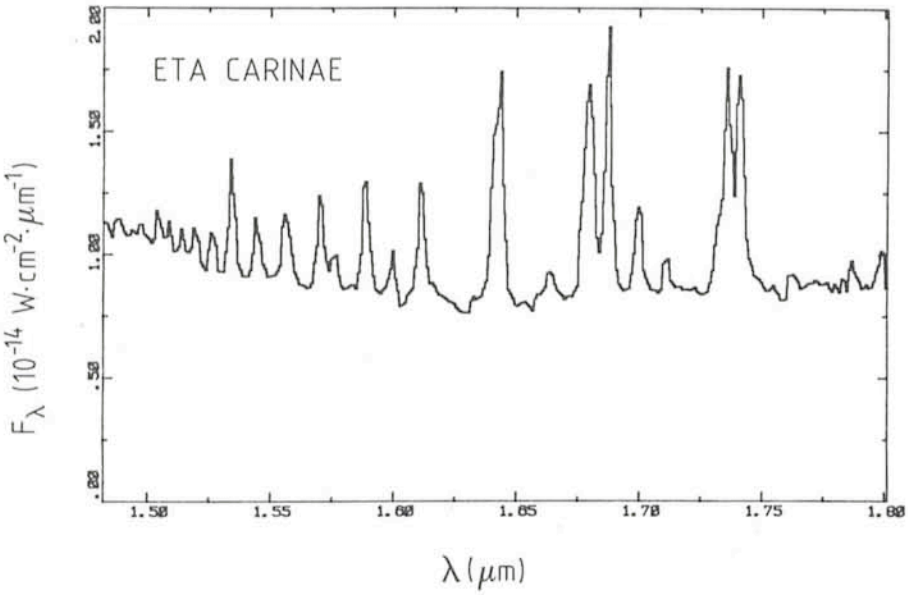

Figure 7: *H band spectrum of η Carinae obtained at R = 1,100 in the Continuous mode with sky chopping and 8s integration. Lines are from HI (Brackett series 28 to 10-4), HeI, FeII and [FeII].*

rebinning to a linear wavelength scale. Flux calibrations have been applied by interpolating between broad-band photometry of the standards and should be considered preliminary. Specific points of interest are mentioned in the relevant captions where all the integration times quoted refer to the total measurement time at each grating position.

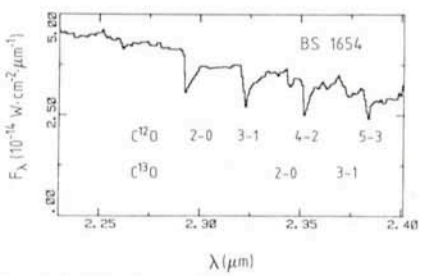

Figure 8: *The 2.3μm CO band in the K giant "standard" star BS 1654 measured at R ≃ 1,600 in the Continuous mode, with sky chopping and 4s integration time. Note that the $C^{12}O$ and $C^{13}O$ band heads can be resolved separately at this resolution.*

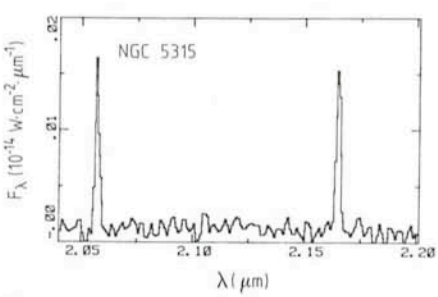

Figure 9: *HeI (left) and HI(Brγ) emission lines in the planetary nebula NGC5315 measured in Continuous mode at R = 1,700 with 24s integration time.*

Future Developments

Further performance gains with IRSPEC are largely dependent on future detector developments. A reduction in read noise would lead to improved sensitivity at $\lambda < 3$ μm while smaller pixels could yield resolving powers up to $\simeq 10^4$ with a $\geqslant 1$ arcsecond slit. The present design also already incorporates the possibility for long slit (~ 120 arcseconds) observations. Various possibilities for better exploiting these intrinsic capabilities of the instrument using an improved linear or, ideally, 2 D array are currently being investigated in Garching.

It is also planned to transfer IRSPEC to one of the 3.5-m NTT Nasmyth foci once this telescope is operational. Although unlikely to yield any significant performance gain directly, this move should bring considerable operational advantages and, hopefully, an increase in the available observation time.

Acknowledgements

Many people have contributed to the design and development of IRSPEC. In Garching we wish particularly to thank B. Delabre and H. Dekker for their contributions to the optical design; G. Hess,

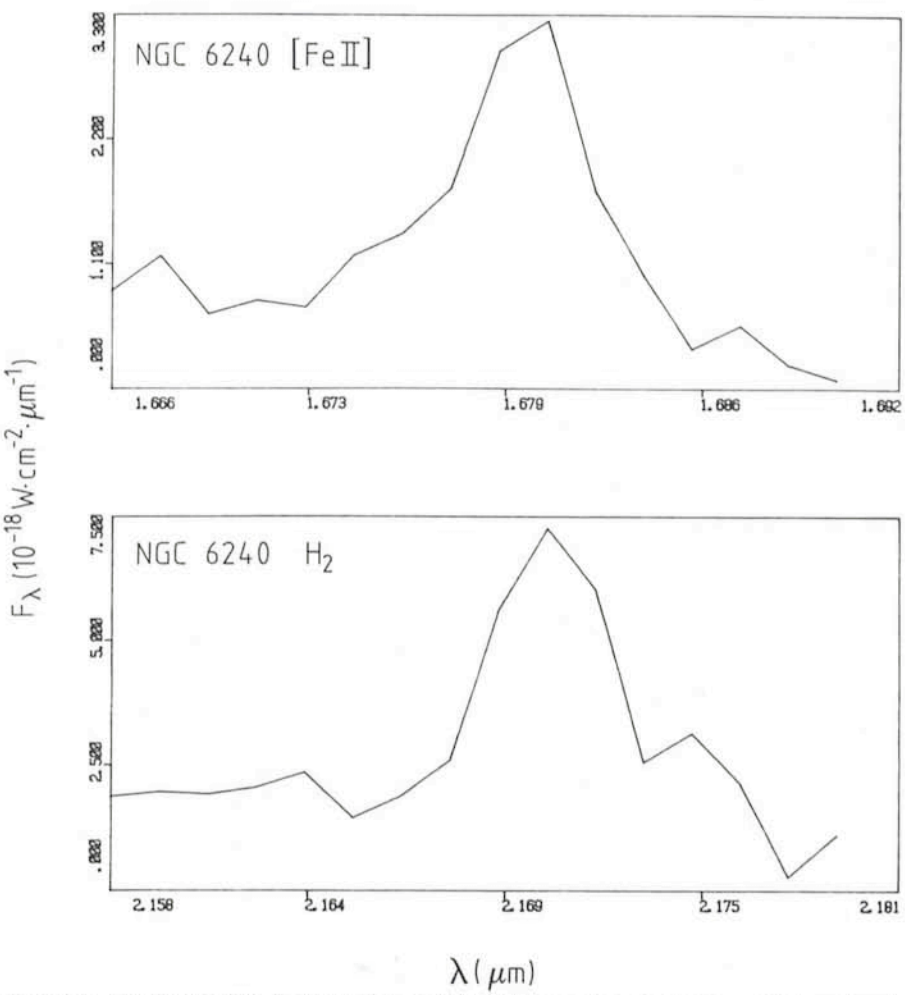

Figure 10: *"Profiles" of the [FeII] (1.64μ) and H_2[S(1)] lines observed to be ≃ 900 kms^{-1} and 500 kms^{-1} broad respectively in the merging galaxy system NGC 6240 (z = 0.025). These measurements were made in the Discrete mode, with sky chopping and integration times of 40 minutes and 20 minutes respectively.*

G. Huster and S. Malassagne for mechanical design support and A. van Dijsseldonk for help during the integration and testing phases. We also wish to thank T. Bohl, F. Gutierrez, D. Hofstadt and T. Le Bertre for their help during the installation and tests on La Silla.

NTT Mirror Leaves Factory

Early June 1986, the 6-ton mirror for the New Technology Telescope was being prepared for transport from the Schott factory in Mainz. The 3.58 m mirror of Zerodur, which is only 24 cm thick, was lowered into the steel frame in which it will be transported to Zeiss Oberkochen. The transport, which in-

Model of the ESO New Technology Telescope.

ESO NTT mirror leaves factory.

volves careful planning by the German traffic authorities, will take place during the night of 23 to 24 June. Once at Zeiss, the optical figuring will start immediately. It is expected that this process will be finished by July 1988 and that the shipment to La Silla can take place soon thereafter.

List of ESO Preprints

(March–May 1986)

425. M. Azzopardi, J. Lequeux and B.E. Westerlund: New Carbon Stars in Spheroidal Galaxies: II. Draco, Ursa Minor and New Data on Sculptor, Carina and Leo I. *Astronomy and Astrophysics.* March 1986.
426. R.G. Gratton, A. Tornambè and S. Ortolani: Spectroscopy of RR Lyrae Stars in Baade's Window and ω Centauri. *Astronomy and Astrophysics.* March 1986.
427. M. Rosa: Star Formation, Giant H II Regions and Spiral Structure. To appear in *Highlights of Astronomy,* Vol. 7, ed. J.-P. Swings. Joint Discussion VI. March 1986.
428. O. Stahl: On the Relationship of the Variable Stars AG Car and HDE 269852 to the Ofpe/WN 9 Objects. *Astronomy and Astrophysics.* March 1986.
429. E. Brinks and E. Bajaja: A High Resolution Hydrogen Line Survey of Messier 31. III. HI Holes in the Interstellar Medium. *Astronomy and Astrophysics.* March 1986.
430. M. Iye: High Resolution Spectrum of the Peculiar Optical Counterpart of an X-ray Binary Pulsar 4U1907+09. *Publ. Astron. Soc. Japan.* March 1986.
431. M.H. Ulrich and M.A.C. Perryman: The Remarkable Absorption-Line Systems in the Quasar Tololo 1037–27. *Monthly Notices of the Royal Astronomical Society.* March 1986.
432. G. Contopoulos: Bifurcations in Systems of 3 Degrees of Freedom. *Celestial Mechanics.* March 1986.
433. G. Contopoulos and P. Magnenat: Simple Three-Dimensional Periodic Orbits in a Galactic-Type Potential. *Celestial Mechanics.* March 1986.
434. F. Matteucci: The Effect of the New ^{12}C (α, γ) ^{16}O Rate on the Chemical Evolution of the Solar Neighbourhood. *Astrophysical Journal,* Letters. March 1986.
435. J.M.R. Espinosa, R.J. Rudy and B. Jones: Extended Non-Nuclear Infrared Emission from Seyfert Galaxies. *Astrophysical Journal.* March 1986.
436. G. Contopoulos: Qualitative Changes in 3-Dimensional Dynamical Systems. *Astronomy and Astrophysics.* March 1986.
437. V. Castellani, A. Chieffi, L. Pulone and A. Tornambè: On the Advanced Evolution of Intermediate Mass Stars: Induced Semiconvection, Breathing Pulses and the Upper Mass Limit for Carbon Deflagration. *Astrophysical Journal.* April 1986.
438. T.J.-L. Courvoisier, A.N. Parmar, A. Peacock and M. Pakull: The Discovery of 3.9 Hour Periodic Dips in the X-Ray Intensity of XB 1254–690. *Astrophysical Journal.* April 1986.
439. J. Lequeux, N. Meyssonnier and M. Azzopardi: An Objective-Prism Survey of Emission-Line Objects in M 33 and IC 1613. *Astronomy and Astrophysics Supplement Series.* April 1986.
440. J. Melnick, M. Moles, R. Terlevich and J.-M. García-Pelayo: Giant H II Regions as Distance Indicators I: Relations Between Global Parameters for the Local Calibrators. *Monthly Notices of the Royal Astronomical Society.* April 1986.
441. M. Pettini and S. D'Odorico: A Search for Million Degree Gas in the Galactic Halo and the LMC Through [Fe X]

λ 6375 Absorption. *Astrophysical Journal.* April 1986.
442. E. Giraud: The Dependence of the Tully-Fisher Relation on Morphological Type. *Astrophysical Journal.* May 1986.
443. P. Magain: Contribution Functions and the Depths of Formation of Spectral Lines. *Astronomy and Astrophysics.* May 1986.
444. A.F.M. Moorwood: 3.28 μm Feature and Continuum Emission in Galaxy Nuclei. *Astronomy and Astrophysics.* May 1986.

MIDAS Memo

ESO Image Processing Group

1. Application Developments

In this summer release of MIDAS a great step towards hardware independence has been achieved: First, the AGL library from ASTRONET is now used by all graphics applications in MIDAS. The metafile oriented AGL package already supports a lot of different graphic devices and backend drivers for other devices may be added easily. Second, all image display applications of MIDAS are now based upon a proto-type of the IDI* interfaces. An actual implementation of the IDI interfaces has been done at ESO for the DeAnza IP 8500 and also at Trieste for an EIDOBRAIN 7001. The concept of these IDI routines was successfully tested in Trieste. We implemented MIDAS on the EIDOBRAIN machine by simply replacing the DeAnza IDI interfaces with the IDI interfaces of the Trieste group!

A set of commands for reduction and analysis of one-dimensional spectra is now available. For a long time this was a main missing area of applications that was not considered until now due to the excellent performance of IHAP. The commands use AGL as standard graphics package. Functions included are wavelength and flux calibration tools and some interactive analysis facilities. More developments are expected in this area in the near future.

Another area of activity was the fitting package. New methods are now available to perform Least-Squares approximations to images and tabular data.

* Image Display Interfaces which have been presented at the Data Analysis Workshop at ESO in February 1986.

2. Distribution Policy

The distribution policy for MIDAS has been revised to ensure a better service for the growing number of users at other institutes. The basic scheme has been modelled after the concept used by AIPS. There will be two major releases of MIDAS taking place January 15 and July 15 each year, i.e. this July release is denoted 86JUL15. In addition, minor releases will be made April 15 and October 15 when required. New reduction packages and significant modifications will be distributed with major releases while minor ones will contain bug-fixes and small enhancements only.

The release tape contains installation procedures, help files and MIDAS code needed for generating the system except commercial libraries. All application programmes are available in FORTRAN source code, whereas monitor and libraries are distributed as object code for VAX/VMS, since parts of the latter code may be written in other languages. Source code as well as executable images and test files are available on special request. Two special libraries are needed for linking MIDAS, namely: NAG for mathematical routines and AGL for graphics. The latter can be obtained through ESO or directly from ASTRONET.

A request form for MIDAS releases was sent to all institutes on our present tape mailing list in early June. Other institutes which would like to use MIDAS are kindly requested to contact the Image Processing Group in ESO directly. The MIDAS distribution kit is provided free of charge to all non-profit research organizations. New releases will be mailed automatically if we have received the returned distribution tape at least one month prior to the release date.

3. A Portable MIDAS Version

Most new computers are offered with the UNIX operating system which has been adopted also by major European vendors. In order to provide MIDAS for such systems (e.g. workstations), a portable version of MIDAS will be developed. This version will run under both VAX/VMS and UNIX, and be upgraded with real-time features for data acquisition and network capabilities. The design specifications will be presented to the community in the fall of this year while a release is expected in the spring of 1988.

4. Computer Upgrade

The main scientific computer facilities of ESO were upgraded at the end of June to meet the growing demand from users. The VAX 11/780 and VAX 11/785 computers are replaced by two VAX 8600 machines increasing the total performance by more than a factor of 3 to 8.4 MIPS. The I/O performance of the system is also increased by a second SBI bus on one VAX 8600 computer and the use of faster Winchester disk drives from System Industries. Further, a VAX station II/GPX was purchased for image processing applications. This workstation runs UNIX and will be used for the first implementation of the portable MIDAS version under UNIX. The computers are interconnected with a Local Area Network which uses Decnet protocol between DEC equipment and TCI/IP for communication to other systems such as HP computers and measuring machines.

Remote Control of 2.2-m Telescope from Garching

G. RAFFI and M. ZIEBELL, ESO

A Remote Control (RC) run of the 2.2-m telescope at La Silla was carried out from Garching during six observing nights in the period March 23–29, 1986. This was the next logical step after the test run of La Serena in June 1984. The instruments used, each for 3 nights, were the Adapter with CCD and the Boller & Chivens with CCD, so that the astronomers involved had a chance to work both with images and spectroscopic data.

The RC concept implemented and tested in this run is what we call "Interactive Remote Control", to point out that the user works at the computer consoles with the same degree of interaction available as in the 2.2-m control room at La Silla, without the need to have a fixed and predetermined observing programme.

The Telephone Link

The RC set-up consisted of two HP 1000 computers, one being the control computer of the 2.2-m telescope at La

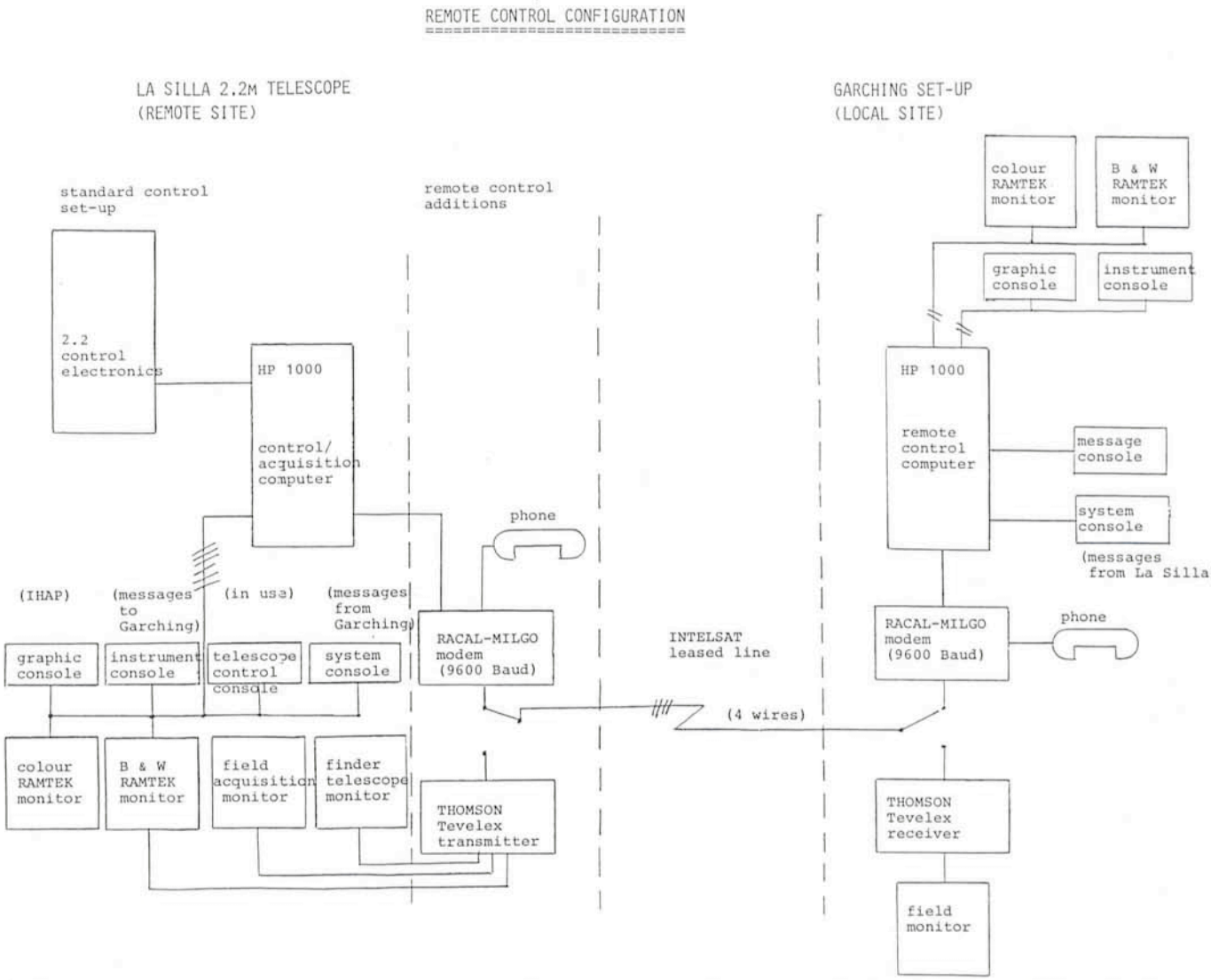

Figure 1: *The complete remote control configuration. One can see that the telephone line is time-shared between digital- and analogue communication, this last both for telephone and TV monitor frames.*

Silla (remote computer), and the second being located at Garching (local computer = near the user). They were connected via a leased telephone line, with a standard bandwidth from 300 Hz to 3.4 kHz, available full-time to ESO during the test period. The telephone line consisted of the following trunks (starting from La Silla):

- a 500-m cable from the 2.2-m telescope to the Chilean Post repeaters at La Silla,
- a microwave link between La Silla and Santiago,
- a satellite link on Intelsat over the Atlantic up to Raisting, FRG,
- a leased ground line from Raisting to Garching.

The line was a 4-wire line, conditioned (equalized) in Munich and Santiago, to provide a good-quality transmission. The digital communication was via 2 modems, with adjustable speeds up to 9,600 baud, belonging to ESO. To have own modems is allowed on a leased international line and solved the problem of different "quasi-compatible" modems, which is what one would get asking the German and the Chilean Post to rent modems. The communication was point-to-point, full-duplex and the protocol used was HDLC. The communication software used at system level was DS/1000 from HP, and the ESO software was developed over it.

The System Configuration

Figure 1 gives a complete picture of the RC configuration. It shows how the leased line was shared, so that it was possible to have telephone communication and analogue image transmission in addition to digital data transmission, by means of a manual switching procedure. In particular, telephone conversation was possible via special telephone sets connected to the modem.

Another possibility offered was the use of a system built by Thomson for the transmission of analogue video frames. This system was used in conjunction with the field acquisition monitor and finder telescopes to send a reduced TV image to Garching in a very short time.

It should be noted that the use of the line in an analogue way (either for telephone or for video frames) was an alternative to computer communication. So this could only be done when no data transmission was going on, but otherwise it did not have other effects on computer operations, which could continue unaffected at the end.

The RC Software

One aim of the RC software was the possibility to offer exactly the same interface to the 2.2-m telescope instrumentation from Garching as from La Silla (e.g. same softkey menus and forms as on the 2.2-m instrument console). It was, however, preferred to leave the control of the telescope via the telescope control console to the night assistant at La Silla, following the usual practice of work sharing at the tele-

Figure 2: *The remote control room for the 2.2-m telescope in Garching. 1 = messages from La Silla, 2 = messages to La Silla, 3 = modem, 4 = TV images receiver, 5 = field acquisition TV monitor, 6 = phone, 7 = Ramtek monitors, 8 = instrument console, 9 = graphic console, 10 = hard copy.*

scope between night assistant and astronomer.

Figure 2 shows the RC room for the 2.2-m telescope in Garching. Figure 3 shows how the RC software was implemented. At the top the ESO control/acquisition software is shown, where the control functions, dealing with the interfaced electronics and user end part, are implemented in separate packages. The two parts communicate via mailboxes. This was done some time ago having RC control in mind.

For RC a remote mailbox mechanism was implemented over the DS/1000 software. This allowed us to keep the controller programmes totally unchanged. They communicate under RC via a link – rather than a normal – mailbox with the user end programmes. On the user side, while the user end interface was kept unchanged, some interface subroutines had to be added.

Data Flow

Following the data flow in Figure 4 one sees that data acquisition was done on the control computer of the 2.2-m telescope (according to commands sent from Garching). Afterwards data were sent from La Silla via a compression/expansion package to Garching. Data went directly from an image processing (IHAP) file at La Silla to a corresponding file in Garching, with an option to display them on an image display monitor. It should be underlined that this activity could go on in parallel both with the sending of new commands or with local image processing in Garching. This means also that transmission times were much less noticeable than if the user had been idle and waiting.

Results

– The leased line, once set-up and equalized, was reliable and stable in time.
– The line was operated at 9600 baud for data transmission.
– Transmission times for a full CCD frame (around 170KW) took about 10 minutes, which is some 40% worse than the net throughput of the La Serena test. This is not due to an increased error (and therefore retransmission) rate, but simply to greatly increased transmission delays.
– On the whole, the line (including modem and computer cards) was adjusted with the main aim to have it working reliably. This was successfully achieved: there were no hang-ups.
– Typical data transfer times were however smaller than the times given above: 7 minutes for images, 2,5 minutes for spectroscopic data. This is because data compression/expansion was applied and, for spectra, only the relevant part of an image was sent. Data were sent in these times complete, i.e. without loss of information.
– Data transmission times could be reduced even more, applying cut levels and division factors in the compression algorithm, but in practice one never felt so time critical that this should be done.
– The good pointing of the 2.2-m telescope helped a great deal, so that no field monitoring was needed for direct imaging. In spectroscopic mode, field acquisition TV frames were sent via the Tevelex device. This is capable of sending a TV frame, reduced to 50% (every other line) in 25 seconds.

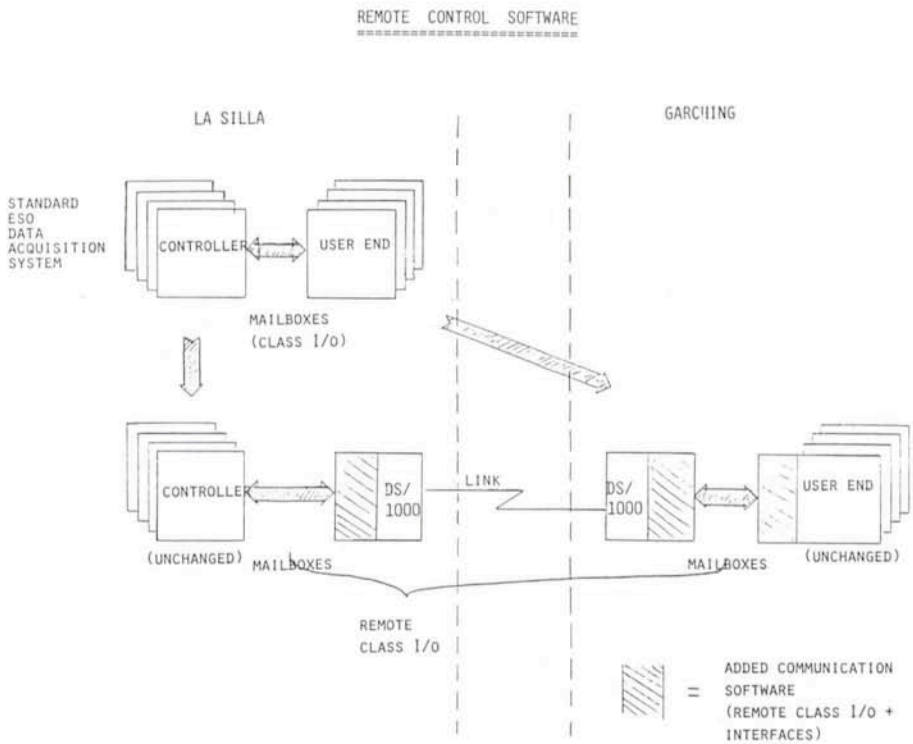

Figure 3: *The control/acquisition software, as implemented in ESO, was adapted to remote control with the insertion of a remote mailbox package.*

– About global reliability one should say that very few restarts of the control software environment were ever needed. Once computers had been started properly at the beginning of the night, they would go on with less than one restart per night. Even short accidental interruptions of the line, by using the telephone when data transmission was going on, were recovered.
– The manual switching procedure among telephone, Tevelex and computer mode demanded for a precise operating discipline, which would not be needed if a way were found to have everything, including switching, under computer control.
– More shall be done and can easily be implemented in the direction of automatic data transmission, after every exposure, on the basis of computer procedures.
– During the day-time, the link was used for telephone communication between La Silla and Garching. A permanent open line between these two ESO sites is important to further improve communication and collaboration.
– Any kind of files and data can be transferred at day time. A significant example was the transmission of Halley images coming from the Wide Field CCD Camera telescope, transferred to Garching in the morning following the La Silla observation within a matter of minutes.
– The large amount of data involved plus the additional advantages just mentioned for day-time use of the line make a leased line a preferable solution with respect to packet switching from an economic point of view. Reliability, reduced delays and all-time availability of a leased line are additional bonuses. However, packet switching communication will also be tried with La Silla during pending RC tests. This could become a general-purpose tool for exchanging messages and short files.
– The 2.2-m telescope was taken as a test case, but also other telescopes and instruments at La Silla could in principle be operated under RC.

Conclusions

We feel that the test was quite successful in showing the potential of "Interactive Remote Control". Astronomers have been working quite efficiently, not too far from what they could do by being physically at La Silla. The efficiency could easily be further improved by simple measures and procedures in the software.

The approach of using a leased line seems correct; though the case for a wider bandwidth is still open, particularly in view of larger size CCDs and in order to allow more parallelism for voice and video information. Also from the point of view of cost, the large amount of data transferred and the use of the line for telephone communication during day time, seem to justify the use of a leased line.

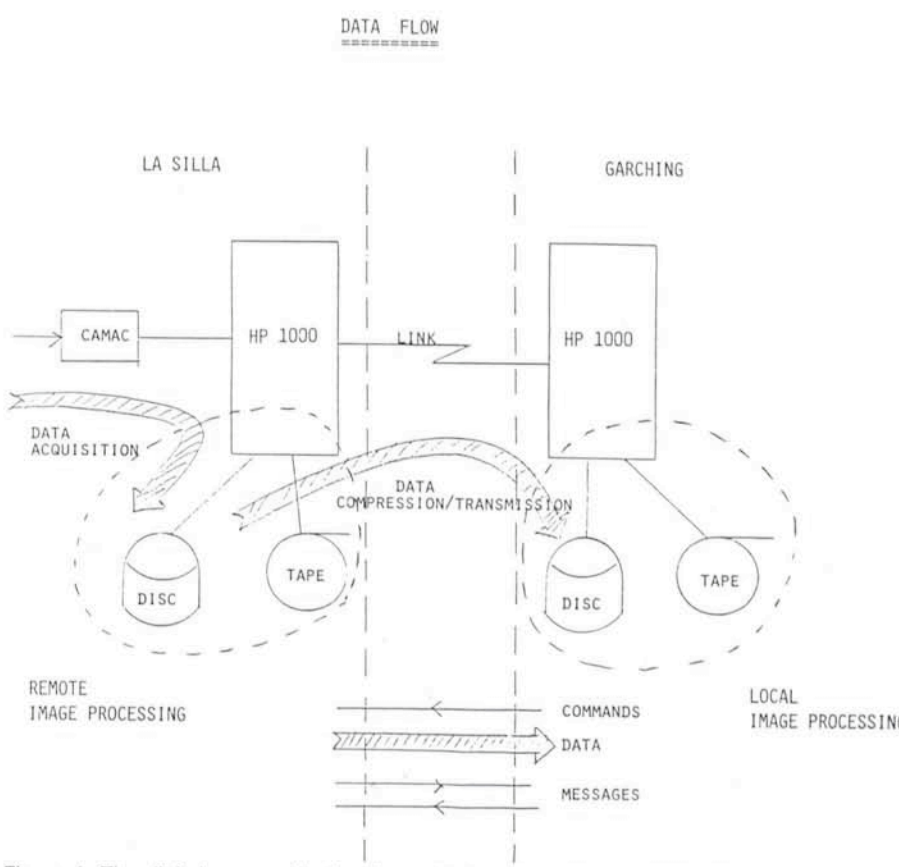

Figure 4: *The digital communication flow of information both for commands and data. The control, acquisition and transmission of data was all under remote control commands sent from Garching.*

It is also clear that interactive remote observing, in the way it was tested, offers entirely new working conditions to astronomers. Flexible scheduling, a few hours work on a telescope, recovery of lost nights at La Silla are all concepts which find a solution under remote control from Garching.

The test run also provided us with a lot of feedback in terms of desirable improvements which should be made in order to have a friendly-and-easy-to-use permanent remote control facility in Garching. We now feel confident that future implementations of RC, like in the case of the NTT, can be based on experience and are technically understood.

The net price of RC features, when cost of operations in Garching versus costs at La Silla are taken into account, seems to be reasonable. RC from Garching becomes therefore an open option, even for the near future.

Acknowledgements

We wish to acknowledge the relevant contribution of P. Biereichel, W. Nees and the TRS division at La Silla to the success of this test. Thanks also to the astronomers who took part in the remote observations: H.-M. Adorf, P. Angebault, J. Danziger, E. Giraud, P. Grosbøl, S. Jörsäter, M. Tarenghi, M.-H. Ulrich in Garching and S. Cristiani at La Silla.

Computer Aided Design of Printed Circuit Boards at ESO

H. KASTEN, ESO

Whenever a new ESO instrument is made available to visitors, they receive a well functioning device which has been tested over and over again. The astronomer of course expects this, and when he sits in front of the computer terminal, happily monitoring this or that celestial object, he is unlikely to think of the amount of work that has been performed before. He is rarely aware of the densely packed electronics racks in the other room and even less of the rows and rows of "cards" within them.

ESO designs its own instruments because it would be very difficult, if not impossible, to contract this work to outside firms. However, after the initial design phase, industries in the member countries are often asked to build parts according to the detailed plans produced at ESO. This is also the case for some electronic components. In order to accommodate modern electronics and to facilitate maintenance, it has since long been customary to design Printed Circuit Boards which can easily be plugged into the cabinets. The design of such boards (PCB) was always rather difficult and time-consuming, but a new computer-supported technique (CAD = Computer Aided Design) has now for some time greatly facilitated this kind of work at the Electronics Group at ESO.

The new system increases the reliability and precision and significantly reduces the time needed to design a board. It is based on a Prime Computer 2250 and two software packages, Autoplan and Autoboard. The CV-Grado system was installed in early 1984 and has since been used extensively. The production rate is now several dozen of new boards/year, each having up to 300 electronic components. The starting point is a "messy" circuit diagram and the result is a well organized, (near)-optimal configuration of the PCB, with all wiring, etc. specified.

The operator starts by inputting the connection list, i.e. which components shall be connected with each other at which points. The programme then places the components within the board perimeter. This can be done automatically or interactively to obtain the best possible component-to-board area

Figure 1: *The CAD-PCB system at the ESO Electronics Group in Garching.*

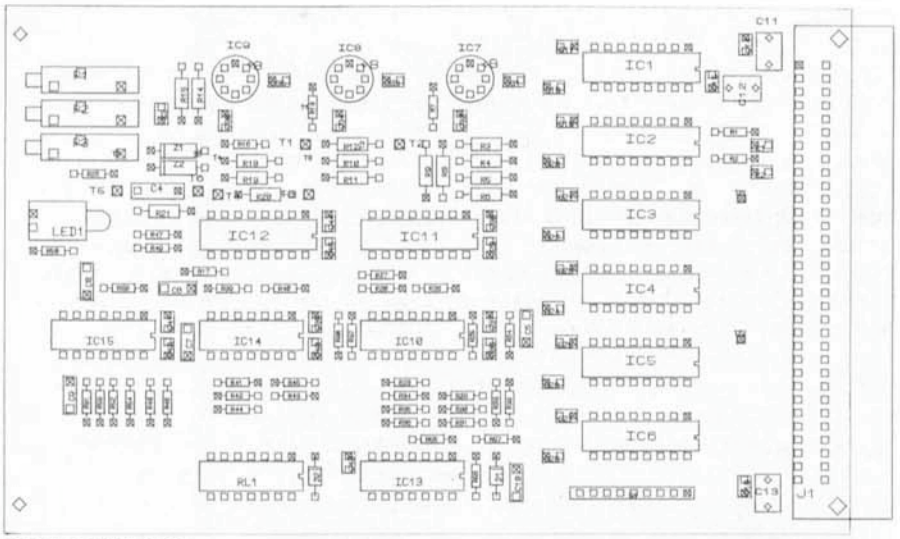

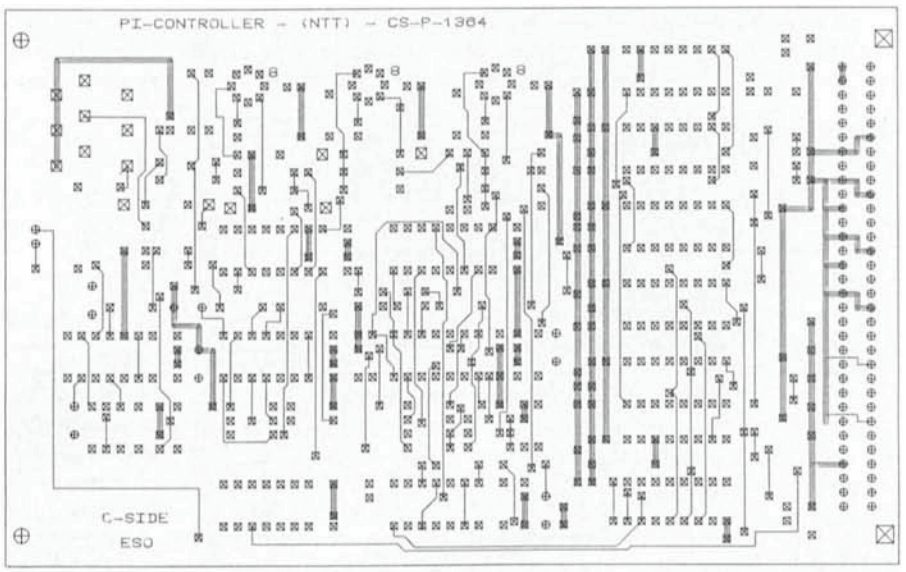

Figure 2: *Example of PCB board design for the PI controller at the NTT. The board measures 100 × 160 mm (Europe size) and contains 82 components with 316 connections; component-to-board ratio is 45 per cent. Upper: Placement of components. Lower: Wiring diagram on component side.*

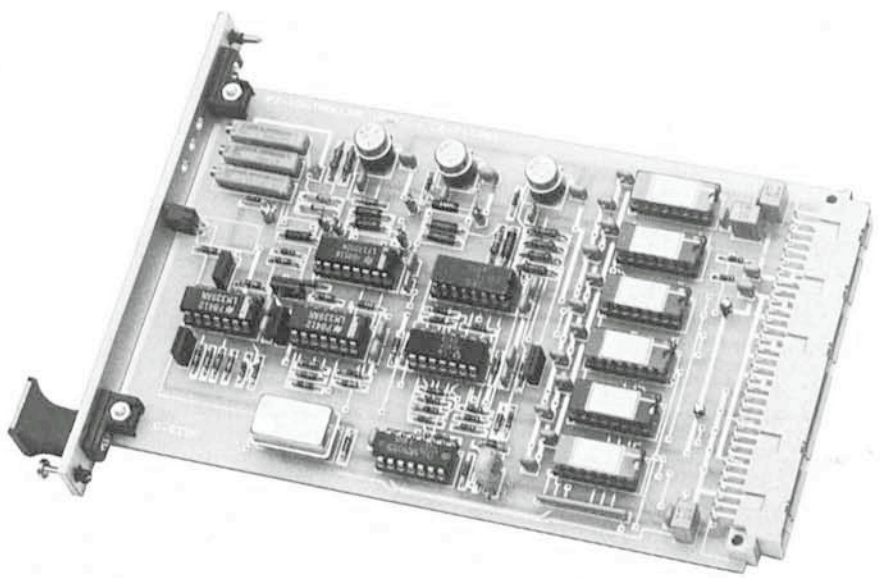

Figure 3: *Photo of board for which the design is shown in Figure 2.*

GRADO-CV-Configuration at ESO

1. CPU: Prime-Computer 2250 (32 Bit)
   Memory – 0.5 MB Autoboard
   – 1.0 MB Autoplan + Autoboard
   Disk – 60 MB
2. Peripherals: System console, printer, tape drive
3. Graphic workstation: Ramtek-Colardisplay, Summagraphic Tablet, Alphanumeric Terminal
4. Hardcopy: Facit printer
5. Plotter: Penplotter BENSON, Photoplotter (Quest) GQ-40 (external). All data storage is brought on a magnetic tape-cassette.

ratio; normally around 50 per cent. Then follows the crucial operation: the automatic process to determine the optimal routing of connections (Autorouter). The two algorithms from Stitching and Lee are used. The problem reminds us of the classical one known as the "travelling astronomer" (what is the shortest route, if he has to visit *x* observatories?).

For a dense PCB, the Autorouter routine can take up to 16–24 hours. Therefore, we normally run these programmes overnight or during weekends. Even then, a few connections are sometimes not found. Then an iterative, interactive process is needed. Once the operator is satisfied, detailed drawings of the PCB design are output, including all layers of the board, which are needed for the fabrication. This entire procedure also guarantees full correspondence between the PCB and its documentation, a fact that greatly facilitates maintenance. Moreover, the software automatically rejects "errors", which might otherwise have gone undetected until the board had already been produced.

The work as PCB-designer has changed drastically with the introduction of CAD at ESO. In less time, we can produce more and better boards and on top of it, it is also interesting to use modern techniques.

ESO Publications and Picture Catalogue Now Available

A catalogue of books, prints, posters, slides, etc. which can be obtained from ESO will be available from mid-July 1986. It will be sent upon request. Please write to the ESO Information and Photographic Service (address on last page).

Extinction Variations at La Silla

F. RUFENER, Geneva Observatory

1. Introduction

The observations made in the seven-colour photoelectric photometry of Geneva Observatory are carried out in a very systematic mannner with equipment which allows a precise and stable definition of the passbands. During these last ten years, the Geneva observers have had permanent access to a small telescope installed at La Silla (altitude: 2,400 m; latitude: −29°). These circumstances have allowed us to undertake several programmes which we have already presented here (*The Messenger* No. 31, 1983). Retrospectively, this series of observations has been reexamined with the aim of extracting a precise appreciation of the atmospheric extinction in each passband as well as its evolution with time. Actually, during 4 nights out of 5 we do not measure the value of the atmospheric extinction: the reduction to outside the atmosphere of the measurements is then made by using the mean extinction values. Simplifying the problem, we can summarize the computation of the magnitudes outside the atmosphere by the following formula.

$$m_{o,\lambda} = m_{z,\lambda} - k_\lambda F_z + C_\lambda \qquad (1)$$

where:
- $m_{o,\lambda}$: magnitude reduced to outside the atmosphere for the mean wavelength λ.
- $m_{o,\lambda}$: magnitude for the same wavelength measured at ground level.
- k_λ: atmospheric extinction coefficient by unit of air mass.
- F_z: air mass expressed in units of zenithal atmosphere thicknesses passed through along the line of sight ($3 > F_z \geq 1$).
- C_λ: Constant allowing the adjustment of the scale of magnitudes.

The inconvenience due to the ignorance of the exact value of the extinction coefficient and its replacement by a mean coefficient ($\bar{k}_\lambda$) is much reduced if the observations are planned in such a manner that the air mass (F_z) passed through varies within very small limits from one measurement to another. This enables the main part of the error on k_λ to be compensated for by a corresponding adjustment of the zero point of the magnitude scale.

On the other hand, for about 1 night out of 5, a particular procedure is used which enables a precise estimate of the extinction to be made even if the latter is not absolutely stable over the night. This is the M and D method, the advantages and peculiarities of which have been described in detail by Rufener (1964, 1986). It differs from the classical Bouguer method which directly applies relation (1). This last case only requires the measurement of a given star at several air masses. The extinction k_λ is then obtained either graphically or by computation. The Bouguer method implicitly assumes the extinction to be stable during the time (4 to 6 hours) necessary for its measurement. This hypothesis is, however, seldom true. Without entering into the details discussed by Rufener (1964, 1986) we can state that the M and D method, which uses pairs of quasi-simultaneous observations of two stars, the one chosen ascending (M) and the other descending (D), allows a subsequent estimate of the instantaneous extinction prevailing at the time of the measurement of each pair to be made. Although this method allows the extinction to be slowly variable during the night it assumes, on the other hand, that it is isotropic at a given moment. This last condition is well confirmed during the clear nights qualified as "photometric". The application of the M and D method leads to a particularization of the extinction as a function of time during the night by interpolating between the moments when the 4 to 6 pairs of M and D measurements were made.

For the period situated between November 1975 and March 1985 we dispose of 452 M and D nights. For each night and for each one of the seven colours we have computed the monochromatic extinctions corresponding to the mean wavelength (λ_o) of each passband. The extinction k_λ adopted is the mean over the 8 to 12 estimates given by the M and D method. We also obtain for each night and each colour a standard deviation ($\sigma_{k\lambda}$ = r.m.s. deviation) which provides an estimate of the fluctuation of the nocturnal extinction. Figure 1 shows the chronological evolution of this estimation of the atmospheric extinction for 3 wavelengths corresponding to the filters

[U]: λ_o = 3456 Å
[B]: λ_o = 4245 Å
[V]: λ_o = 5500 Å

Some points earlier than November 1975 are visible in this figure. They correspond to M and D nights recorded with the aid of ESO telescopes equipped with photometers in which the filters of the Geneva system had been installed. Several remarkable features can be seen in Figure 1.

1. An important dispersion of the daily values, with a pronounced seasonal trend.
2. A slow decrease before the El Chichón event and a more rapid trend following the discontinuity.
3. A marked discontinuity in October 1982. It is a consequence of the eruptions of the El Chichón volcano in the Mexican state of Chiapas on March 23 and April 4, 1982.

Let us examine in more detail these three observational facts and their significance.

2. Mean Extinction and Seasonal Variations

Our observations of the mean daily extinctions show a dispersion $\sigma_{k\lambda}$ (r.m.s. deviation) which varies from night to night. A typical value of this dispersion is 0.007; this implies peak to peak variations of the extinction of 0.02 to 0.03 per night. We quite often (10 % of the M and D nights) find amplitudes of variation of twice these values. The dispersion observed over the series of daily values is larger, clearly more pronounced for the ultraviolet than for the visible. Figure 1 shows peak to peak variations ranging from 0.05 for $k_{[V]}$ to 0.10 for $k_{[U]}$. It is readily apparent that this dispersion is seasonal. By taking into account the 321 m and D nights preceding the El Chichón event and by subtracting the slow decrease we obtain the annual variation depicted in Figure 2. The full line is the result of a sinusoidal fit with a period of one year. This same sine curve is plotted in Figure 1 after addition of the slow decrease.

It is generally assumed that the atmospheric extinction is the result of three main causes which add together:

$$k(\lambda_o) = k_{RC}(\lambda_o) + k_{03}(\lambda_o) + k_p(\lambda_o) \qquad (2)$$

- $k_{RC}(\lambda_o)$ for the Rayleigh-Cabannes molecular diffusion.
- $k_{03}(\lambda_o)$ for the selective absorption by molecular bands which in our case are restricted to those of ozone.
- $k_p(\lambda_o)$ for the extinction due to aerosols, dust and condensations of various natures.

Each of these 3 components varies as a function of several parameters; let us point out the main ones: For $k_{RC}(\lambda_o)$ these are the atmospheric pressure and temperature, for $k_{03}(\lambda_o)$ it is the reduced height of ozone and for $k_p(\lambda_o)$ the quantity of aerosols, whose vertical distribution and origin can be variable.

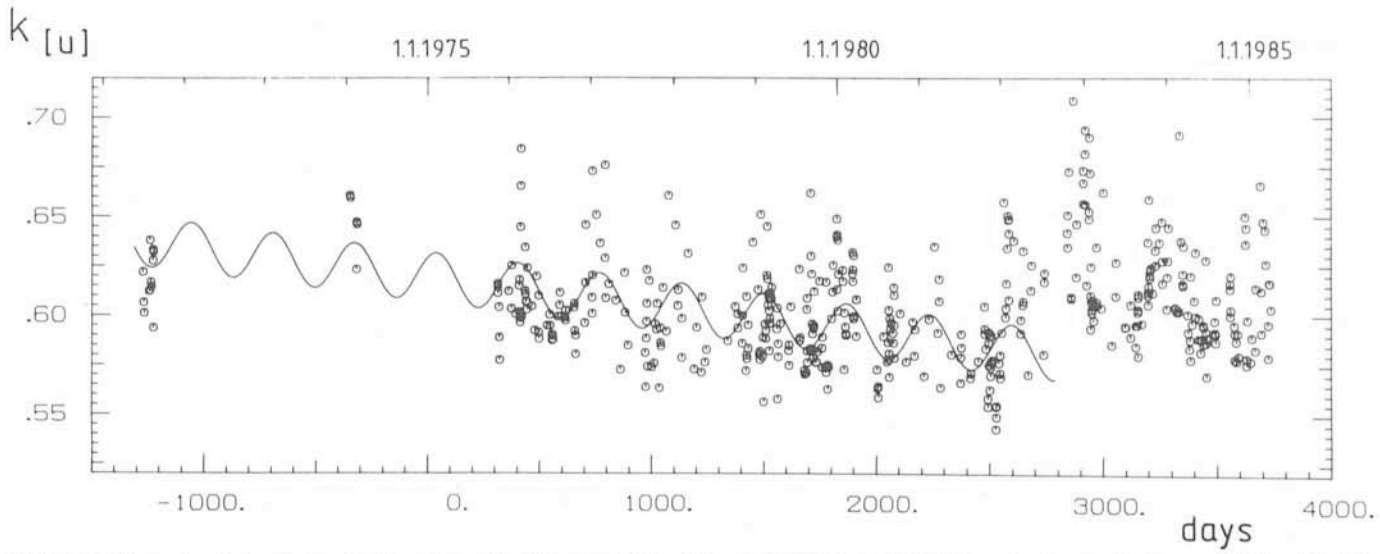

Figure 1a: *Chronological variation for the colour [U] of the mean atmospheric extinction coefficient ($k_{\lambda_0} = k_{[U]}$) computed for each M and D night (see text for details). The discontinuity at the abscissa 2800 is due to the eruption of the El Chichón volcano. A slow decrease of the minimum and maximum values is clearly visible over the 2500 preceding nights. This is also the case for the mean value $\bar{k}(t)$. The sine curve represents the annual variation of $\bar{k}(t)$ as obtained in Figure 2a. The site of the observations is the ESO observatory at La Silla (Chile). The zero point of the abscissa corresponds to 1.1.1975.*

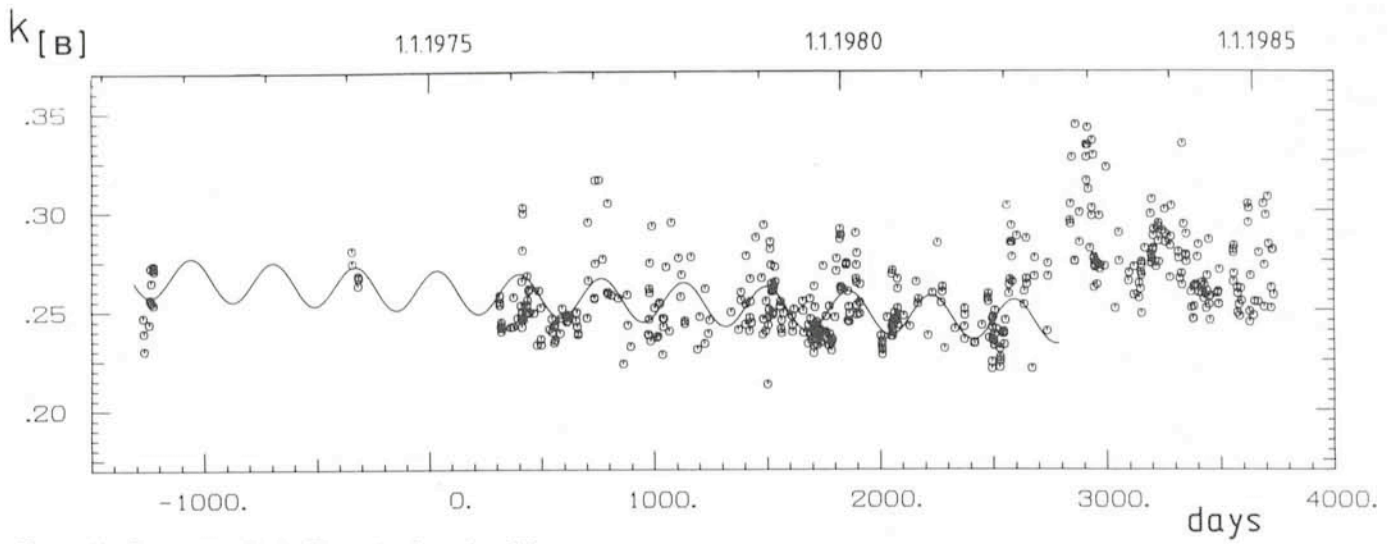

Figure 1b: *Same remarks as Figure 1a, for colour [B].*

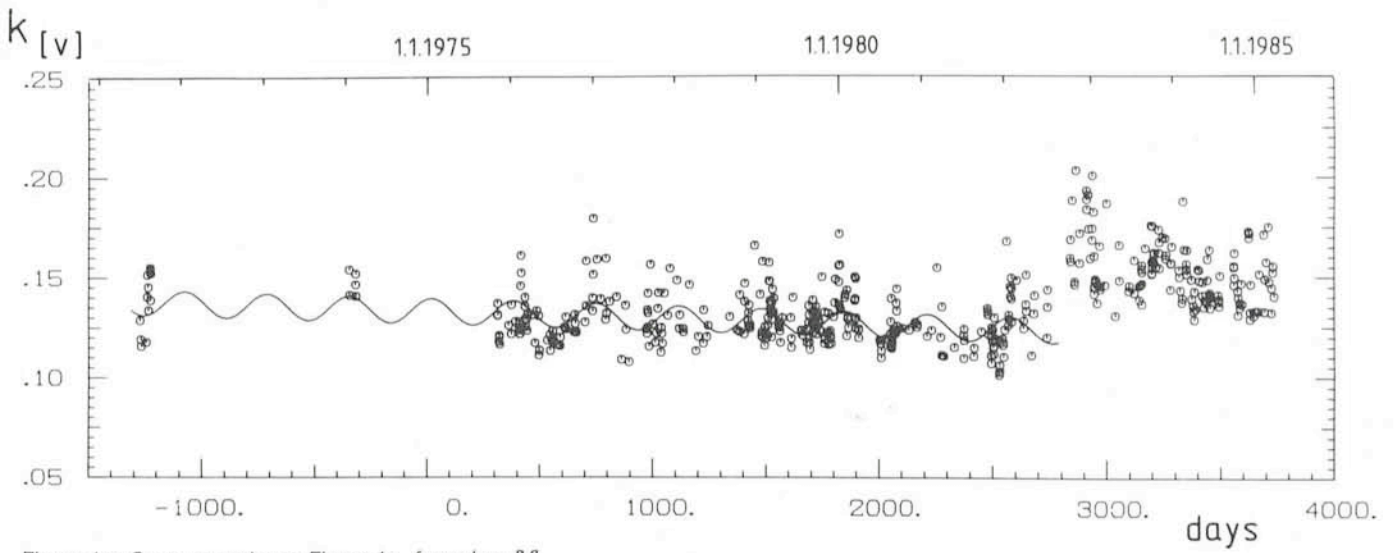

Figure 1c: *Same remarks as Figure 1a, for colour [V].*

The mean values and minima shown in Figure 2 are characteristic for the period preceding the El Chichón eruption; they are given in Table 1. The interpretation of these values enables an appreciation of the minimal effect of aerosols possible at La Silla. Indeed, by subtracting probable estimates of k_{RC} (λ_o) and k_{03} (λ_o), taken from Penndorf (1957), Van Allen (1976), Gast (1960) we get for k_p (λ_o) the values of Table 1. The mean minimum extinction by aerosols can then be expressed by

$$k_p(\lambda_o) = b\,\lambda_o^{-\alpha} = 0.006\,\lambda_o^{-1.3} \qquad (3)$$

(k_p in magnitudes per unit of air mass, λ_o in μm). The value of the coefficient b = 0.006 is exceptionally small if one considers the work of Siedentopf (1948). The important fluctuations of the observed extinctions, be they seasonal or not, result on the one hand from the variation of the physical parameters which control molecular diffusion and, on the other hand, from seasonal variations of the reduced thickness of ozone and of the various aerosols present in the lower atmospheric layers. The altitude reached by the latter is clearly greater during the southern summer, its upper limit being situated above La Silla.

3. Slow Variations of the Extinction

If we consider the 2,500 days preceding the El Chichón eruption we notice, in spite of the strong dispersion of the points in Figure 1, a slow and regular decrease of the mean as well as the extreme values (minima and maxima). This decrease is strongly chromatic, more pronounced for [U] than for [V]. For the values observed in the seven colours and calling this decrease over 2,500 days $d_{\lambda o}$, we find the relation

$$d_{\lambda o} = 0.002\,\lambda_o^{-2.3} \qquad (4)$$

($d_{\lambda o}$ in magnitudes by unit of air mass, λ_o in μm). This decrease cannot be related with a drift of the parameters which control molecular diffusion or the absorption by ozone, since no variation of that nature is known. On the other hand, if we compare our observations with those of Moreno and Stock (1964) and Gutierrez-Moreno et al. (1982), we are led to the conclusion that this decrease is the continuation of the diminishing diffusive and absorbant effects caused by the aerosols emitted in March 1963 by the Mt. Agung volcano (Bali, latitude −8°). Indeed, that volcano was responsible for an exceptional stratospheric load of aerosols with a probable maximum in the southern hemisphere. According to Lamb (1970), the contamination of the stratosphere could have reached an altitude close to 50 km. The

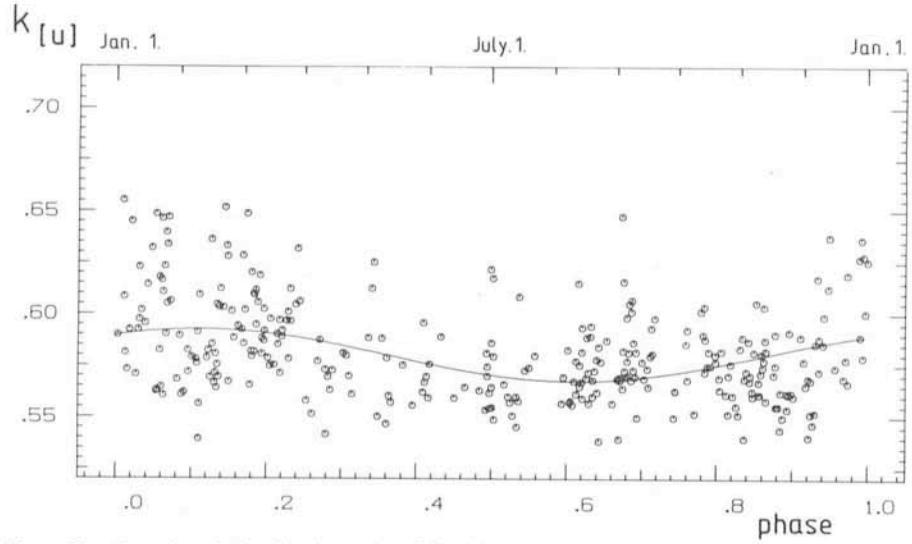

Figure 2a: *Annual variation for the colour [U] of the atmospheric extinction coefficient ($k\lambda_o = k_{[U]}$) observed during the 321 M and D nights preceding the eruption of the El Chichón volcano (positive abscissa in Figure 1a). The slow decrease has been subtracted. The scale of the ordinates therefore corresponds to the period 2800 in abscissa in Figure 1a. The full line is the fitted sine curve.*

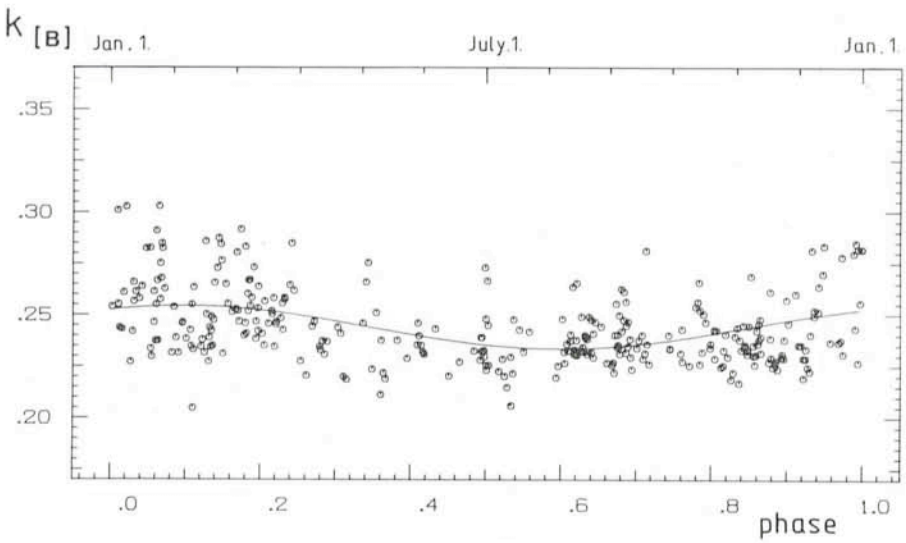

Figure 2b: *Same remarks as Figure 2a, for colour [B].*

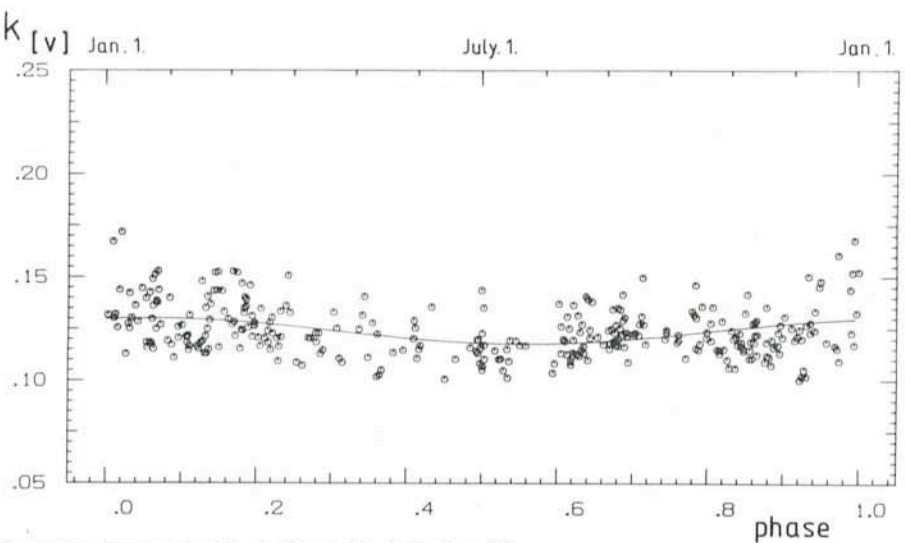

Figure 2c: *Same remarks as Figure 2a, for colour [V].*

TABLE 1

Filters	U	B_1	B	B_2	V_1	V	G
λ_o [nm]	345.6	402.4	424.5	448.0	540.5	550.0	580.0
k_{RC} (λ_o) [magn. air mass^{-1}]	.550	.289	.230	.185	.085	.080	.065
k_{03} (λ_o) [magn. air mass^{-1}]	.016	.000	.000	.001	.025	.030	.039
$< k >$ [magn. air mass^{-1}]	.589	.308	.246	.206	.126	.124	.114
k_p (λ_o) [magn. air mass^{-1}]	.023	.019	.016	.020	.016	.014	.010
Slope $d_{\lambda o}$ [magn./2500 d]	.034	.012	.015	.013	.008	.009	.010
El Chichón discont. $\varepsilon_{\lambda o}$ [magn.]	.070	.053	.055	.050	.048	.048	.040

eruptions of Mt. Agung and El Chichón are conspicuous by their very strong emissions of sulfuric gases such as sulfur dioxide. In the presence of water vapour this gas can condense in the form of fine droplets of sulfuric acid (Robock, 1983; Keen, 1983). The altitude reached by these droplets and their small size can explain their very slow decantation through the stratosphere. Durations of 10 to 20 years are estimated as possible by Lamb (1970). On the other hand, the fact that these droplets were still in suspension more than 12 years after the Mt. Agung event is consistent with the strong chromaticity of the slow decrease observed. Indeed, the chromatic nature of this type of diffusion is all the more pronounced if the dimensions of the droplets are smaller than the wavelength of the observations. An order of magnitude of the typical dimension of these residual aerosols is ≤ 0.1 μm. On the basis of our observations, we can also conclude that for negative latitudes the period 1978–1982 was the most transparent during these last 20 years.

4. The Discontinuity Following the El Chichón Eruption

We notice no appreciable increase of extinction until the second of July 1982, i.e. three months after the El Chichón eruption. A difference in latitude of 46° separates the volcano from the site of our observations. The strongest extinction is recorded on November 3, 1982, seven months after the eruption. These delays are longer than those recorded at Cerro Tololo (latitude −30°) by Moreno and Stock (1964) following the Mt. Agung eruption. Indeed, they detected a significant increase after only 6 weeks and measured the highest extinction after 5 months. The difference in latitude between Mt. Agung and Tololo is only 22°. The amplitude of the discontinuity was also much larger (about 5 times!). The longer propagation time is certainly due to the greater separation in latitude, whereas the smaller discontinuity following the El Chichón event may reflect the combination of an intrinsic difference between the stratospheric loads injected by each volcano with the effect of difference in latitude or hemisphere. The size of the discontinuity that we have estimated ($\varepsilon\lambda_o$) over the extinction measured in each colour is observed as well for the mean values as for the minima and maxima. It is remarkable that the amplitude of the dispersions computed each night ($\sigma_{k\lambda}$) as well as the night-to-night dispersions are not significantly increased after the discontinuity. This tends to prove that at the latitude −29° the stratospheric load was already well distributed and sufficiently isotropic not to alter these estimators. From the $\varepsilon_{\lambda o}$ values of the discontinuity given in Table 1 we can deduce a chromatic dependence of the form

$$\varepsilon_{\lambda o} = 0.024\,\lambda^{-1} \qquad (5)$$

($\varepsilon_{\lambda o}$ in magnitudes, λ in μm). The exponent of the wavelength in this relation suggests that the size distribution of the supplementary particles has a distinctly larger modal value (0.5 μm) than that of the particles responsible for the slow decrease of § 3. This is consistent with the fact that this additional stratospheric load decreases rather rapidly during the first two years. The largest particles decant most rapidly.

5. Conclusion

This retrospective analysis over ten years of atmospheric extinction observations at La Silla allows one to better understand the nature of its variations. We were able to calculate the sizes of its short, mean and long term fluctuations. We confirm the advisability of taking the necessary precautions to control this parameter which is essential for the precise reduction to outside the atmosphere of ground based photometric observations. Events such as El Chichón induce variations of extinction which are locally quasi isotropic but nevertheless variable in time. Due to the restricted number of its assumptions, the M and D method is very useful for the correct estimation of atmospheric extinction. The analysis of the measured values shows the high quality of transparancy of the best nights at La Silla and the great frequency of nights during which photometric measurements are feasable.

References

Allen, C.W., 1976, *Astrophysical Quantities*, third ed. Athlone Press, London.

Gast, P.R., 1960, in *Handbook of Geophysics*, U.S. Air Force, Cambridge Research Center. Mac. Millan Cp. New York.

Guitérrez-Moreno, A., et al., 1982, *Publ. Astr. Soc. Pac.* **94,** 722.

Keen, R.A., 1983, *Science* **222,** 1011.

Lamb, H.H., 1970, *Phil. Trans. Roy. Soc. London* **266,** 425.

Moreno, H., Stock, J., 1964, *Publ. Astr. Soc. Pac.* **76,** 55.

Penndorf, R., 1957, *Jour. Opt. Soc. Amer.* **47,** 176.

Robock, A., 1983, *Nature* **301,** 373.

Rufener, F., 1964, *Publ. Obs. Genève, A,* **66,** 413.

Rufener, F., 1984, Reduction to outside the atmosphere and statistical tests used in Geneva photometry. In "NASA sponsored Workshop on improvements in photometry", San Diego State University. NASA Conference Publication **2350,** 108.

Siedentopf, H., 1948, *Naturwiss.* **35,** 289.

The trail of a meteor is captured on this 20-minute exposure of the La Silla night sky with the meteo mast in the foreground. Photograph by R. Lukas on Kodak 400 ASA film with a 50-mm f/1.8 lens.

Seeing at La Silla: LASSCA 86

M. SARAZIN, ESO

At the end of January 1986, a team of ten observers gathered at the observatory for a two week experiment of a new kind. Their aim was not to explore remote and fascinating stellar objects. They wanted to track a lifelong enemy, and also inevitable companion of every astronomer: the seeing.

The La Silla Seeing Campaign (LASSCA) was scheduled within the framework of the VLT working group for site evaluation, chaired by H. Van der Laan. The scientific community had immediately agreed to reserve simultaneous observing time on three telescopes. Proverbially, it was obviously necessary to look in detail at what was happening at our own front door before making comparisons with other places. Lassca was certainly the first experiment of this size dedicated to scientific analysis of atmospheric turbulence.

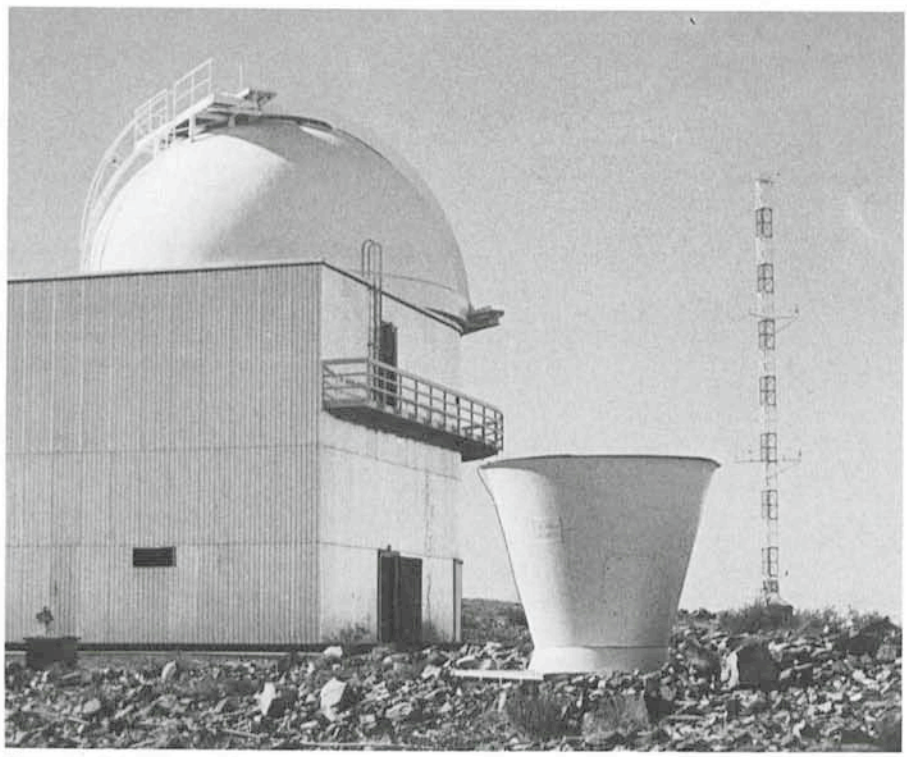

Figure 1: *SODAR antenna and meteo mast near the 1-m telescope at La Silla.*

The permanent site monitoring instrumentation includes a meteorological station and an acoustic sounder also named SODAR (Sound detection and ranging [Fig. 1]). To these devices was added a radar for tracking tropospheric balloons, on loan from the Centre National de Recherches Météorologiques (CNRM, Toulouse [Fig. 2]). A full monitoring of the atmosphere from the ground to more than 20 km altitude was then possible: The acoustic sounder displays the invisible microthermal perturbations which affect starlight between 30 m and 800 m altitude over the site (Fig. 3). It is an ideal tool for understanding the sudden changes in image quality during the course of an observing run. The conversion of its output into equivalent image width is relatively straightforward.

The analysis of the free atmosphere with free balloons permits the detection of any particularity of the site. An example is the Jet Stream whose 200 km wide core sometimes stays over the observatory at 12 km altitude (Fig. 4). The wind velocity there may reach 200 km/h and models are being developed to relate wind shear and temperature gradient to thermal turbulence and thus, to seeing.

Leaving aside the increase in image size, the high atmosphere is also responsible for shortening the lifetime of speckles (by increasing their number and their agitation) and for reducing the isoplanatic angle (solid angle in which two stars may be considered as coherent sources). Such parameters decide the efficiency of interferometric

Figure 2: *Radiosonde tracking system.*

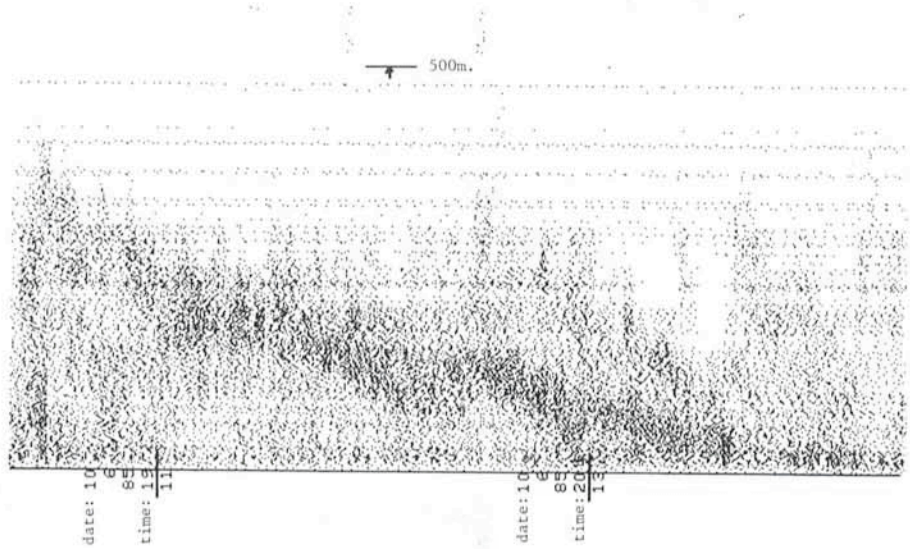

Figure 3: *SODAR display: decrease of turbulence level at sunset.*

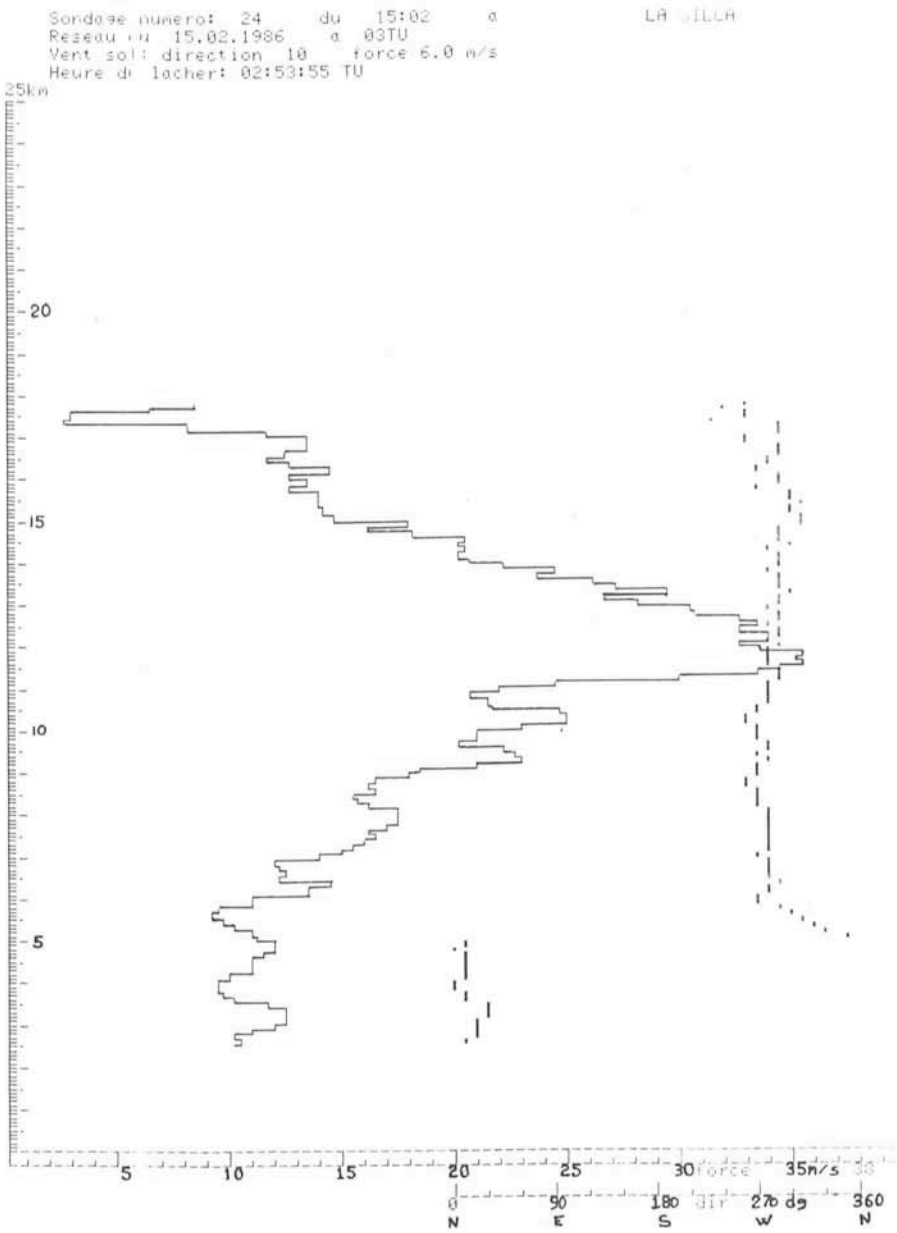

Figure 4: *Tropospheric sounding output in presence of the jet stream.*

methods and are of prime importance for the development of adaptive optics systems foreseen for the VLT.

Speckle lifetime, isoplanatic patch, image size with and without image motion were simultaneously monitored by G. Weigelt, G. Baier and P. Koller at the 2.2-m telescope. Thousands of speckle interferograms from single and double stars have been recorded using ICCD or a movie camera.

From the 1.52-m ESO telescope, J. Vernin and M. Azouit have been observing the scintillation characteristics of the same stellar sources with the SCIDAR technique (Scintillation Detection and Ranging). They could derive the vertical profiles of refractive index inhomogeneities from 1 km up to 10 or even 30 km over the site, according to double star angular separation.

Last but not least, the shearing interferometer of F. and C. Roddier was installed at the focus of the 50-cm ESO telescope. This device is considered as an absolute calibrator for the determination of the atmospheric point spread function since it is not sensitive to telescope optical aberrations or misfocusing.

Processing data and delivering conclusions is not the smallest part of the work but preliminary results allow us to hope that the analysis will be complete by the end of the year. Besides the increase in the knowledge of our observing environment, these measurements will allow some estimation of dome seeing. They also have been of great help for the calibration of the site testing seeing monitor, scheduled to start routine operation in August.

Very Large Telescope: Recent Developments

D. ENARD, ESO

Readers may feel badly informed about the development of the Very Large Telescope project, since no article appeared in the *Messenger* after December 1983 – a time when the VLT concept was still wide open. Since then, a concept – the linear array – has been presented at the IAU Conference in April 1984 at Garching. The internal study group was firmly established and began a thorough investigation of the array concept towards the end of 1984. Quite a number of studies – most of them feasibility studies of critical aspects – have been performed and a synthesis report of this initial phase, roughly equivalent to the phase A of space projects, has recently been issued.

The ESO base-line concept, called the linear array, consists of 4 independent 8-metre telescopes, with alt-azimuth mounts, operating in the open air but protected, when not observing, by removable shelters. The maximum operating wind speed in the free flow has been provisionally set to 9 m/sec which corresponds to about two thirds of the night time conditions at La Silla. For stronger winds, a wind screen is erected and reduces the average wind velocity in the region of the telescope by about 50 %. Because strong winds in Chile are effectively blowing from the same direction (north-south) the wind screen can be fixed independent of the telescope. An aerodynamic numerical analysis has shown that a promising concept would consist of a platform covering the space between the wind screen and the telescope and located at about 10 metres above the ground. Low air layers are captured beneath the platform thus creating a depression behind the wind screen. The result, illustrated by Figure 1, shows that the wind load on the telescope and particularly in the region of the primary mirror is greatly reduced, whereas the air stream is accel-

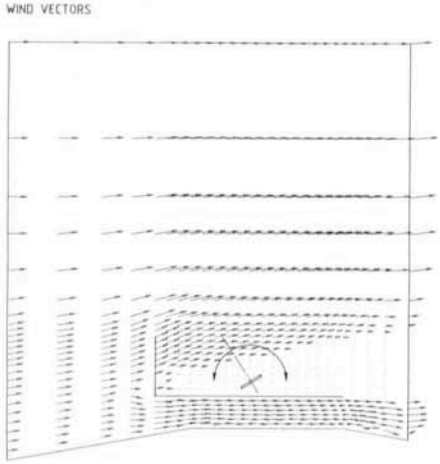

Figure 1: *Wind flow simulation of the proposed VLT building concept, obtained with a 2-dimensional fluid flow finite element model. A wind screen reduces the wind speed on the telescope structure and the primary mirror. A large part of the air flow is captured under the platform which surrounds the telescope up to the wind screen.*

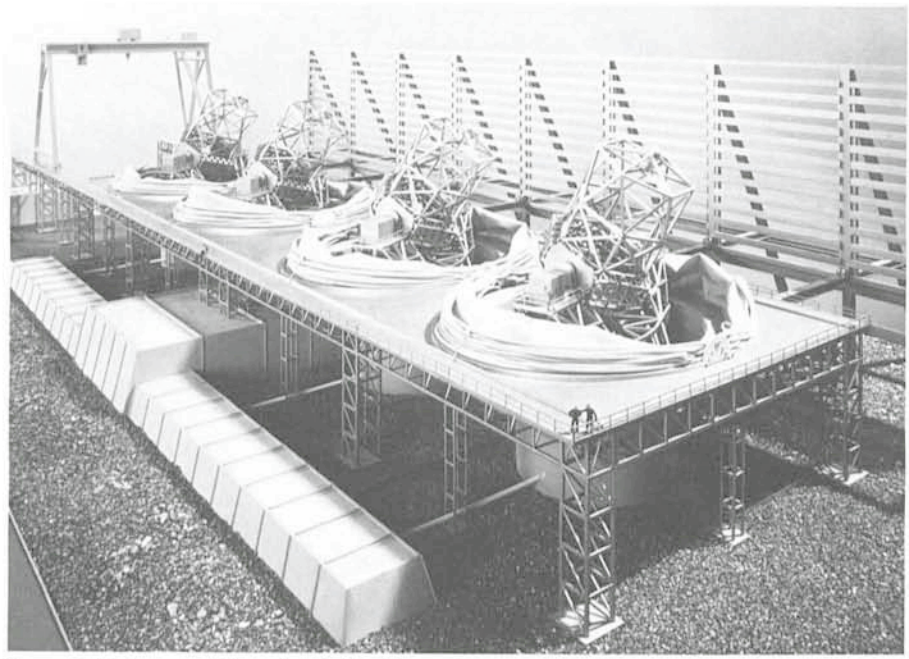

Figure 2: *VLT concept based on inflatable shelters and 2-position wind screen (here in down position for wind speed inferior to 9 m/sec).*

erated beneath the platform. A great improvement of local seeing conditions is expected of this approach.

Figures 2, 3 and 4 show models of two possible concepts for the building and the telescope structure. It is evident from the pictures that both concepts make a large place to innovation. For instance the solution for the shelters of Figure 2 is based on a high-strength double-wall plastic fabric supported by light-weight metallic hoops and inflated so that the effective wind load is always compensated by the internal pressure. The concept of Figure 4, based on metallic movable shelters, is more traditional but provides a safe, although less original, solution.

The coudé light beams transit through the tubes joining the telescope bases. The beam combination is effected either in a central "Combined Coudé Laboratory" for incoherent combination or for the purpose of interferometry in a long building parallel to the array.

The definitive configuration for the 4 telescopes has not yet been finalized and depends largely upon interferometry and on site constraints. The scientific working group on interferometry is very active in trying to define a realistic optimum configuration. The concept of Figure 2 is based on a compact and redundant linear arrangement whereas that of Figure 4 considers a 25–75–50 m arrangement which would provide 6 different base lines. The mechanical structure of the unit 8-m telescopes should be conceived for compactness, high rigidity, and for minimizing the wind load and the thermal inertia. The present analysis shows that it seems possible to conceive a telescope structure (Figures 2 and 3 show two examples) able to sustain an open air operation.

The crucial question of the primary mirror technology is actively investigated. One of the best materials for mirror blanks is Zerodur, a nearly zero expansion glass-ceramic. The presently available Zerodur technology cannot provide blanks larger than about 4 metres, but new technologies could become available within a few years to make 8-metre Zerodur blanks. Alternatives such as metal are also considered. Figure 5 represents an experimental light-weight steel blank recently manufactured. The process with which this blank has been produced seems perfectly extendable up to almost any size. The initial results look quite encouraging. Structure print-through looks less critical than anticipated and the quality of polish does not seem to be inferior to that of glass. Thermal warping and stability is being investigated.

The primary mirrors of the VLT will be active, which means that the mirror figure is corrected in real time. A wavefront analyzer is locked on a reference star and provides information for the mirror correction possibly at a frequency of a few Hertz. This rather high frequency may be necessary to correct for wind buffets. It has been shown that bright enough reference stars will be easily available in the 30-arcminute field of view of the unit telescopes. Indepen-

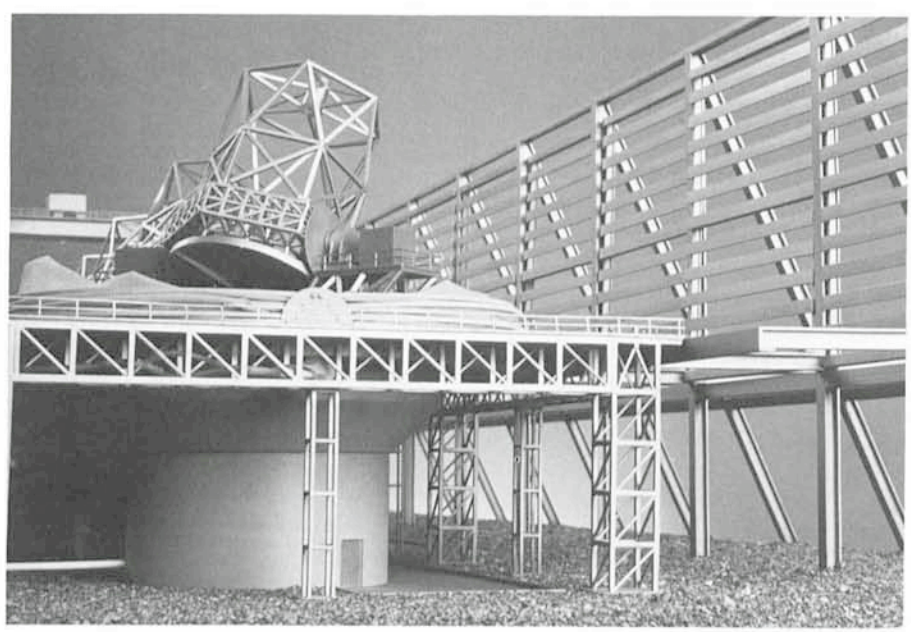

Figure 3: *Same concept as Figure 2 showing the mechanical structure of the telescope and the wind screen raised for wind speeds exceeding 9 m/sec.*

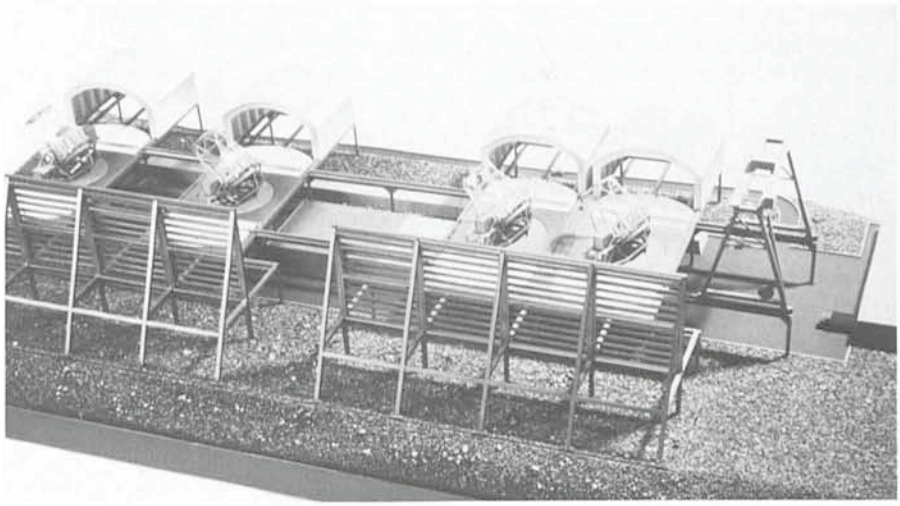

Figure 4: *VLT concept with movable shelters and a non-redundant configuration for interferometry. The 2 shelter doors are hinged on the platform so that the air flow can pass through the opened shelter with little disturbance.*

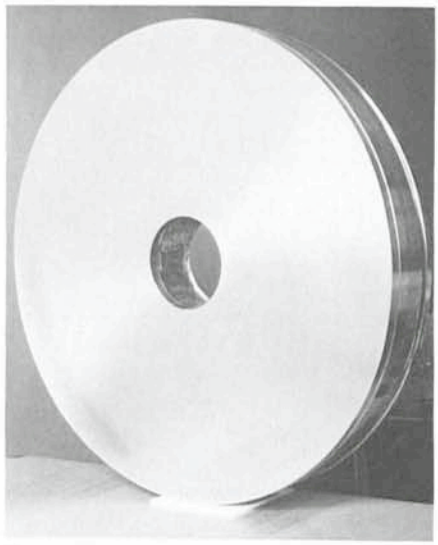

Figure 5: *An experimental steel mirror blank. Although in principle not an ideal material, stainless steel can be polished directly, and has a better thermal conductivity than glass. An active correction system would compensate for thermal and possible long-term warping.*

dently of the correction for wind load, an active mirror is viewed as the only way to obtain a very high imaging performance, whilst keeping the cost and lead time for the production of the mirror within reasonable limits. As an example, it is envisaged to relax considerably the tolerance on low spatial frequency deformations such as astigmatism and to correct it *in situ* with the active system. An active system leaves also the possibility to correct for thermal gradients and long-term warping and thus allows the use of non-zero expansion materials.

The correction of atmospheric phase disturbances with an adaptive smaller mirror is also investigated and small-scale experiments could start in 1987.

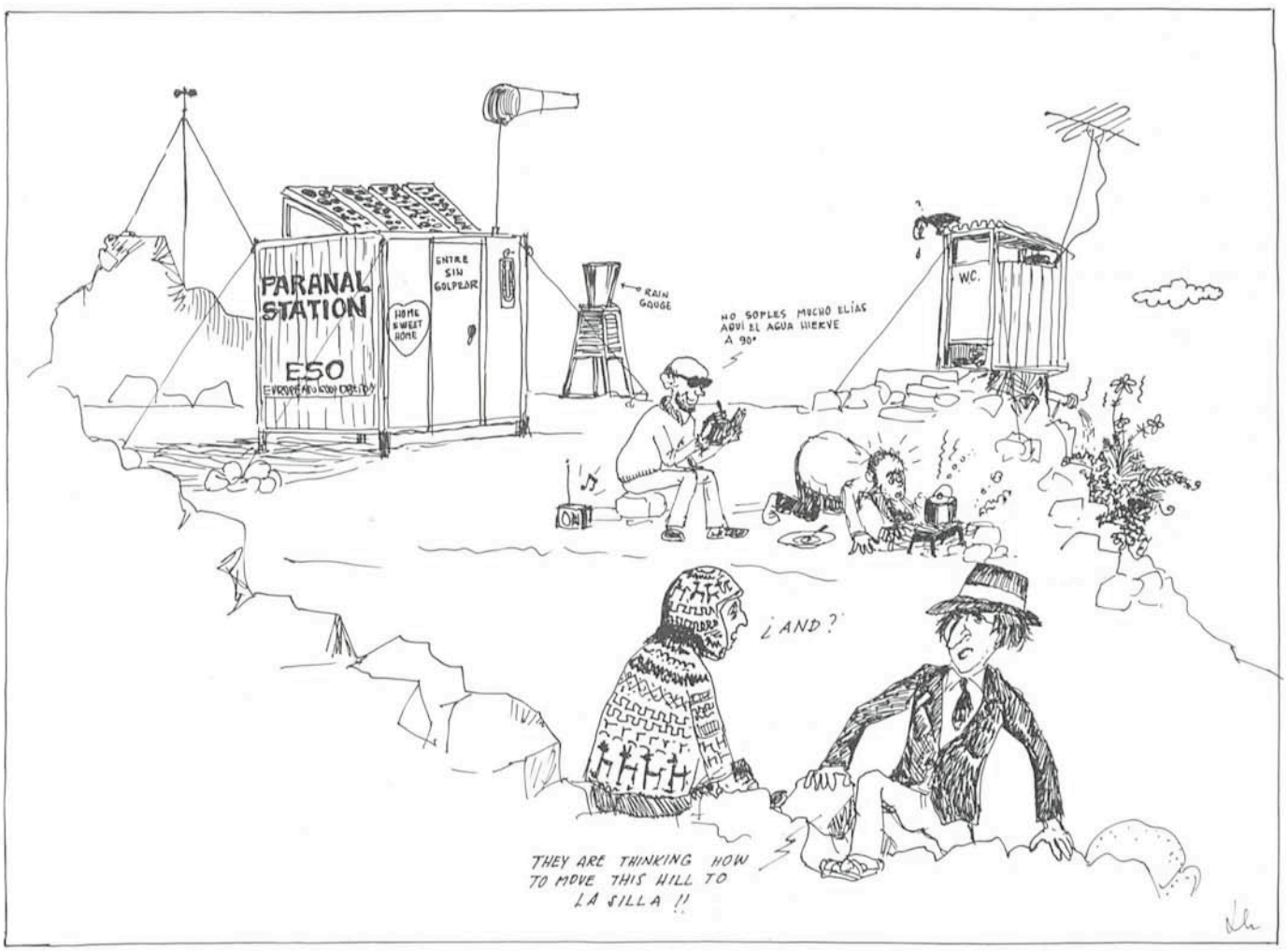

Whither the VLT?

(Drawing by H. Núñez.)

The ESO MESSENGER is published four times a year: normally in March, June, September and December. ESO also publishes Conference Proceedings, Preprints, Technical Notes and other material connected to its activities. Press Releases inform the media about particular events. For further information, contact the ESO Information and Photographic Service at the following address:

EUROPEAN
SOUTHERN OBSERVATORY
Karl-Schwarzschild-Str. 2
D-8046 Garching bei München
Fed. Rep. of Germany
Tel. (089) 32006-0
Telex 5-28282-0 eo d
Telefax: (089) 3202362

The ESO Messenger:
Editor: Richard M. West
Technical editor: Kurt Kjär

Printed by Universitätsdruckerei
Dr. C. Wolf & Sohn
Heidemannstraße 166
8000 München 45
Fed. Rep. of Germany

ISSN 0722-6691

Perhaps the most crucial question for the moment is the development of an adequate facility for the optical figuring and polishing of the 8-m mirrors; this is likely to determine the project lead time.

The priority activities for the next two years will be the detailed analysis of the telescope dynamic behaviour and the definition of the active primary mirror and of its support system.

Parallel to the technical investigations, scientific working groups pursue the analysis of the VLT concept with respect to its various observing goals. They are expected to give their final recommendation by July 1986 before a VLT workshop to be held next October.

Catálogo de ESO de publicaciones y fotografías disponible

A partir de mediados de julio de 1986 estará disponible un catálogo de libros, publicaciones, posters, diapositivas, etc. que se podrán obtener de ESO. Rogamos enviar sus pedidos por escrito al Servicio Informativo y Fotográfico de ESO (ver dirección en esta página).

Exhibiciones ESO

Durante buena parte del paso visible del cometa Halley por los cielos de Chile, la ESO contribuyó a una mejor información del público interesado, ofreciendo sendas exhibiciones en importantes centros culturales de Santiago y La Serena. En la Galería Azul de la Biblioteca Nacional (Santiago), nuestra exposición permaneció abierta entre mediados de febrero y mediados de abril, recibiendo la visita de aproximadamente 15600 personas. Dicha muestra se encuentra actualmente exhibiéndose en Punta Arenas, iniciando un itinerario que la llevará a las principales ciudades del país. Al mismo tiempo, el Museo Arqueológico de La Serena expuso una segunda colección de fotos y explicaciones entre noviembre de 1985 y mayo de este año, siendo admirada por aproximadamente 19500 personas. *R. Huidobro*

Libro de ESO aparecerá en 1987

Fué decidido que el libro de ESO titulado "Visiones del cielo austral" (ver *El Mensajero* N° 43, pág. 36) será publicado en 1987 con ocasión del 25° aniversario de la ESO.

Se están finalizando las negociaciones por un contrato de publicación con una de las editoras más importantes de Europa.

Contents